# Some recent Developments in Astroparticle Theory and Phenomenology

1. Ultra-high energy cosmic rays: Observations
2. Ultra-high energy cosmic rays: theoretical challenges, multi-messenger aspects
3. Axions and axion-like particles as dark matter
4. Astrophysical and experimental signatures
5. Outlook

DFG Deutsche Forschungsgemeinschaft

PROJEKTTRÄGER FÜR DAS Bundesministerium für Bildung und Forschung

UHH Universität Hamburg
DER FORSCHUNG | DER LEHRE | DER BILDUNG

Günter Sigl
II. Institut theoretische Physik, Universität Hamburg

SILAFAE 2018, Lima, Peru, 26.11-30.11.2018

# The All Particle Cosmic Ray Spectrum

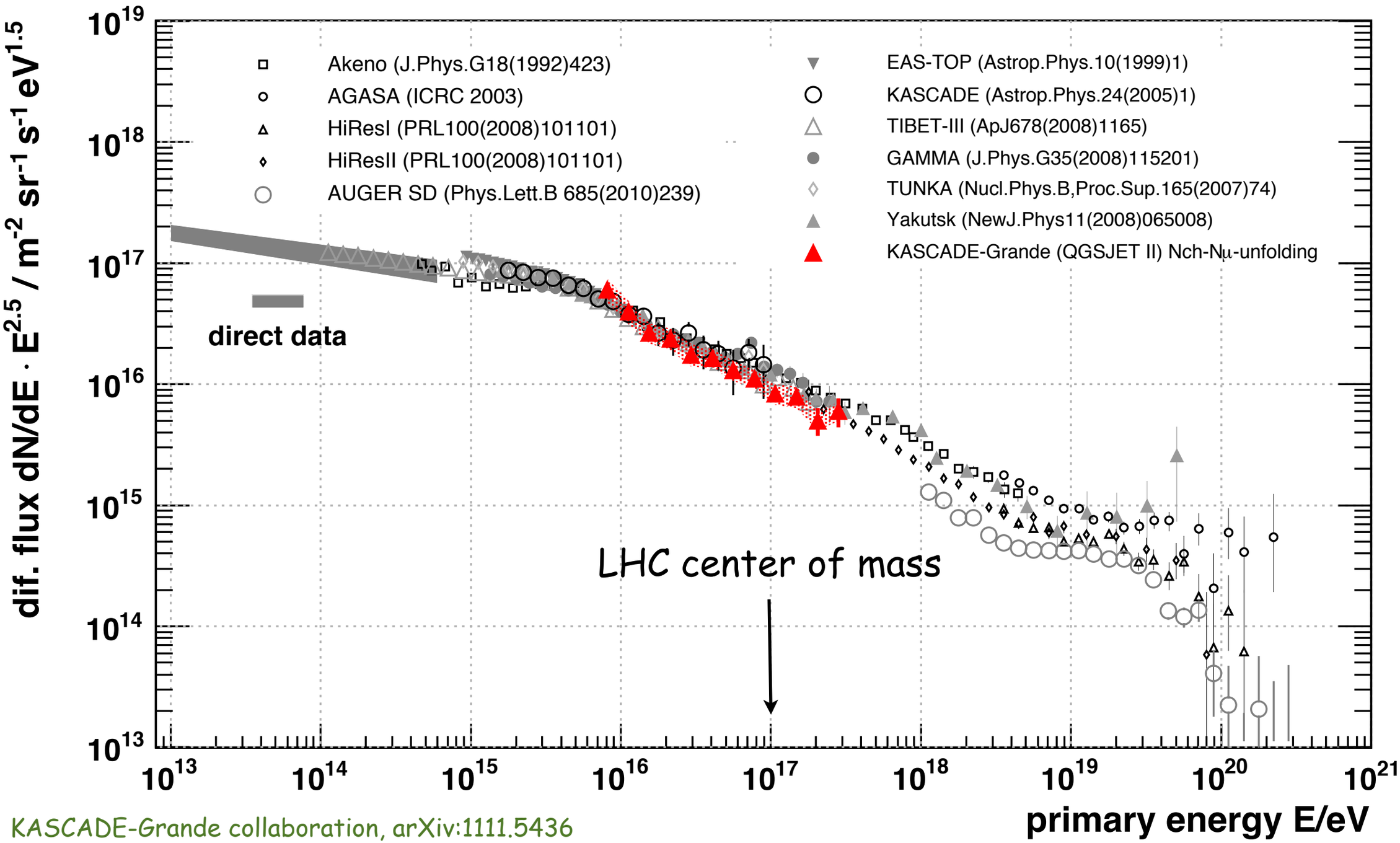


KASCADE-Grande collaboration, arXiv:1111.5436

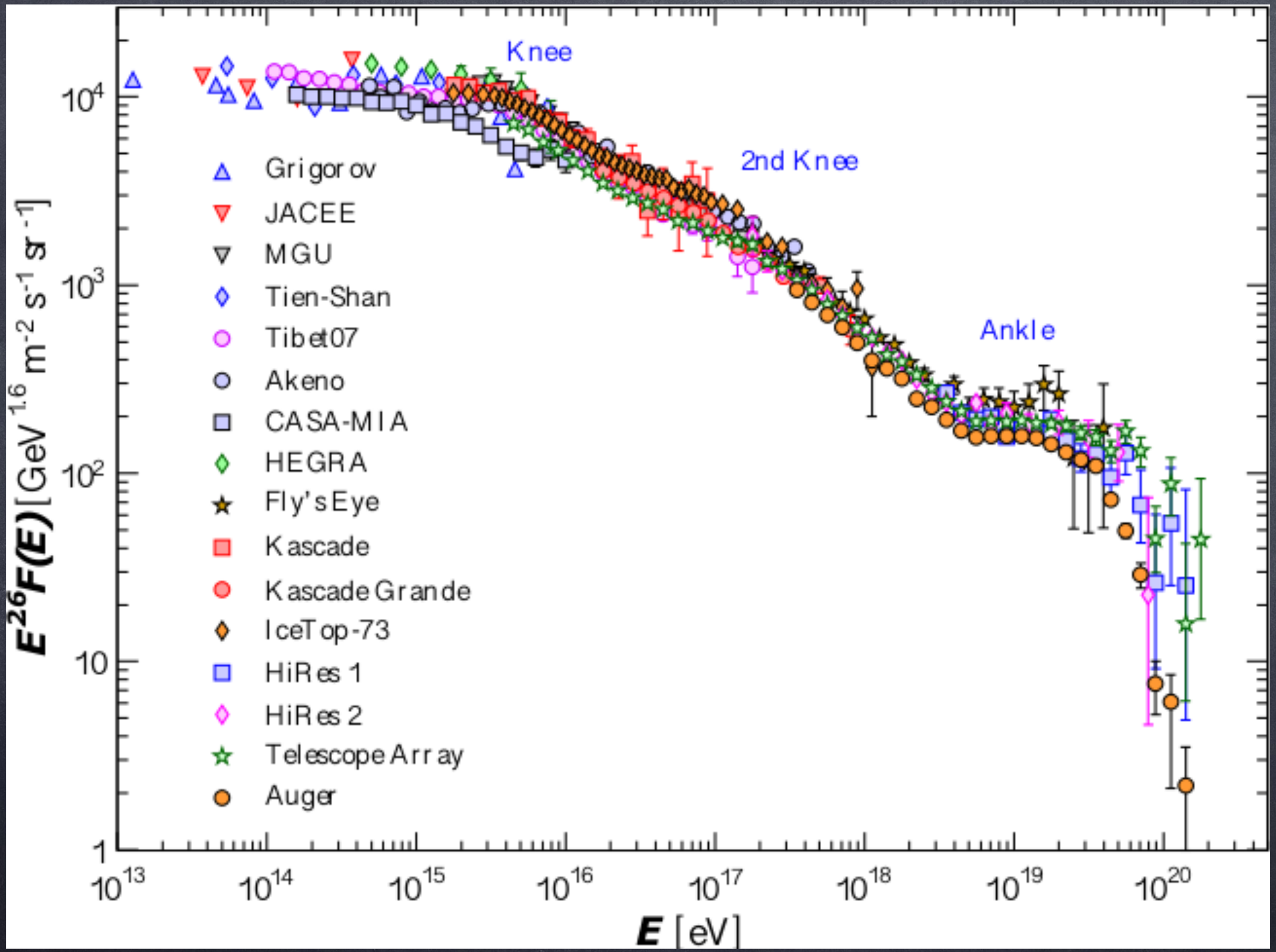
Knee
2nd Knee
Ankle
Grigorov
JACEE
MGU
Tien-Shan
Tibet07
Akeno
CASA-MIA
HEGRA
Fly's Eye
Kascade
Kascade Grande
IceTop-73
HiRes 1
HiRes 2
Telescope Array
Auger
$E^{2.6}F(E)$ [GeV$^{1.6}$ m$^{-2}$ s$^{-1}$ sr$^{-1}$]
$E$ [eV]
$10^4$
$10^3$
$10^2$
10
1
$10^{13}$
$10^{14}$
$10^{15}$
$10^{16}$
$10^{17}$
$10^{18}$
$10^{19}$
$10^{20}$

# Pierre Auger Spectra

**Auger exposure = 50000 km² sr yr, 102901 events above 3x10¹⁸ eV until end 2014**

Pierre Auger Collaboration, PRL 101, 061101 (2008)
and Phys.Lett.B 685 (2010) 239
ICRC 2015, arXiv:1509.03732

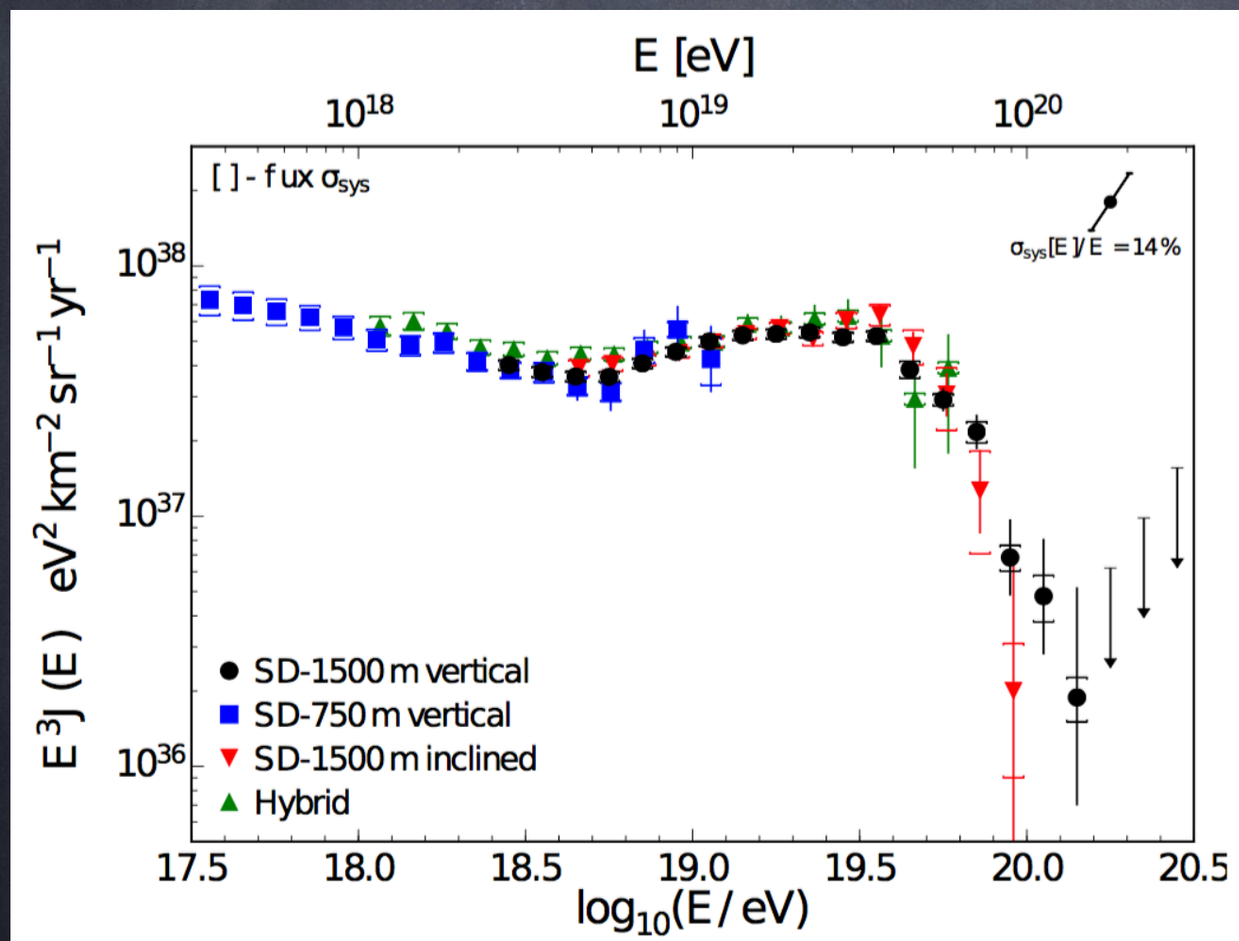


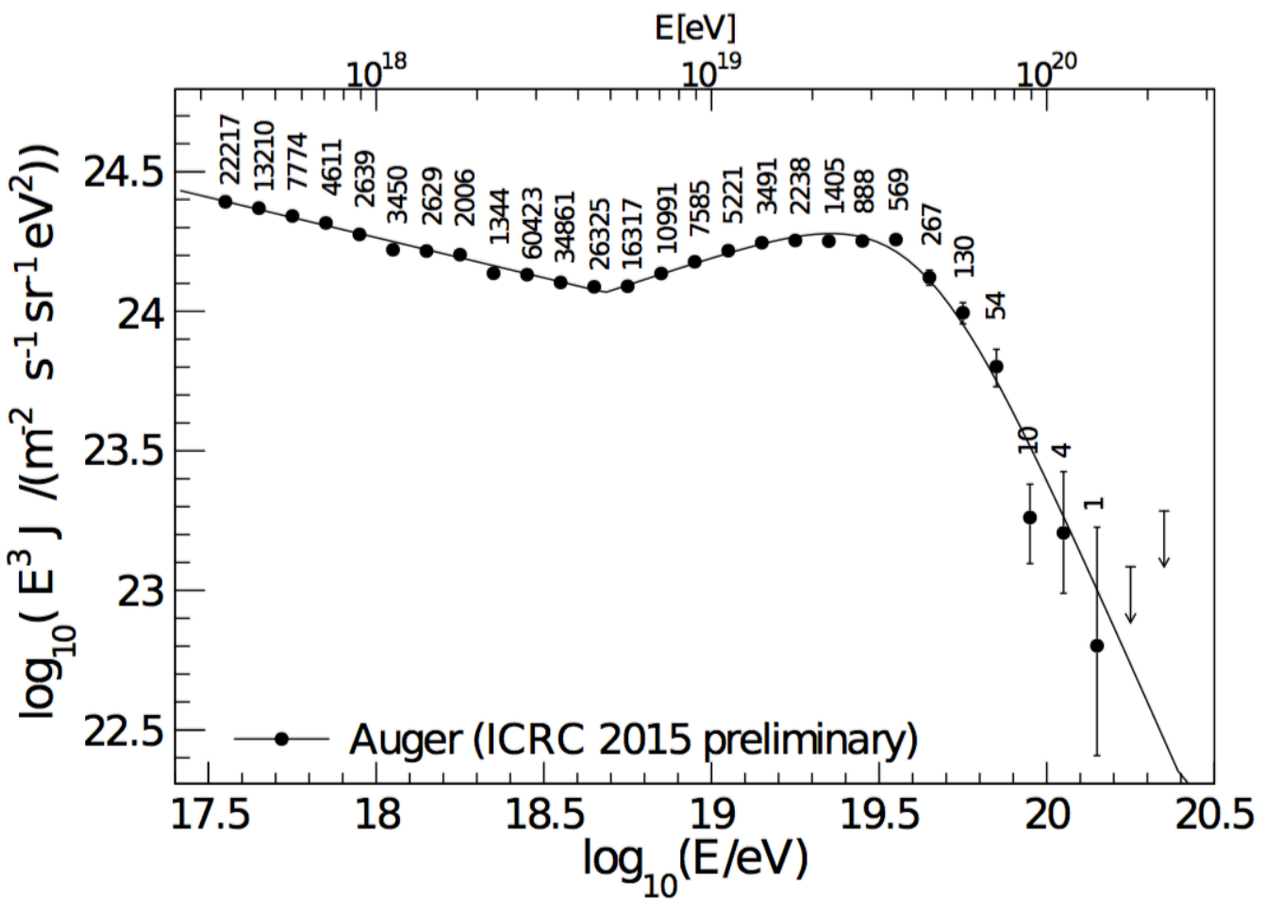

# Atmospheric Showers and their Detection

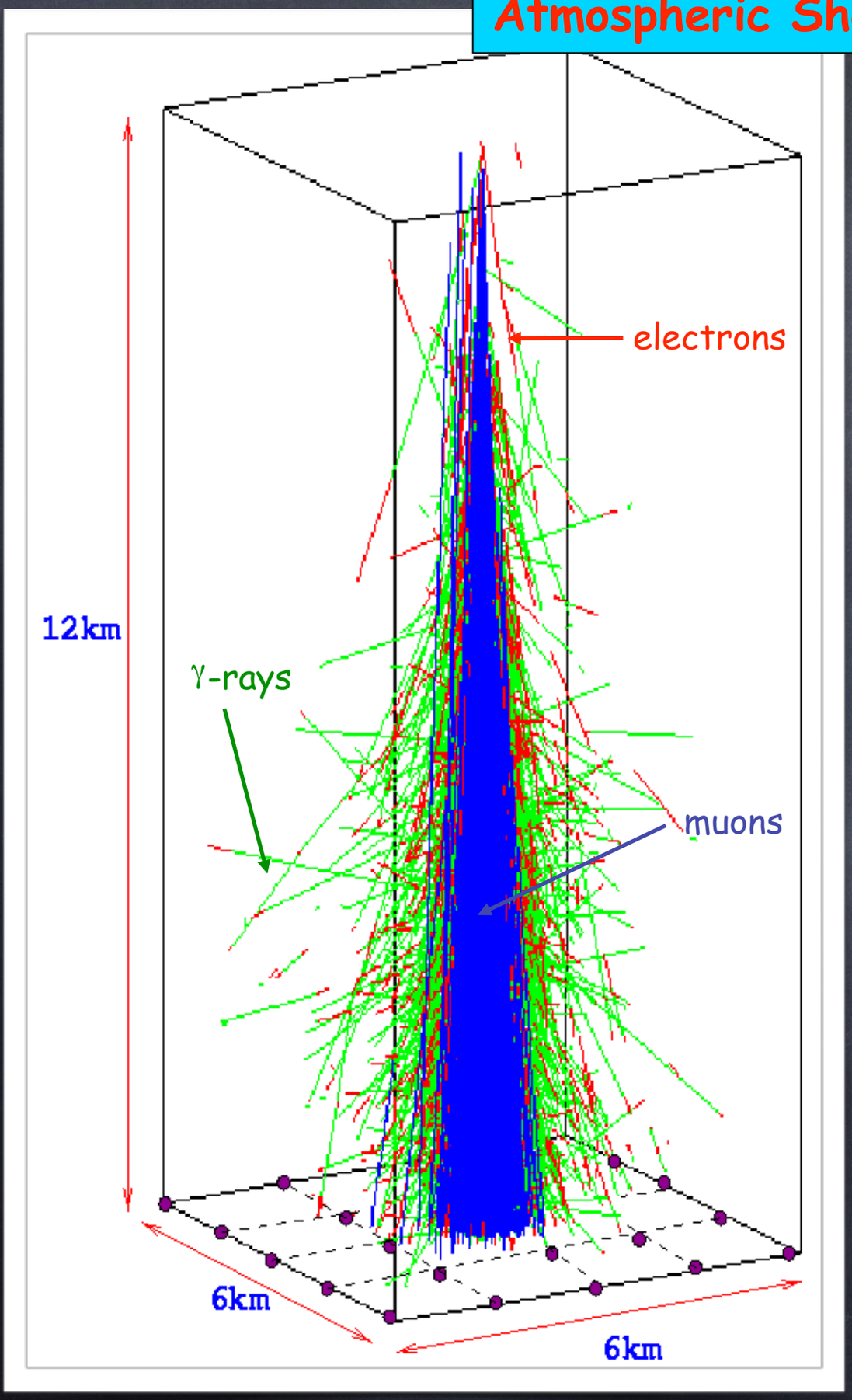

# Atmospheric Showers and their Detection

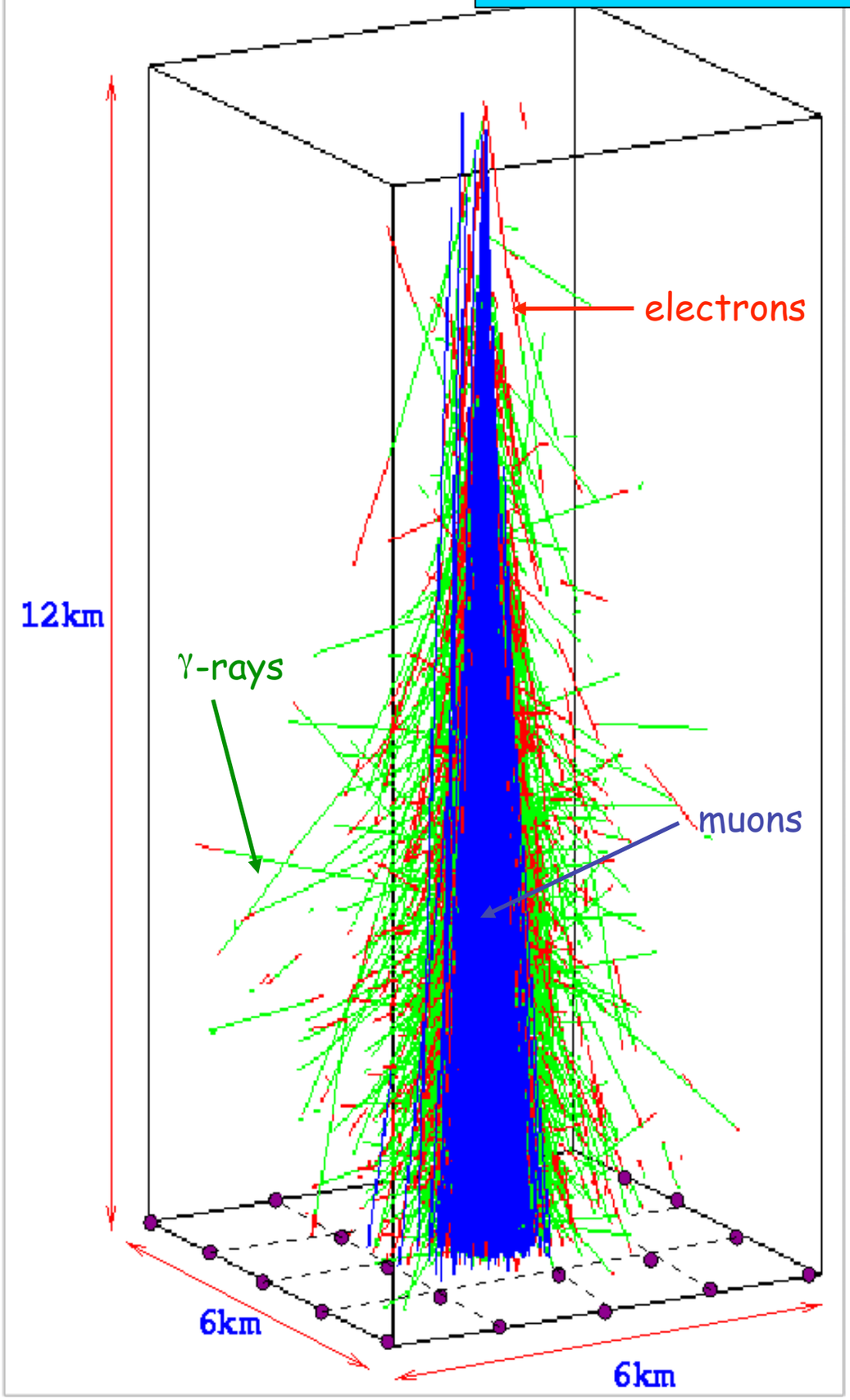


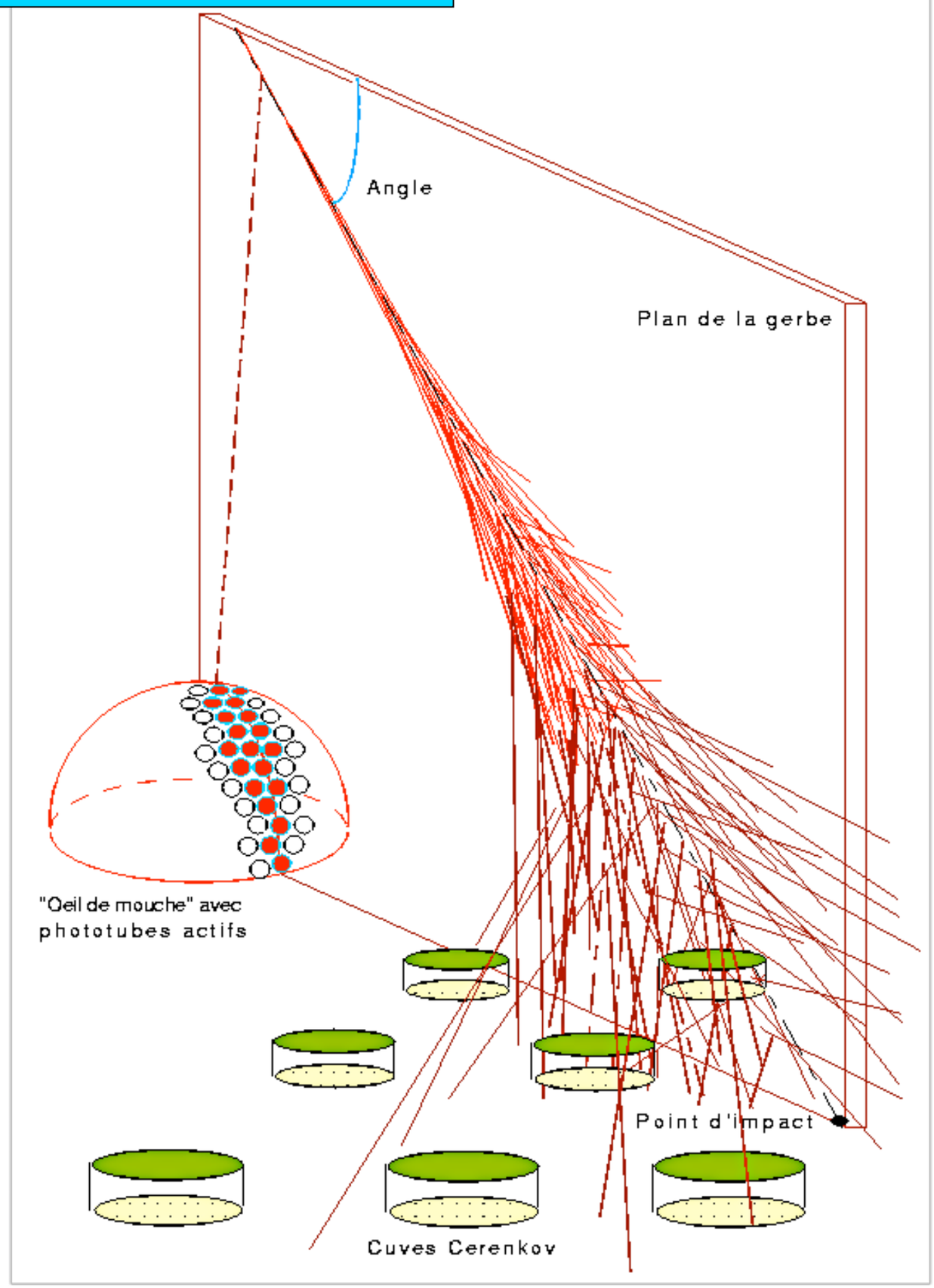

# Atmospheric Showers and their Detection

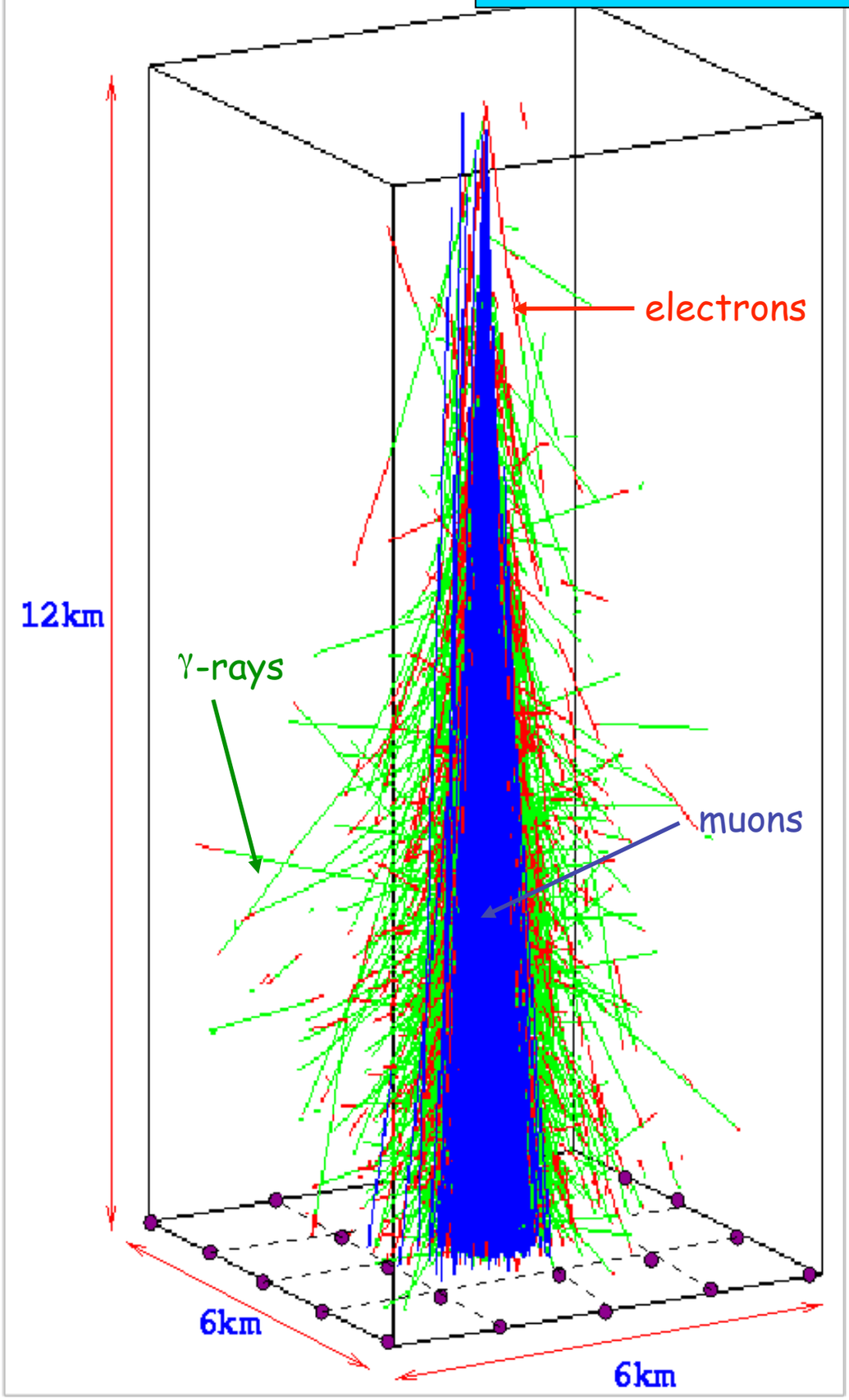


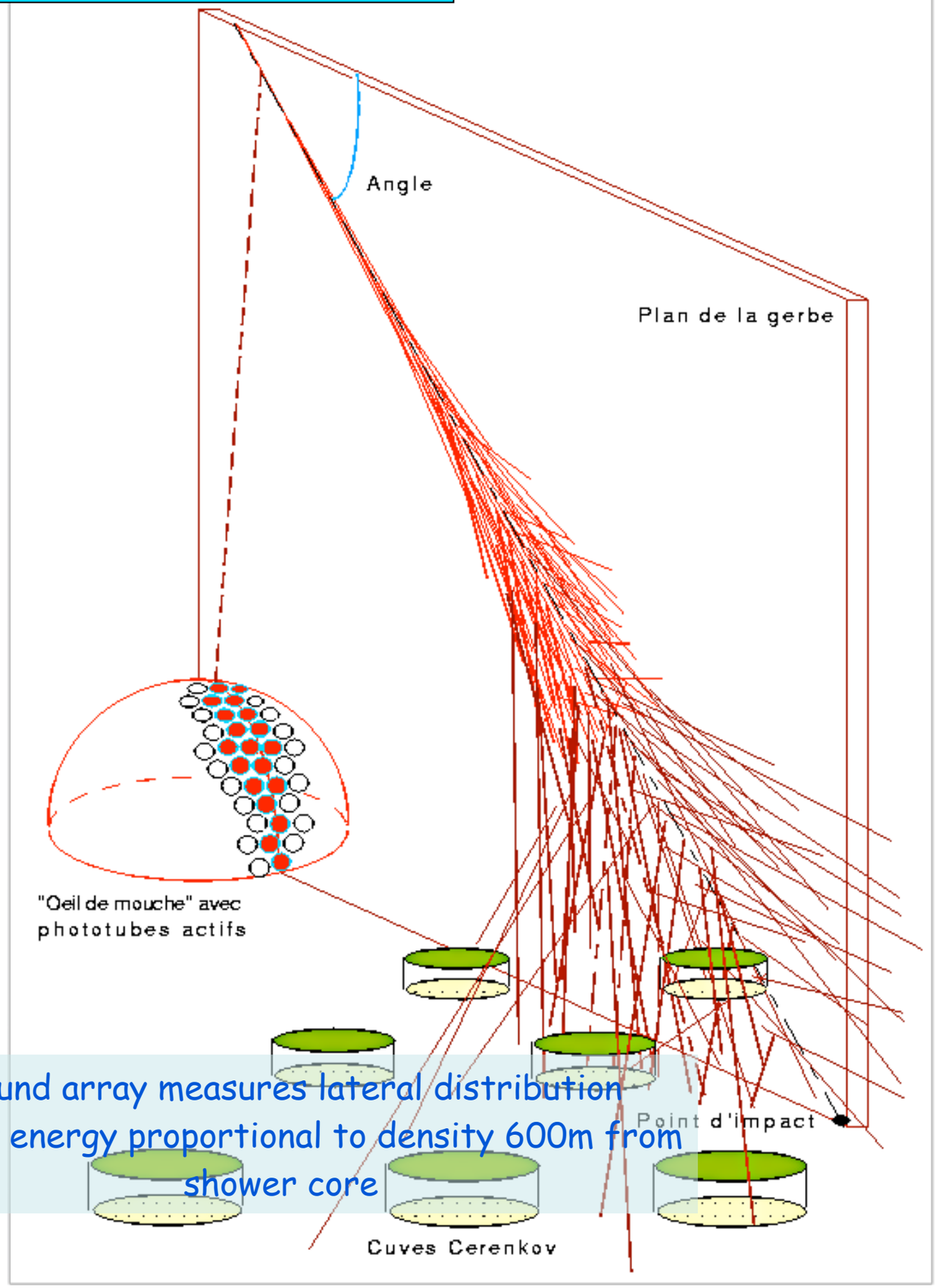


Ground array measures lateral distribution
Primary energy proportional to density 600m from shower core

# Atmospheric Showers and their Detection

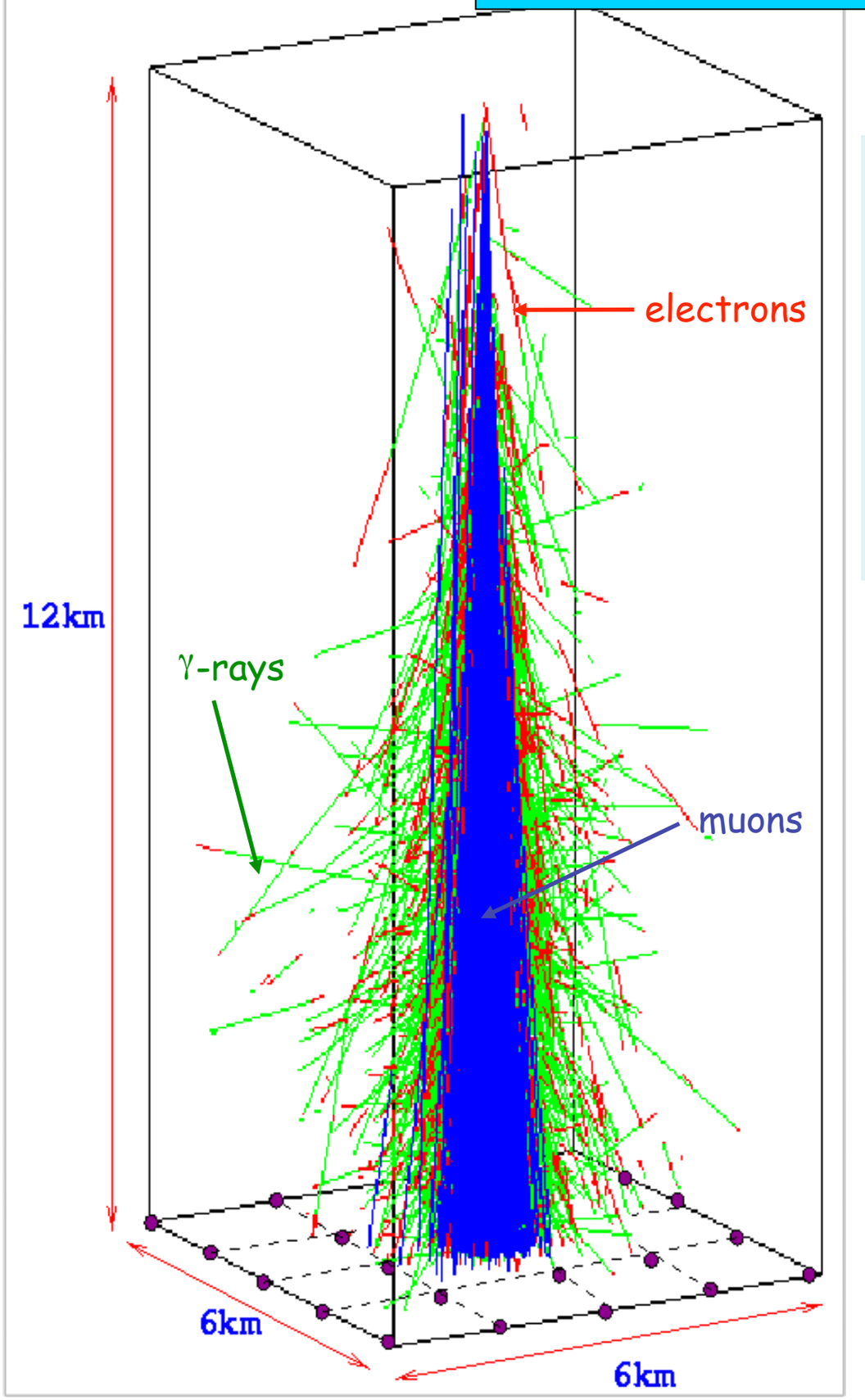


Fly's Eye technique measures fluorescence emission

The shower maximum is given by

$$X_{max} \sim X_0 + X_1 \log E_p$$

where $X_0$ depends on primary type for given energy $E_p$

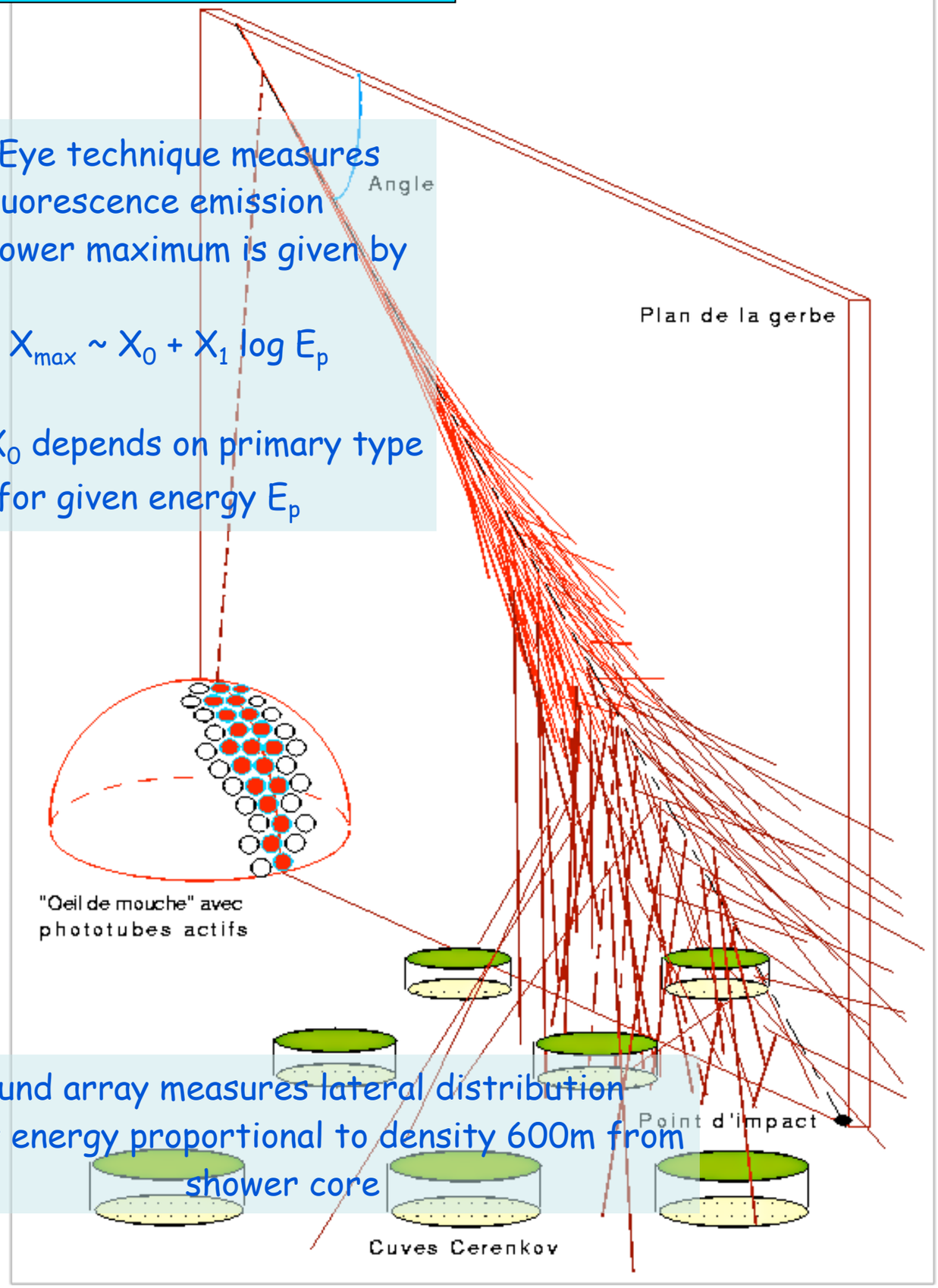


Ground array measures lateral distribution

Primary energy proportional to density 600m from shower core

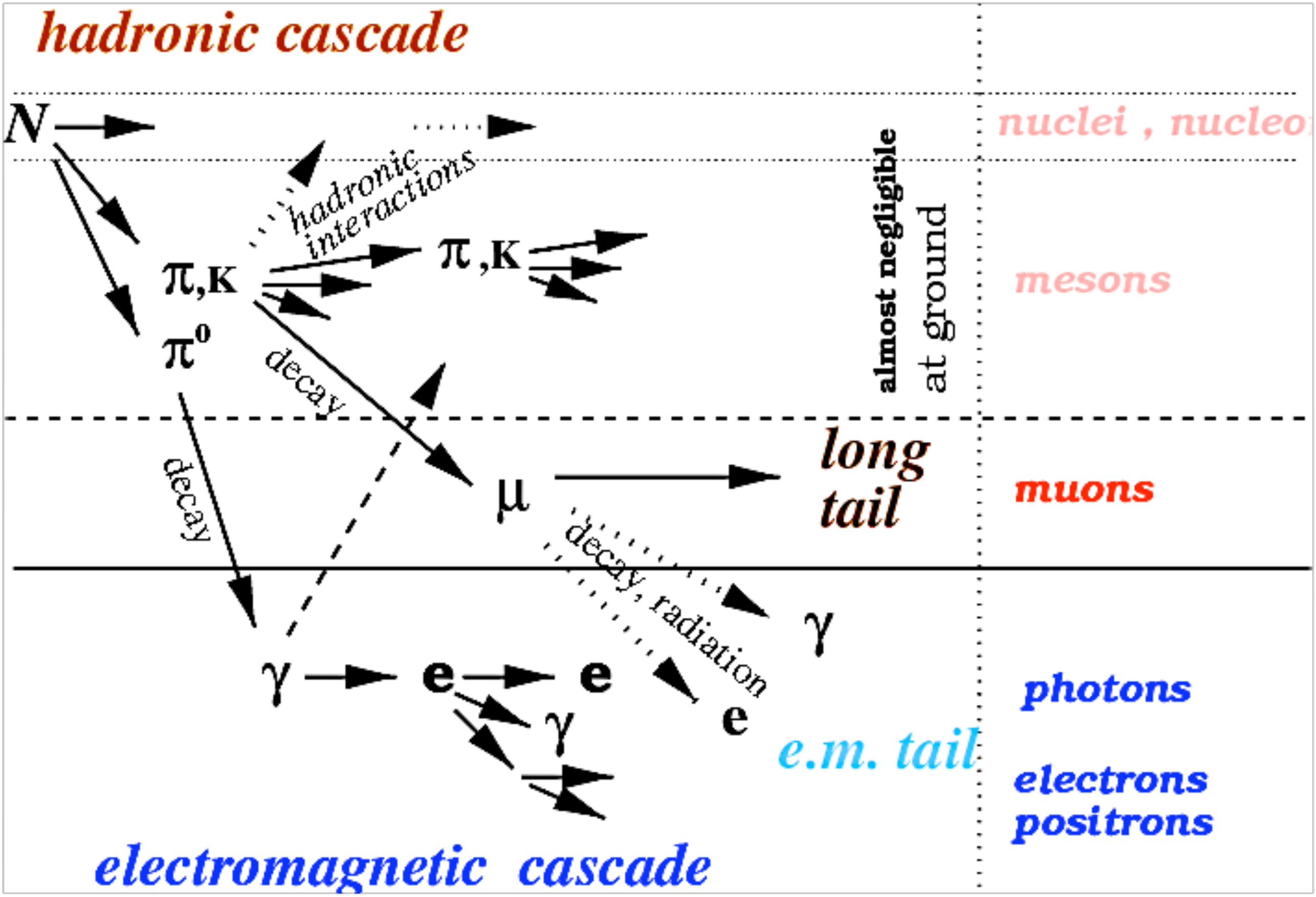
hadronic cascade
N
nuclei , nucleo
hadronic interactions
π,K
π,K
π0
decay
almost negligible
at ground
mesons
decay
μ
long tail
muons
decay, radiation
γ
γ
e
e
e
γ
e.m. tail
photons
electrons
positrons
electromagnetic cascade

# Some Air Shower Physics

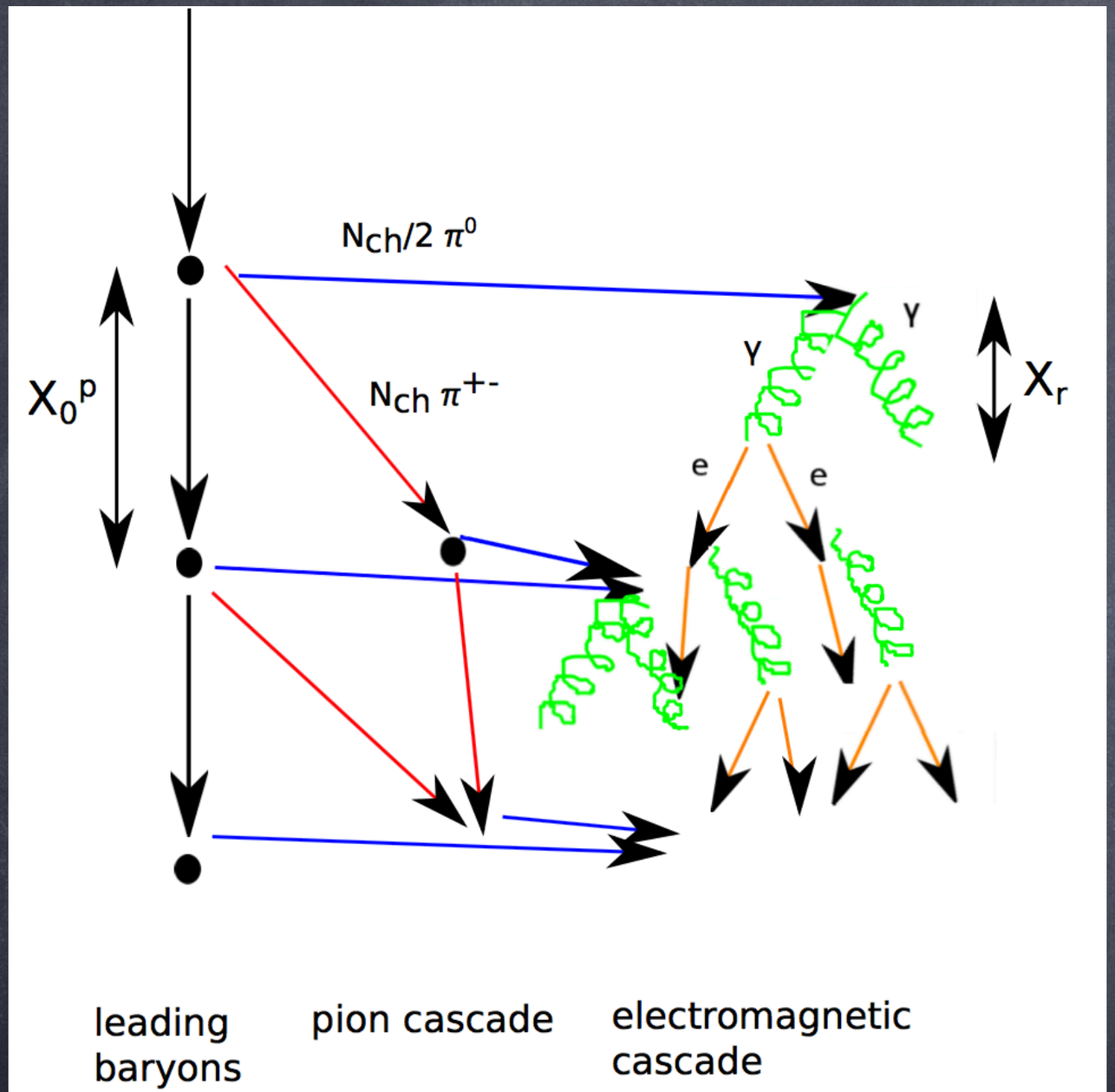


**Fig. 5.2** A sketch of the first two generations of an hadronic cascade in the Heitler Matthews model [232] (left part) and of the first few generations of the electromagnetic cascade in the Heitler model [229] (right part). After each hadronic interaction length $X_0^p(E)$ the *leading baryon* produces $N_{ch}(E)$ charged pions and $N_{ch}(E)/2$ neutral pions. Neutral pions decay into two $\gamma-$rays instantaneously whereas charged pions interact again after column depth $\simeq X_0^p(E)$, producing further pions. High energy $\gamma-$rays produce electron-positron pairs after one radiation length $X_r$ which in turn recreate $\gamma-$rays by bremsstrahlung after a similar length scale.

In this simple picture for a primary energy $E_p$ the depth of shower maximum is the depth of first interaction $X_0$
plus the radiation length $X_r$ times the number of generations n,

$$X_{max} \sim X_0 + X_r \log (E_p/E_c)$$

where $E_c$ is some critical energy

# Cosmic ray versus neutrino induced air showers

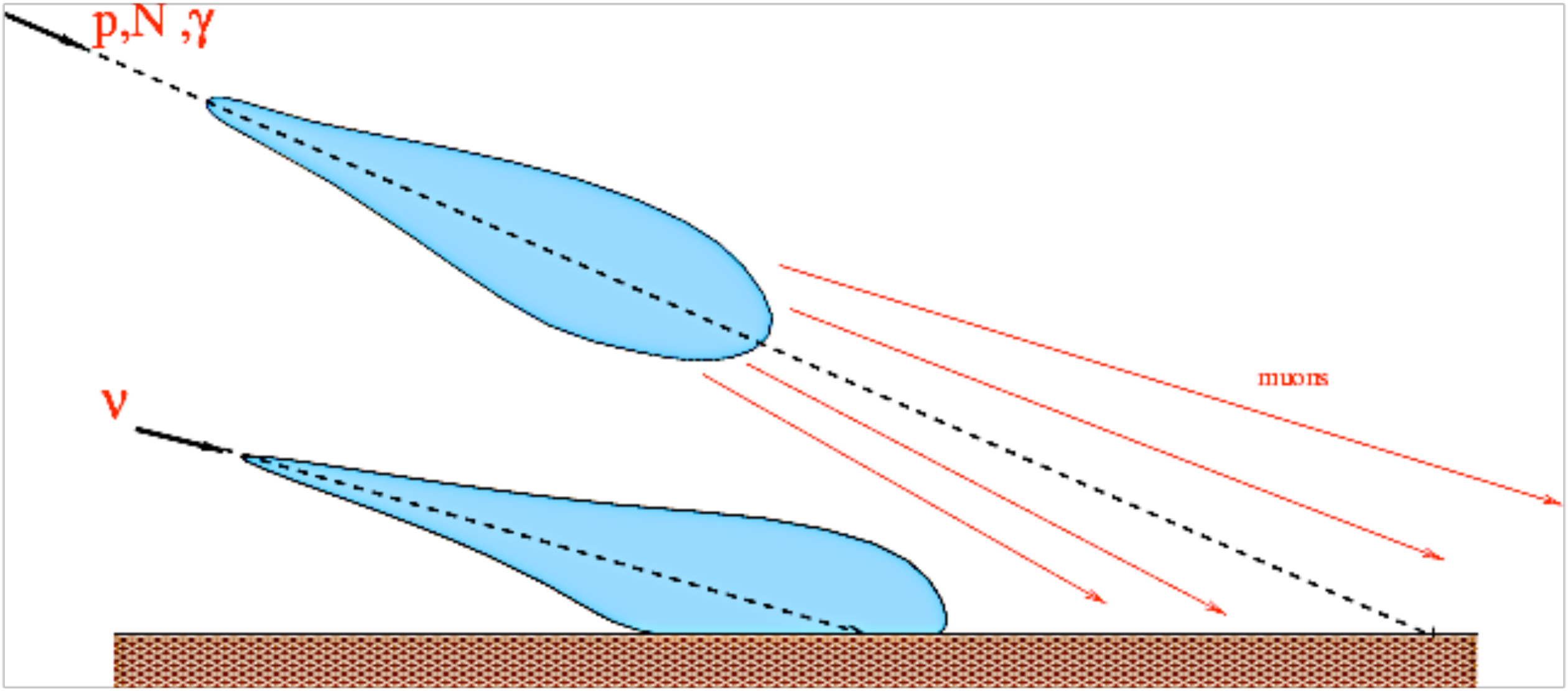

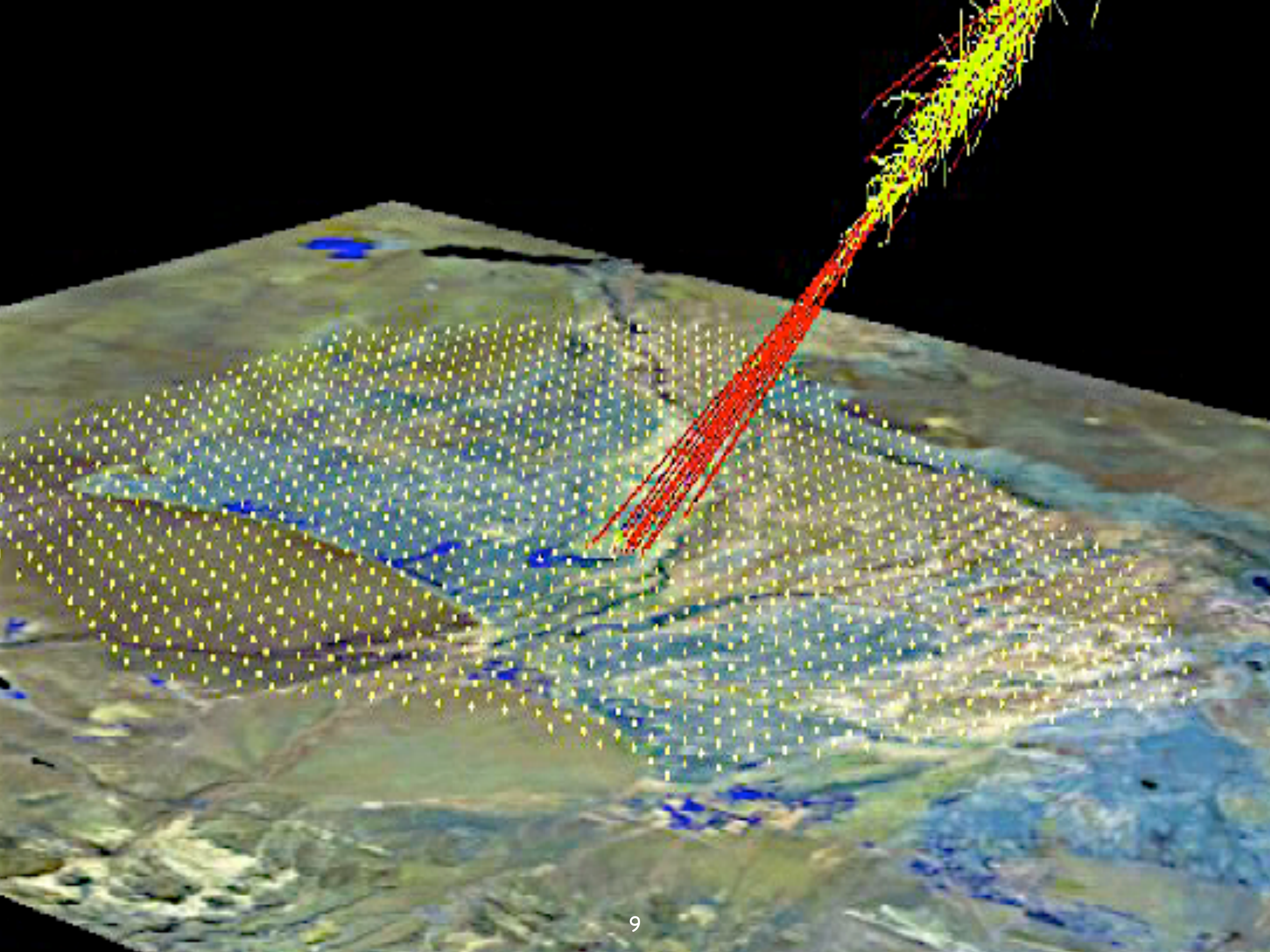

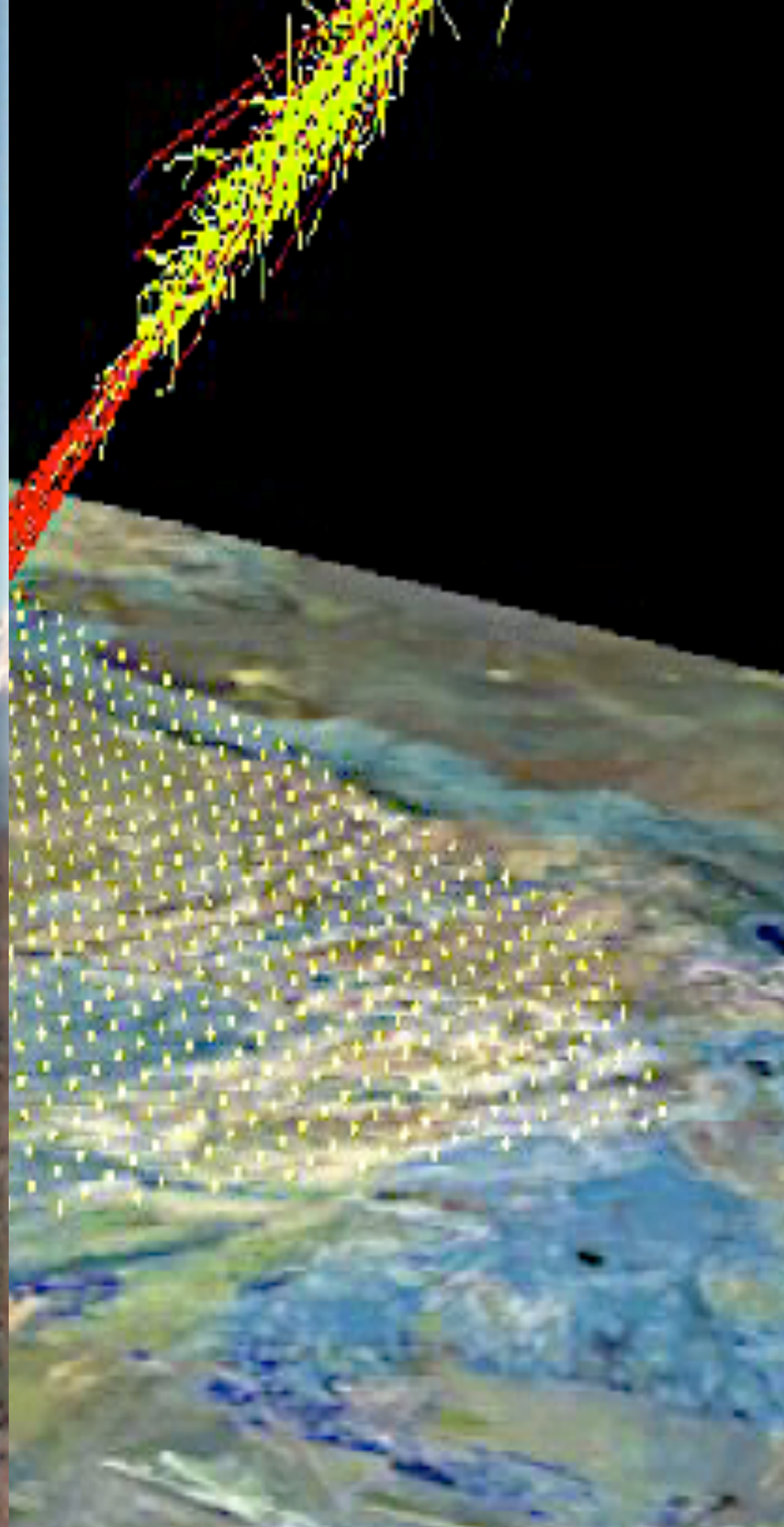

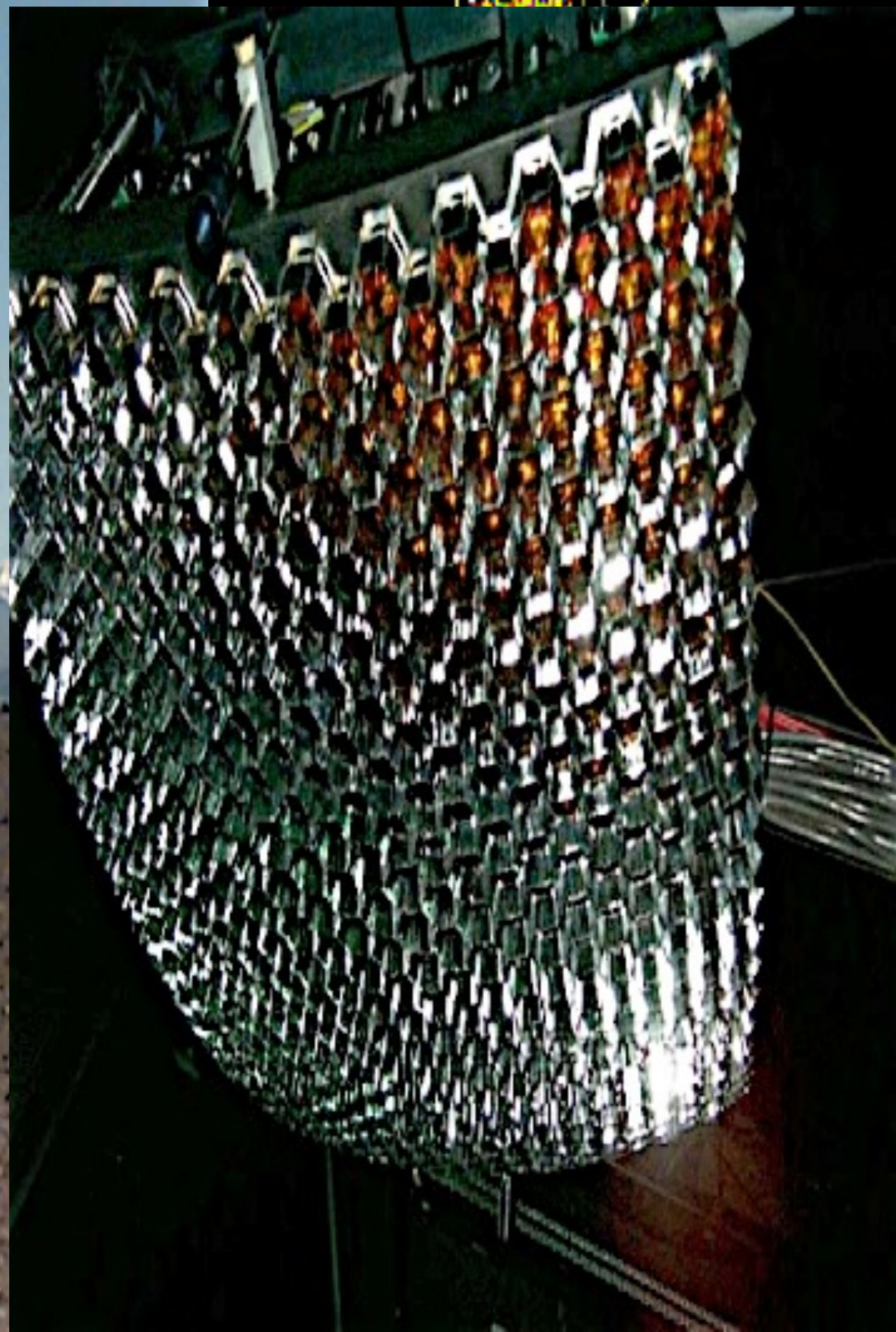

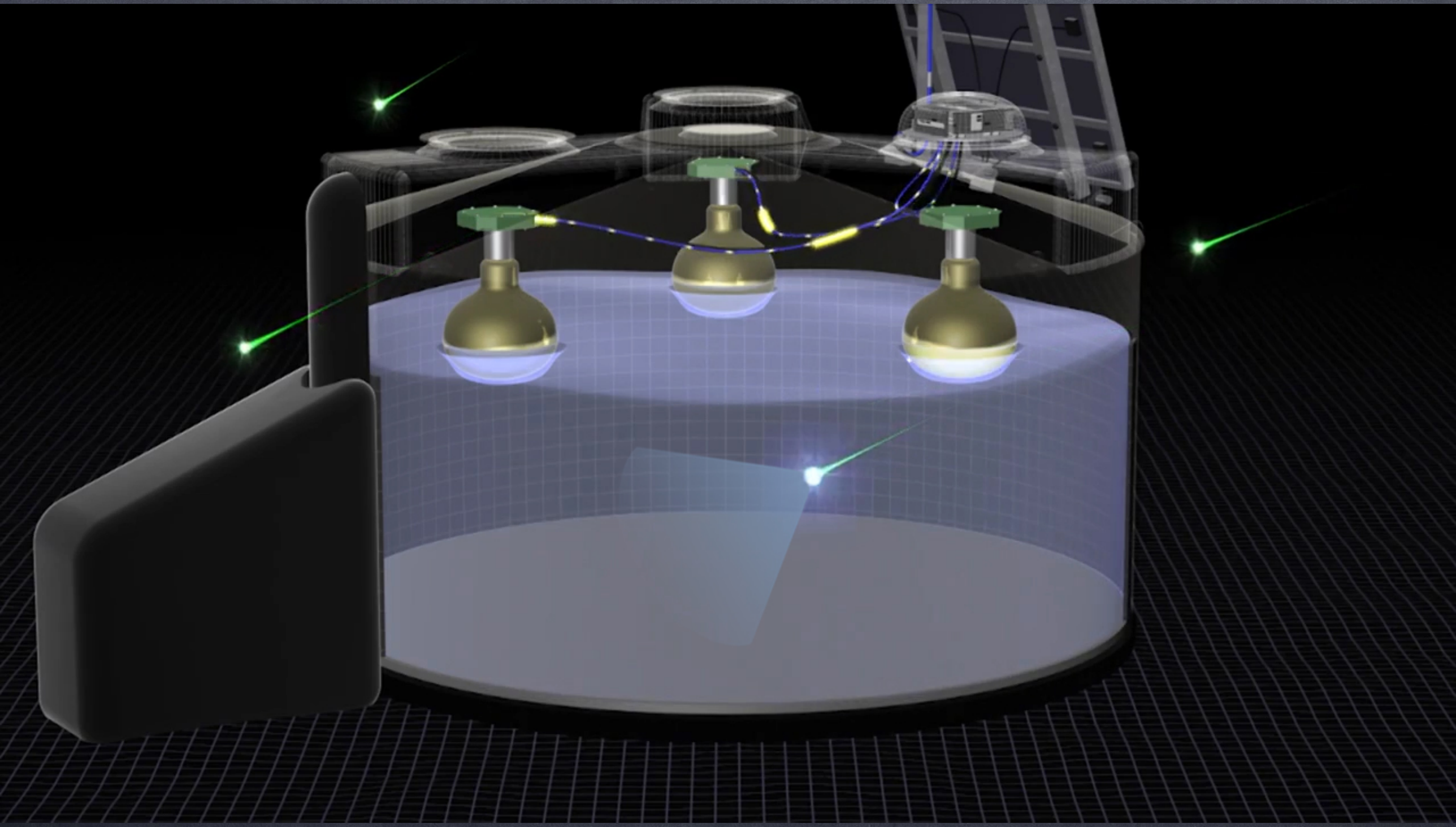

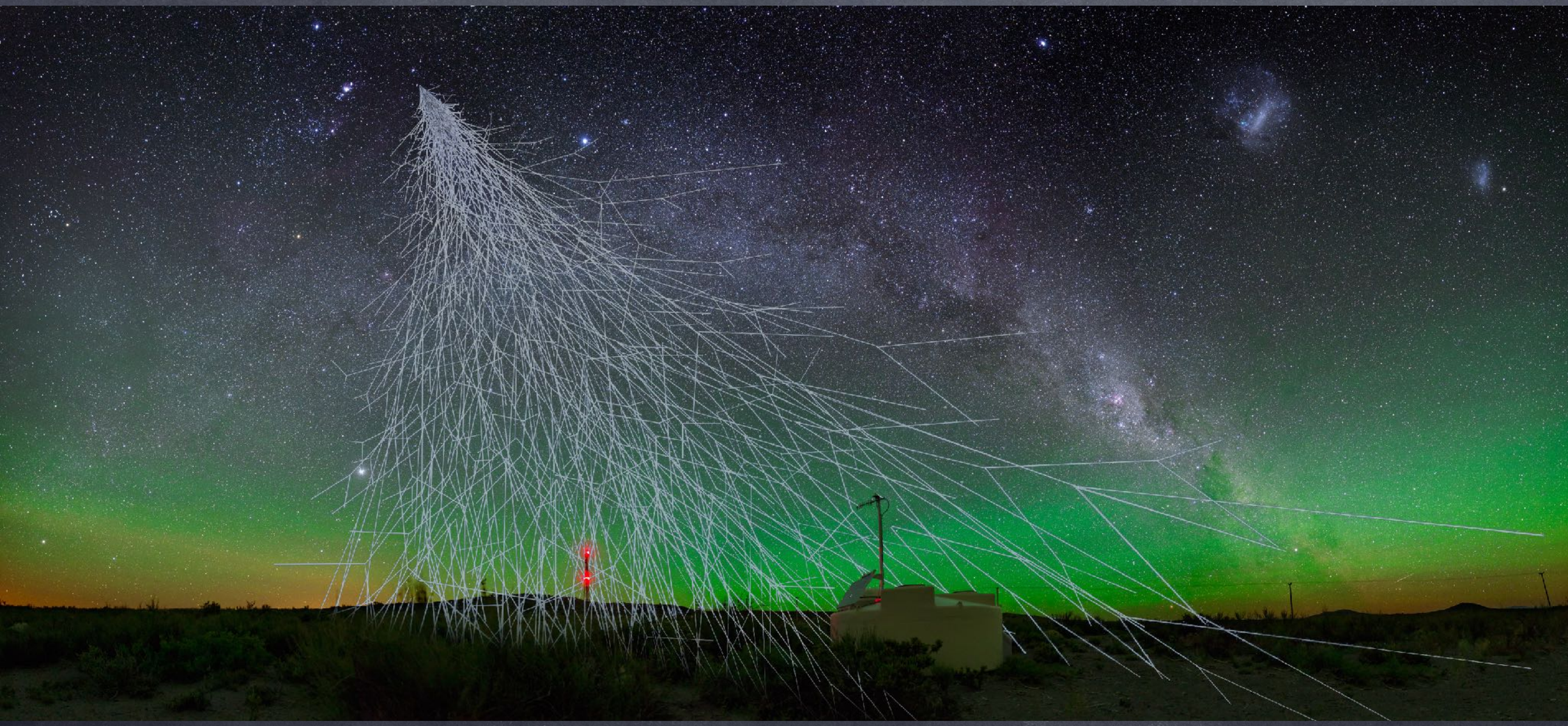

# Southern Auger Site

Pampa Amarilla, Province of Mendoza

3000 km², 875 g/cm², 1400 m

Lat.: 35.5° south

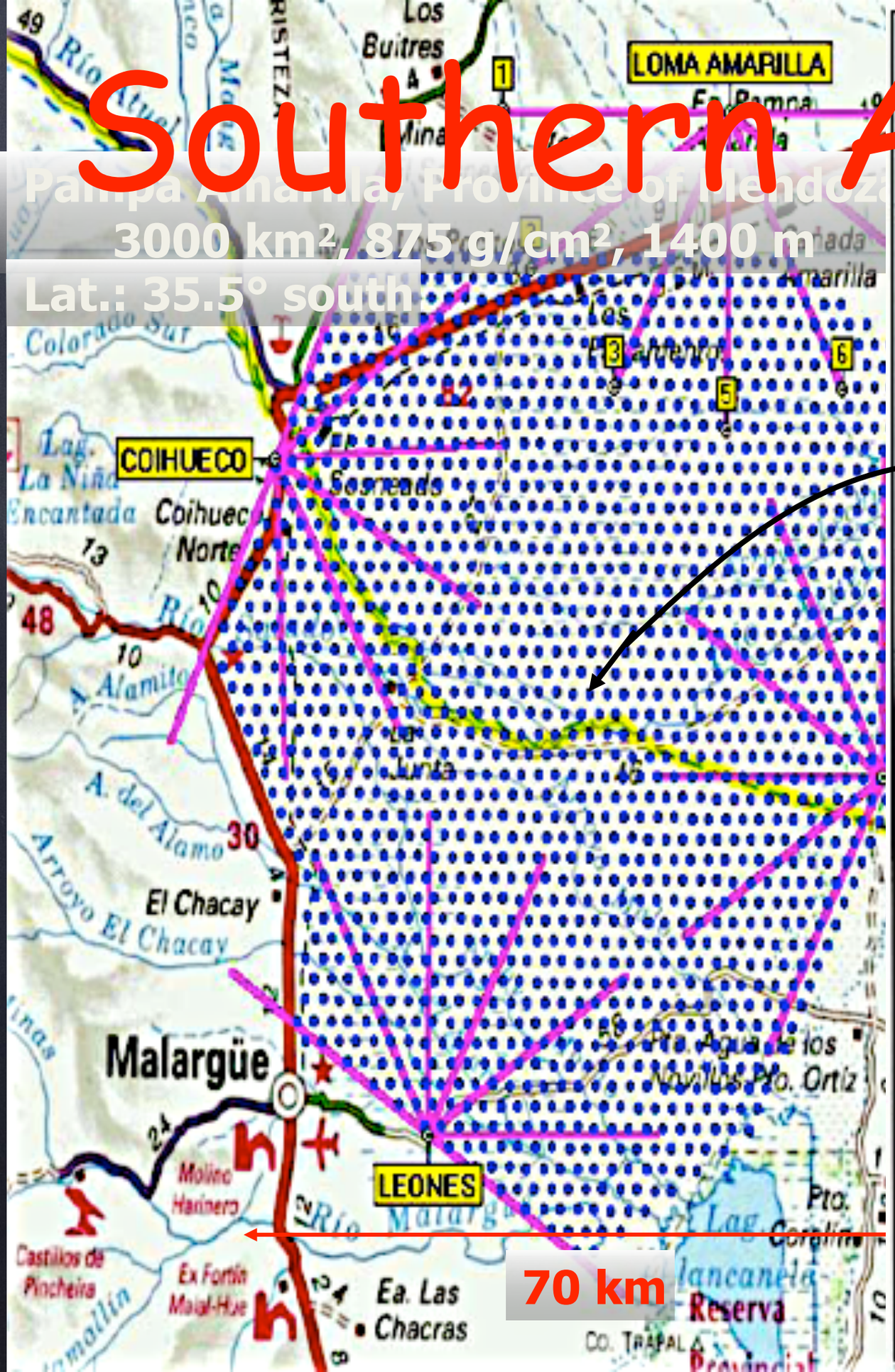


# Southern Auger Site

Pampa Amarilla, Province of Mendoza

3000 km², 875 g/cm², 1400 m

Lat.: 35.5° south

**Surface Array (SD):**

1600 Water Tanks

1.5 km spacing

3000 km²

70 km

# Southern Auger Site

Pampa Amarilla, Province of Mendoza

3000 km², 875 g/cm², 1400 m

Lat.: 35.5° south

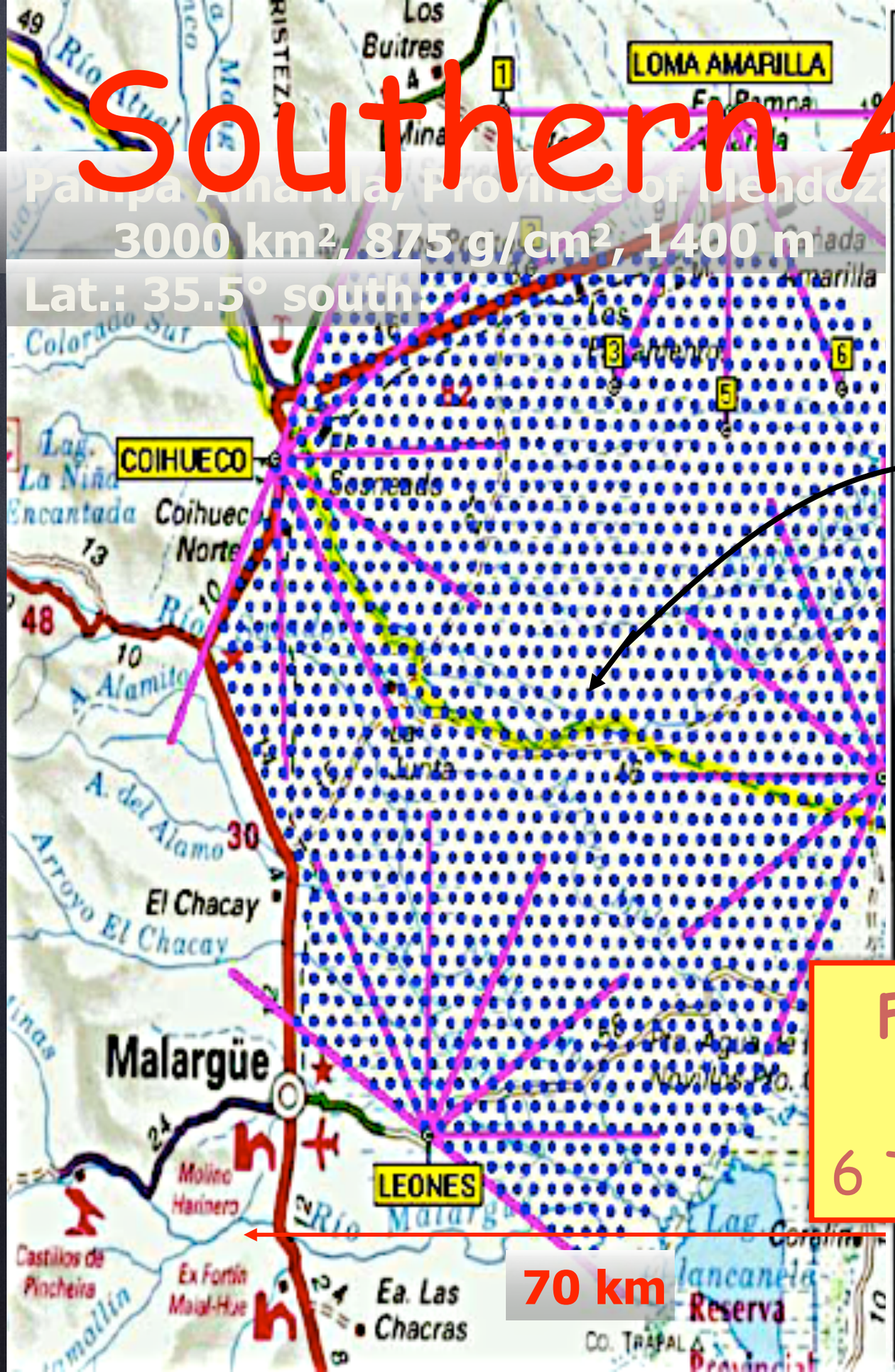


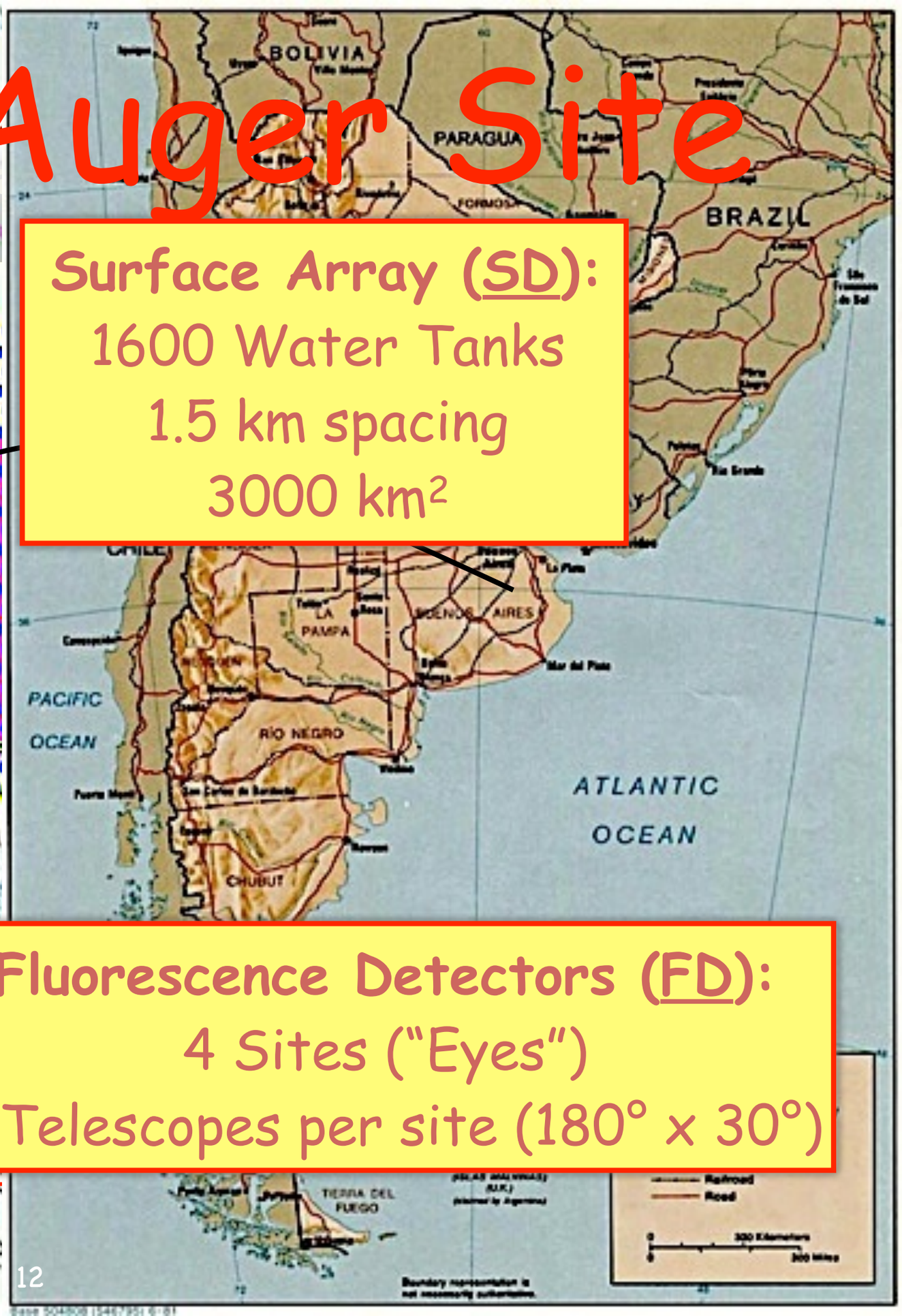


**Surface Array (SD):**
1600 Water Tanks
1.5 km spacing
3000 km²

**Fluorescence Detectors (FD):**
4 Sites ("Eyes")
6 Telescopes per site (180° x 30°)

# The Greisen-Zatsepin-Kuzmin (GZK) effect

Nucleons can produce pions on the cosmic microwave background


$$E_{\rm th} = \frac{2 m_N m_\pi + m_\pi^2}{4\varepsilon} \simeq 4 \times 10^{19}\,{\rm eV}$$

# The Greisen-Zatsepin-Kuzmin (GZK) effect

Nucleons can produce pions on the cosmic microwave background


$$E_{\rm th} = \frac{2 m_N m_\pi + m_\pi^2}{4\varepsilon} \simeq 4 \times 10^{19}\,{\rm eV}$$

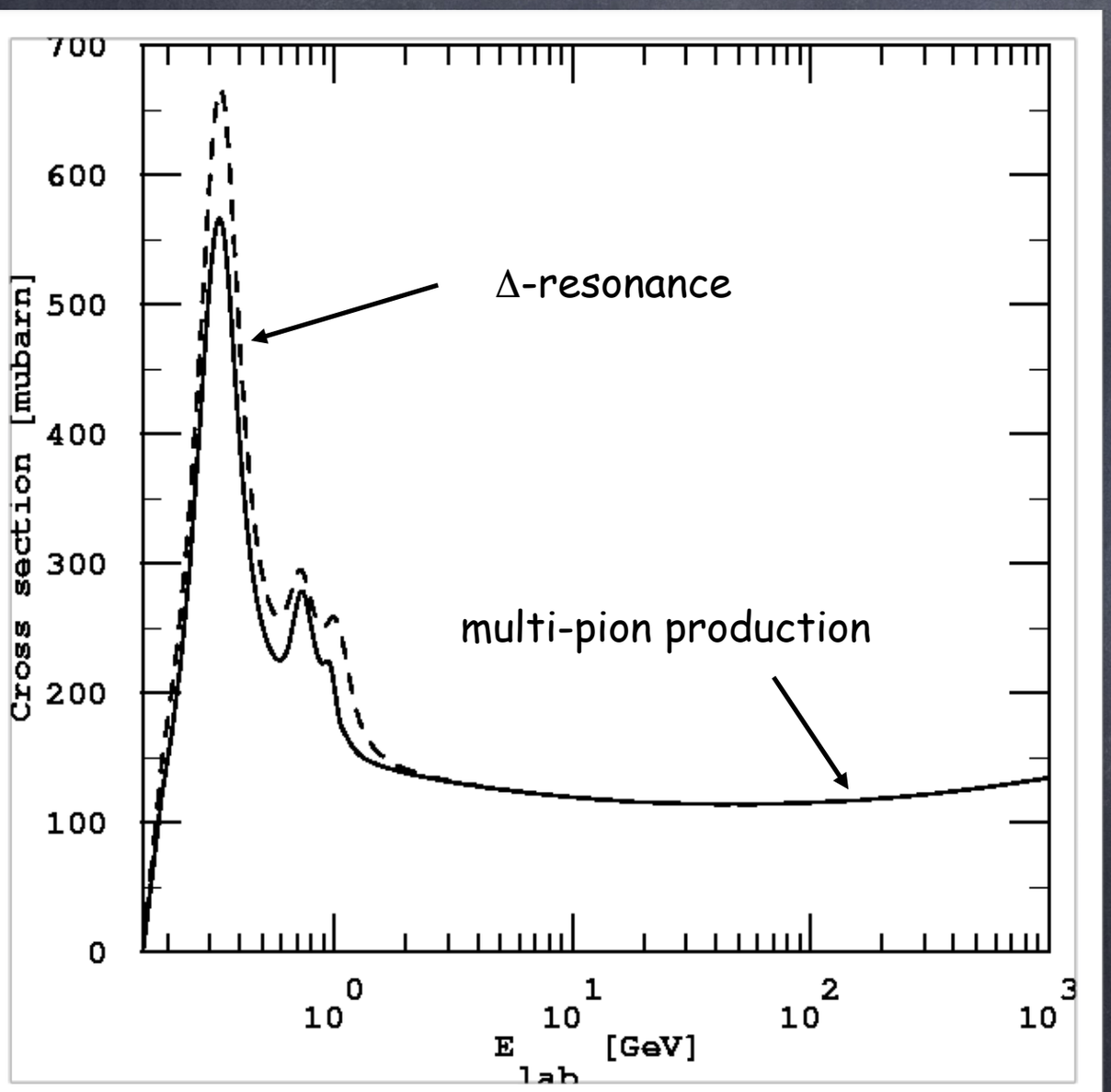

# The Greisen-Zatsepin-Kuzmin (GZK) effect

Nucleons can produce pions on the cosmic microwave background


$$E_{\rm th} = \frac{2m_N m_\pi + m_\pi^2}{4\varepsilon} \simeq 4 \times 10^{19}\,{\rm eV}$$

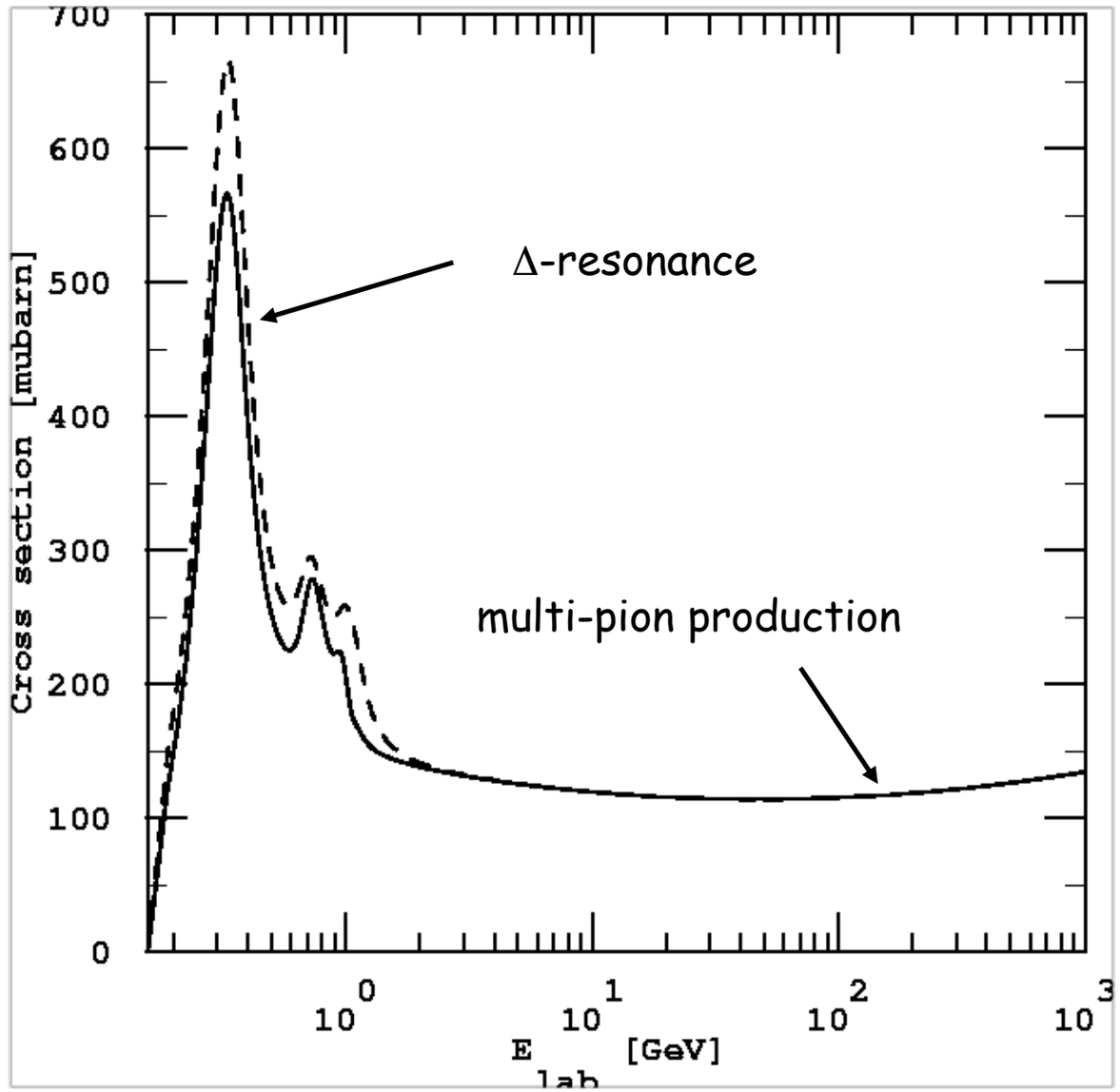


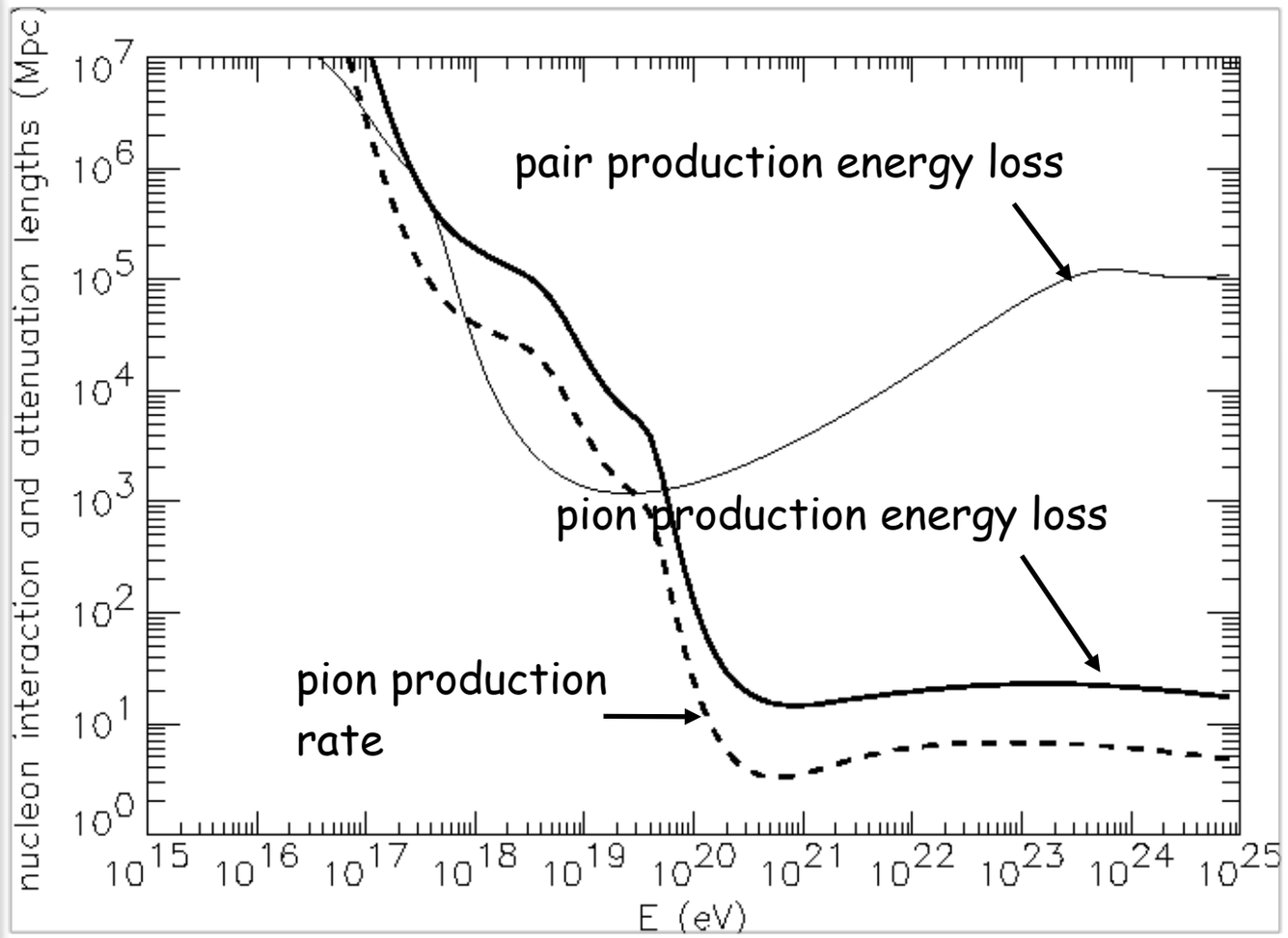

# The Greisen-Zatsepin-Kuzmin (GZK) effect

Nucleons can produce pions on the cosmic microwave background


$$E_{\rm th} = \frac{2m_N m_\pi + m_\pi^2}{4\varepsilon} \simeq 4 \times 10^{19}\,{\rm eV}$$

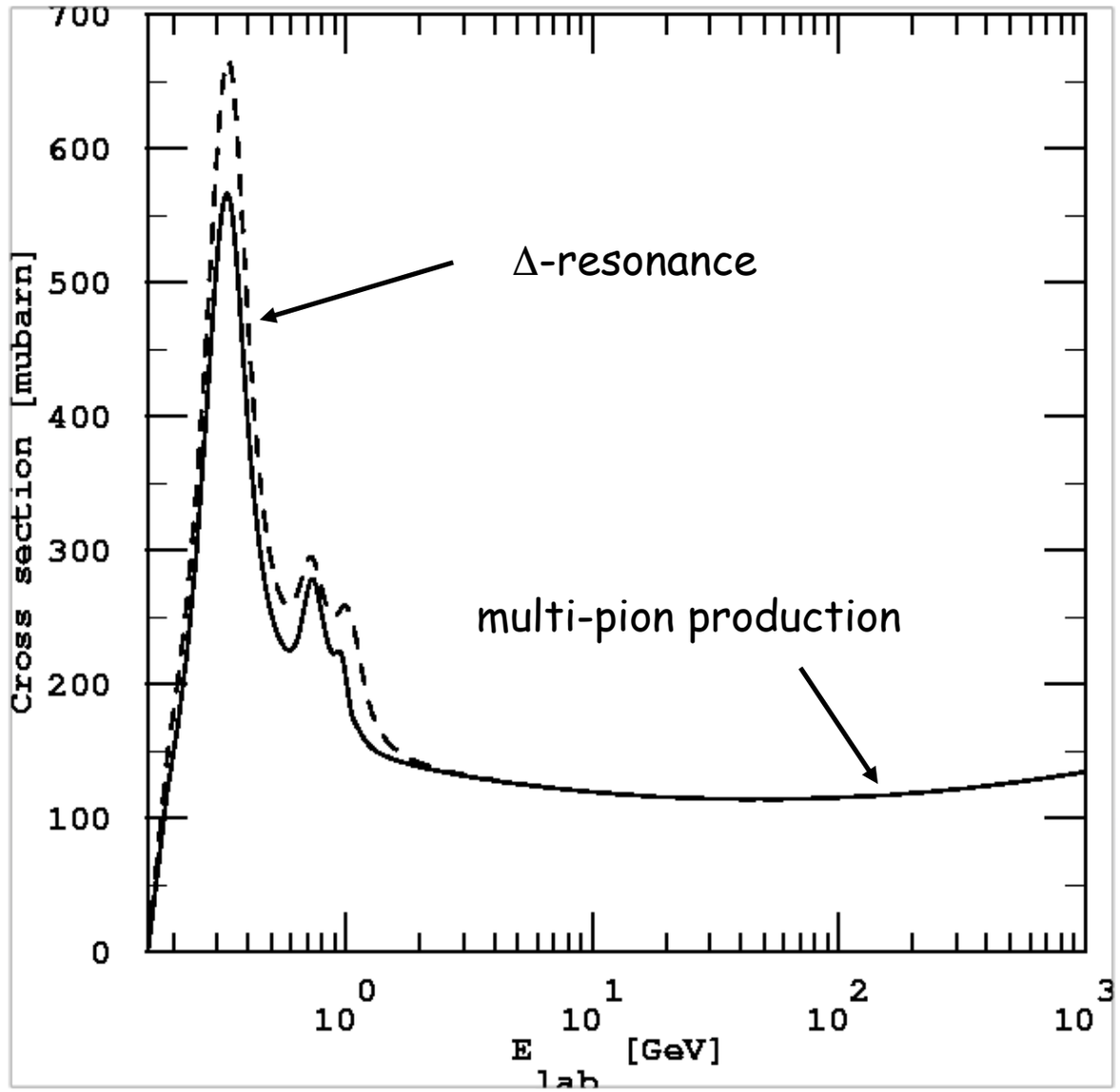


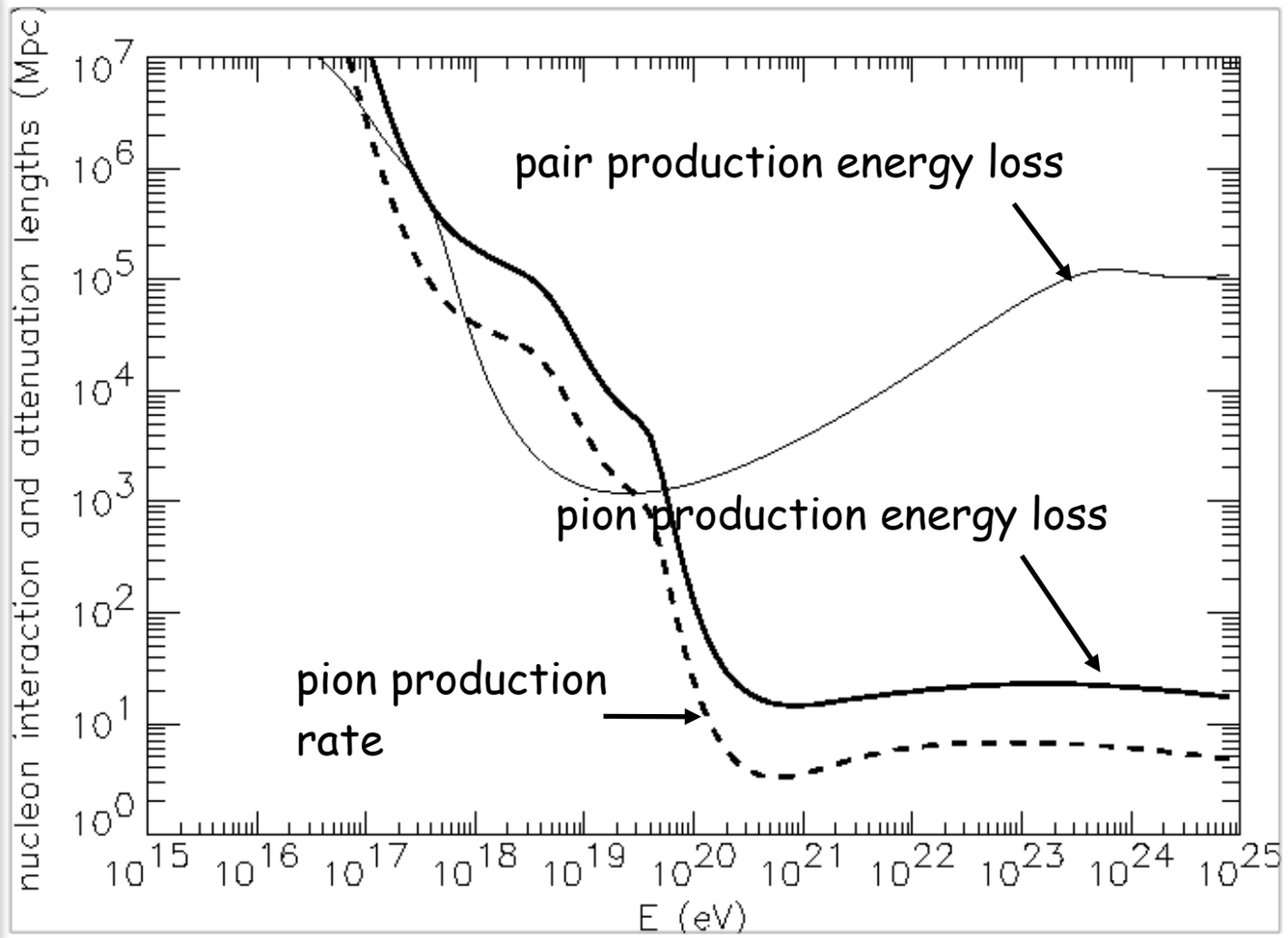


sources must be in cosmological backyard
Only Lorentz symmetry breaking at $\Gamma > 10^{11}$ could avoid this conclusion.

# Length scales for relevant processes of a typical heavy nucleus

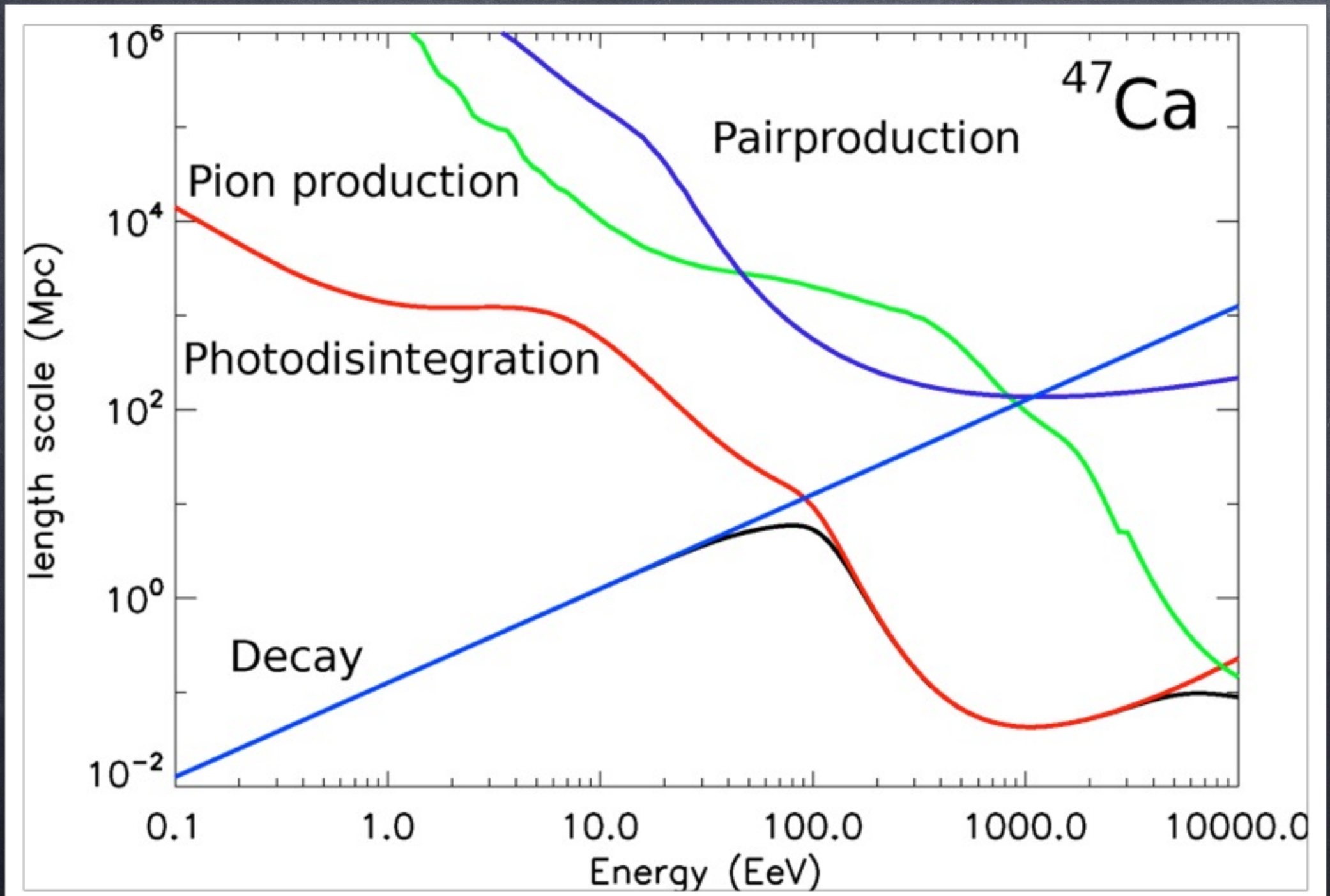

# 1st Order Fermi Shock Acceleration

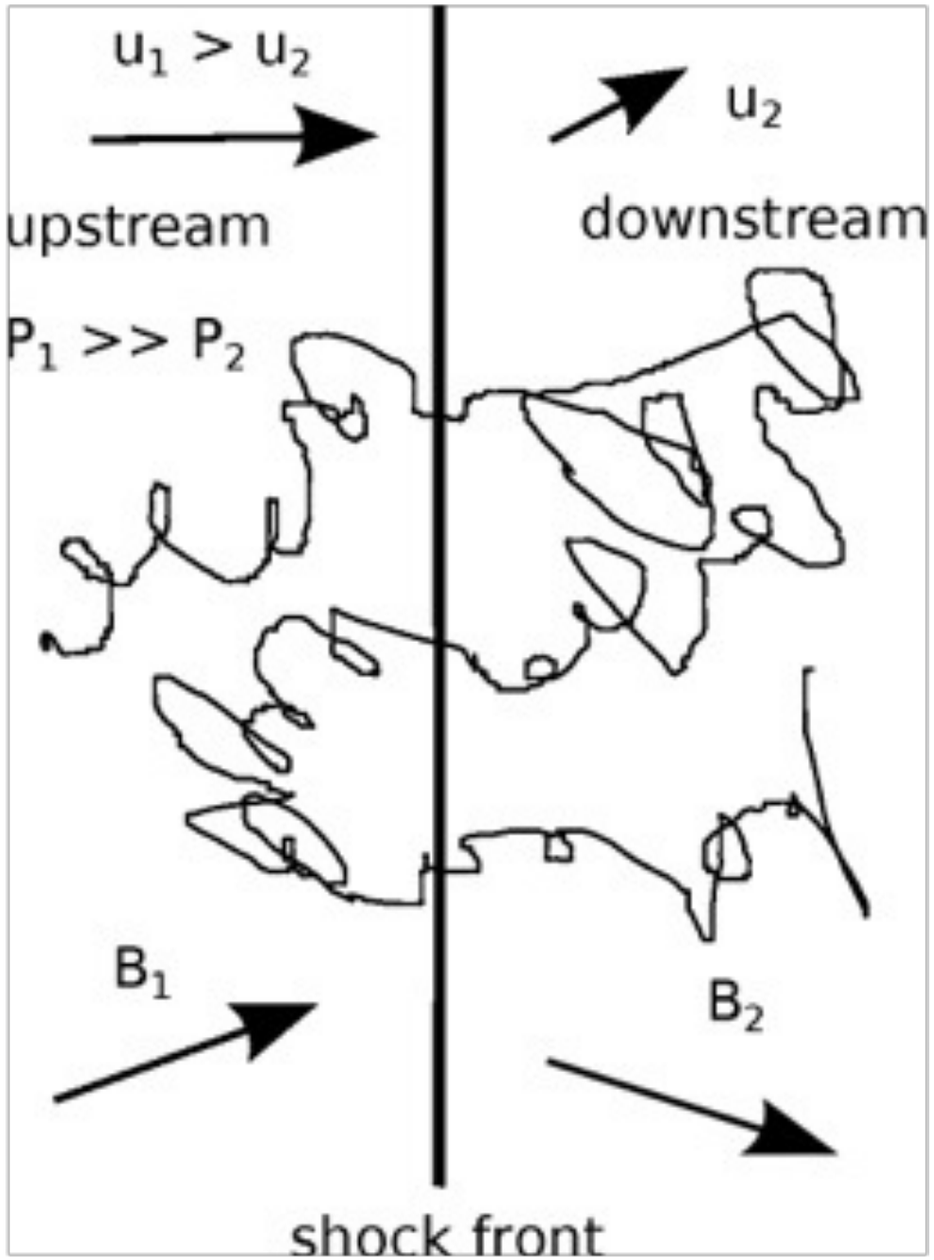


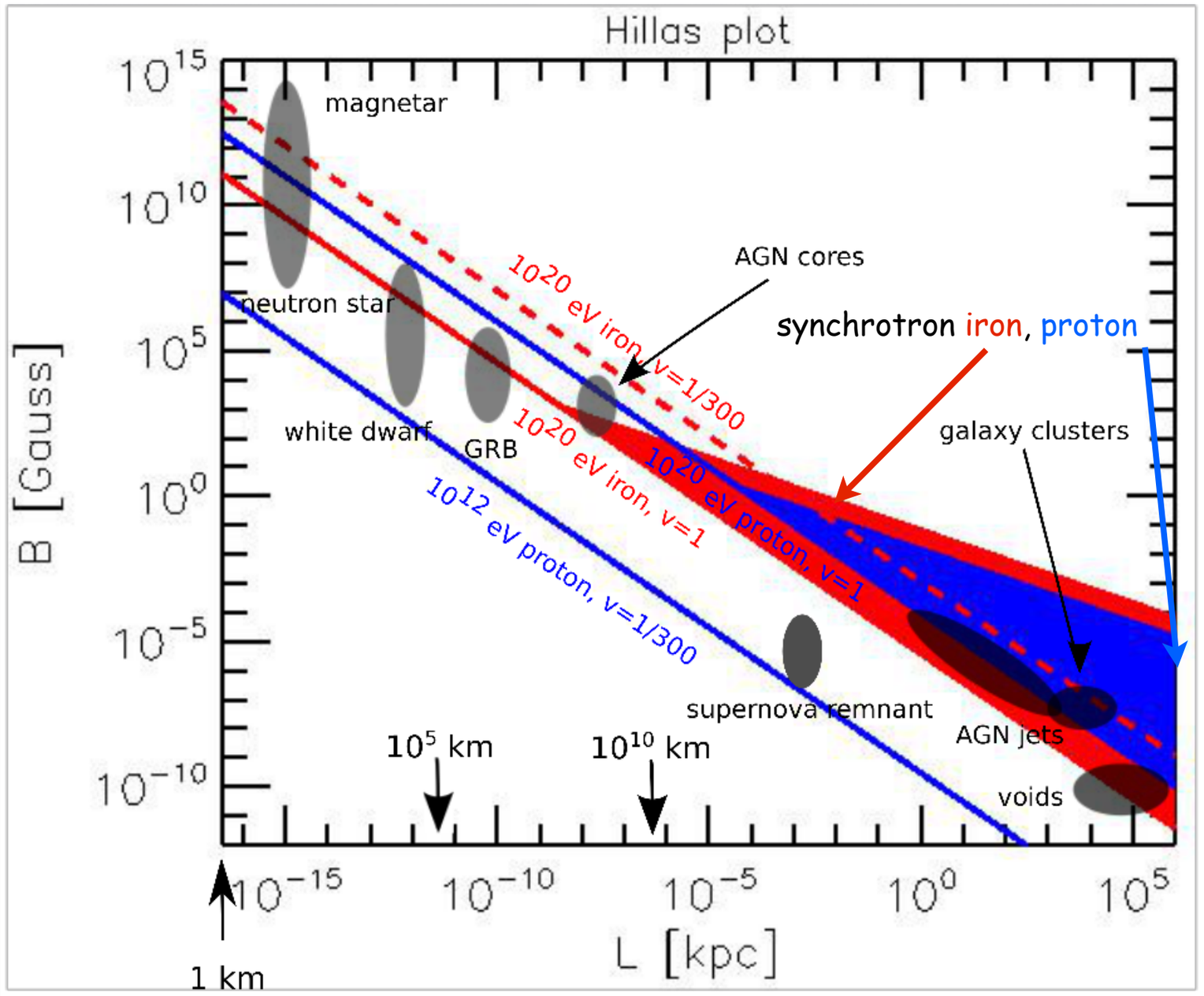


Fractional energy gain per shock crossing $\sim u_1 - u_2$ on a time scale $r_L/u_2$ .

Together with downstream losses this leads to a spectrum $E^{-q}$ with $q > 2$ typically.

Confinement, gyroradius < shock size, and energy loss times define maximal energy

# Some general Requirements for Sources

Accelerating particles of charge eZ to energy $E_{max}$ requires induction $\varepsilon > E_{max}/eZ$. With $Z_0 \sim 100\Omega$ the vacuum impedance, this requires dissipation of minimum power of

$$L_{\rm min} \sim \frac{\epsilon^2}{Z_0} \simeq 10^{45}\, Z^{-2} \left(\frac{E_{\rm max}}{10^{20}\,{\rm eV}}\right)^2 \,{\rm erg\,s^{-1}}$$

This „Poynting" luminosity can also be obtained from $L_{min} \sim (BR)^2$ where BR is given by the „Hillas criterium":

$$BR > 3 \times 10^{17}\,\Gamma^{-1} \left(\frac{E_{\rm max}/Z}{10^{20}\,{\rm eV}}\right) \,{\rm Gauss\,cm}$$

where Γ is a possible beaming factor.
If most of this goes into electromagnetic channel, only AGNs and maybe gamma-ray bursts could be consistent with this.

# A possible acceleration site associated with shocks in hot spots of active galaxies

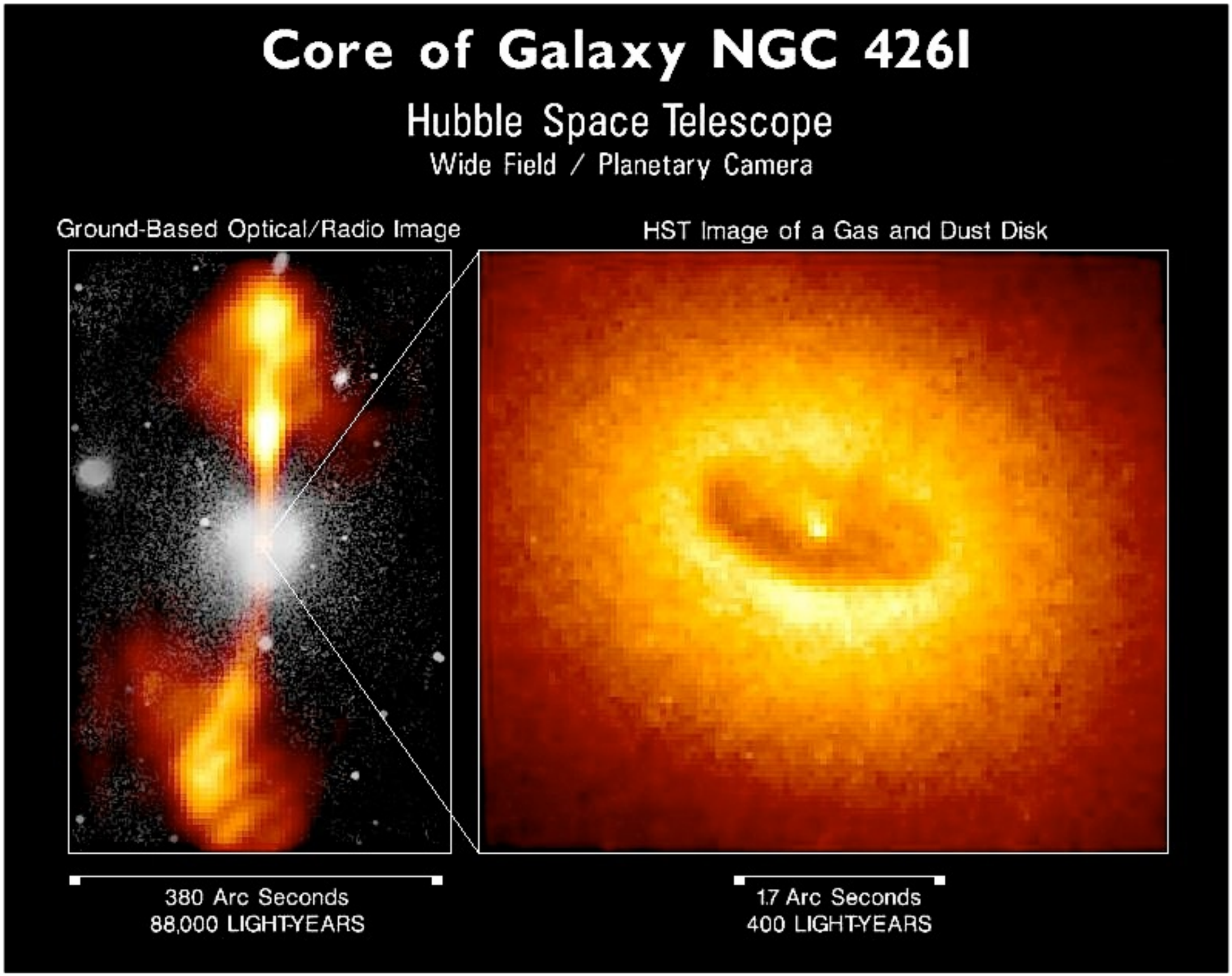

Or Cygnus A

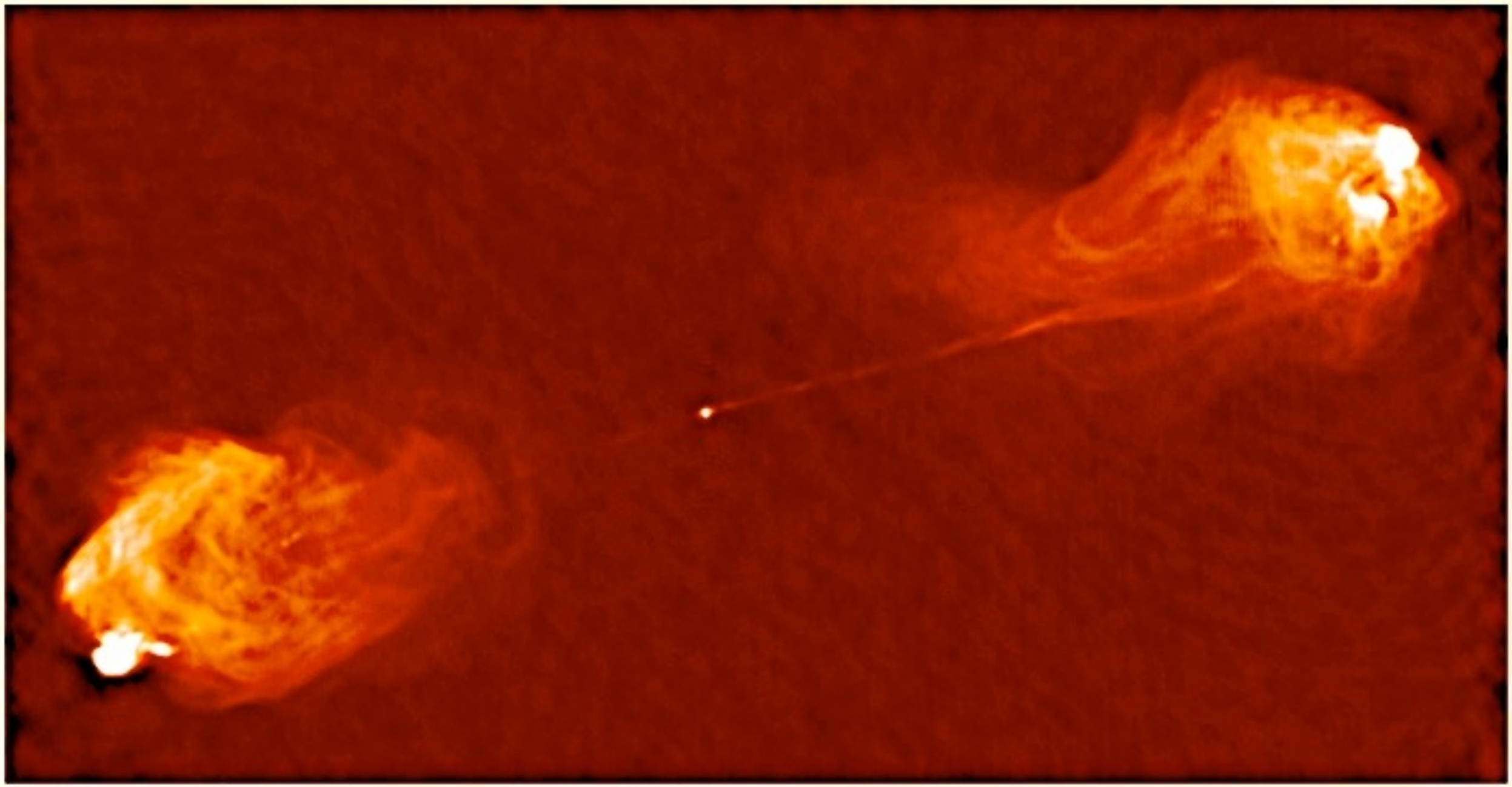

# Mass Composition

Depth of shower maximum $X_{max}$ and its distribution contain information on primary mass composition

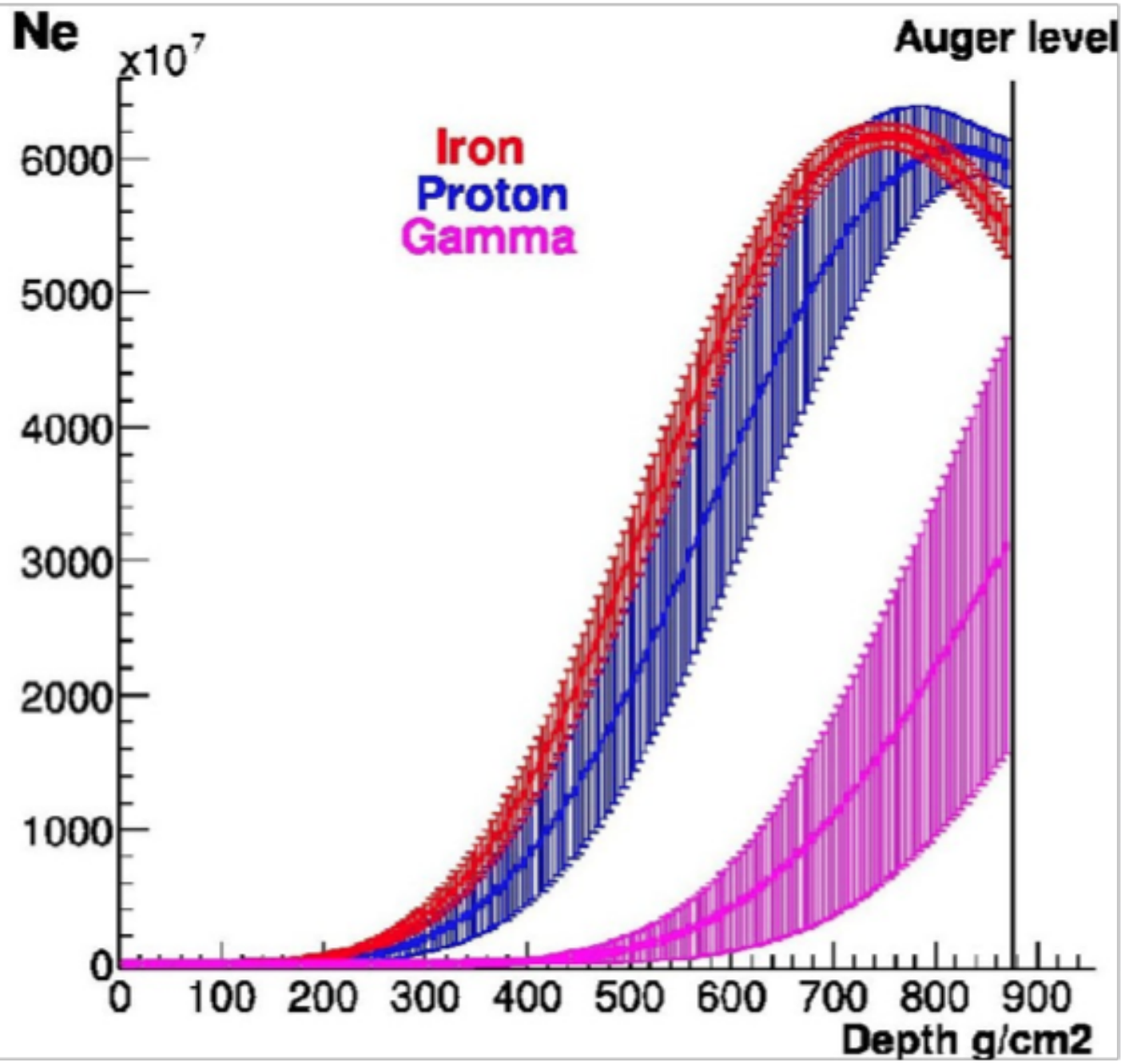


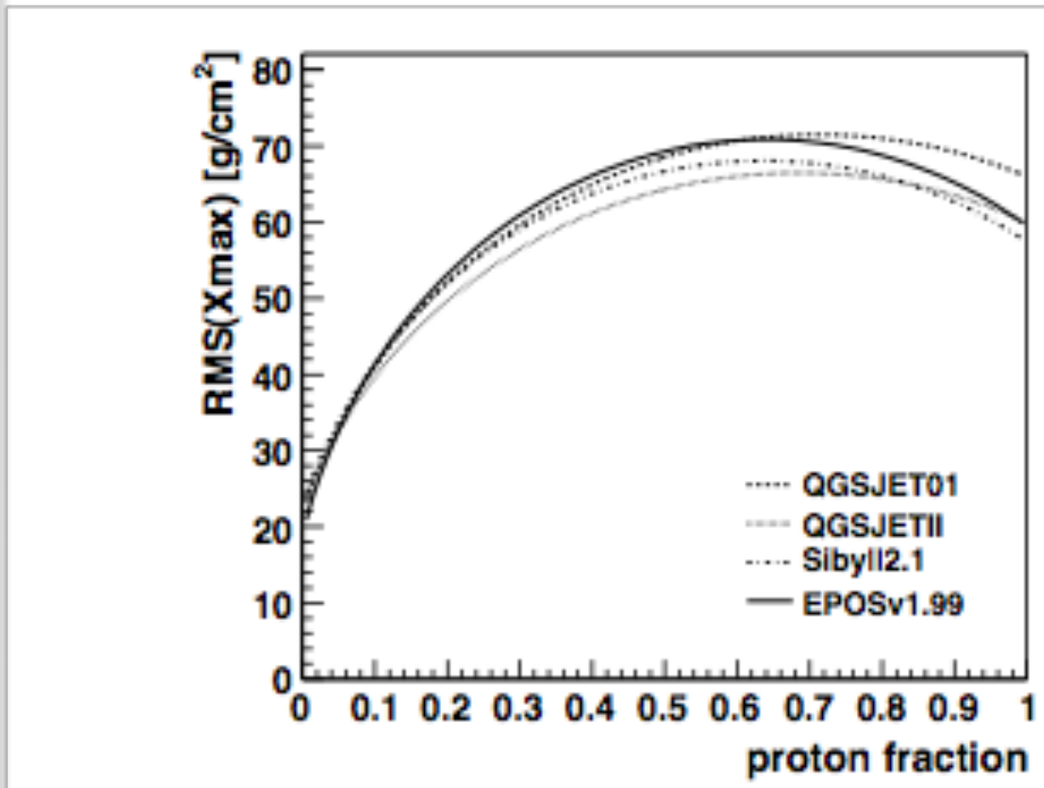


**FIGURE 1.** RMS($X_{\max}$) from different hadronic interaction models [23] and a two-component p/Fe composition model ($E = 10^{18}$ eV).

# Pierre Auger data suggest a heavier composition toward highest energies:

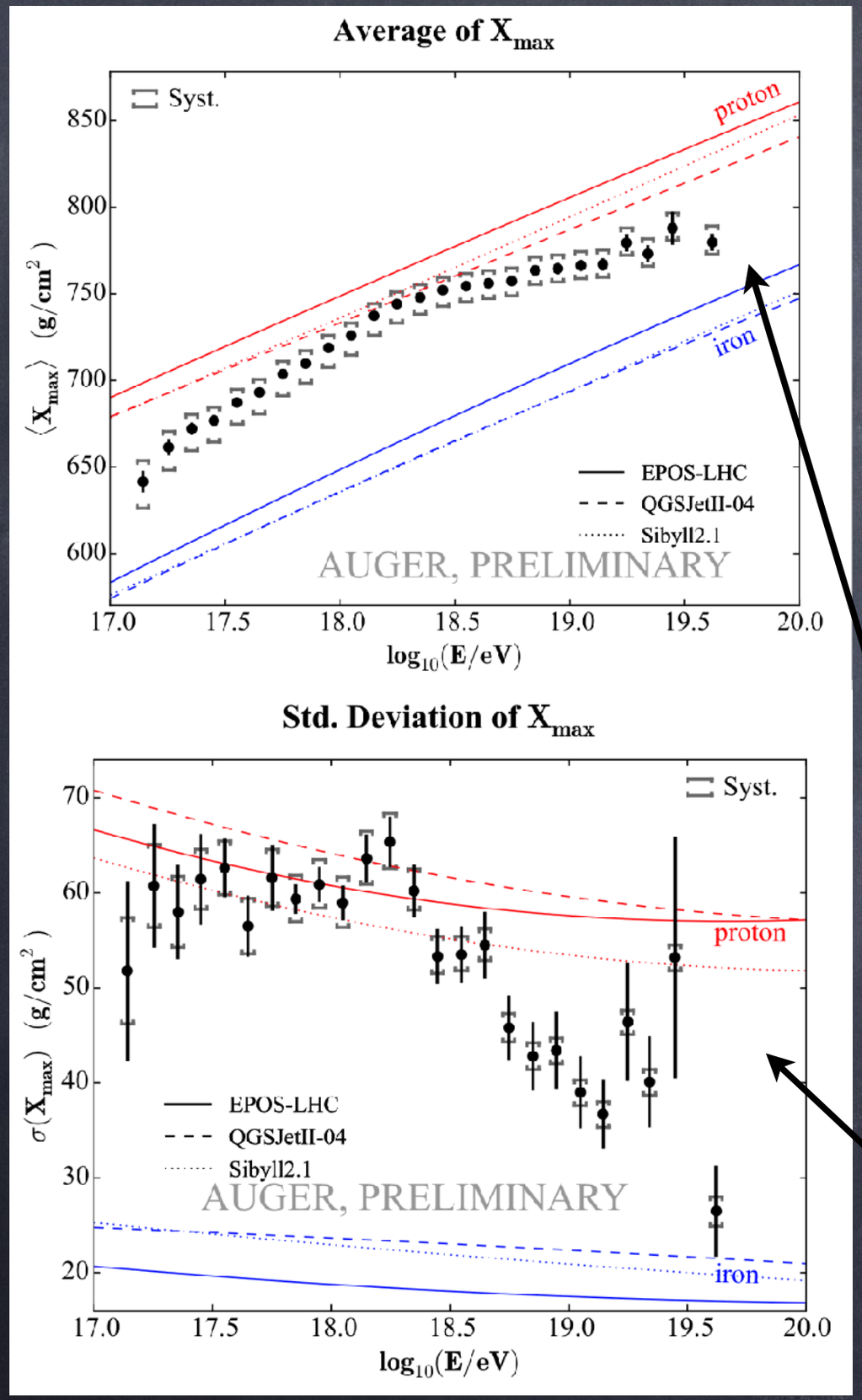


Pierre Auger Collaboration, arXiv:1509.03732

but not confirmed on the northern hemisphere by HiRes and Telescope Array which are consistent with protons

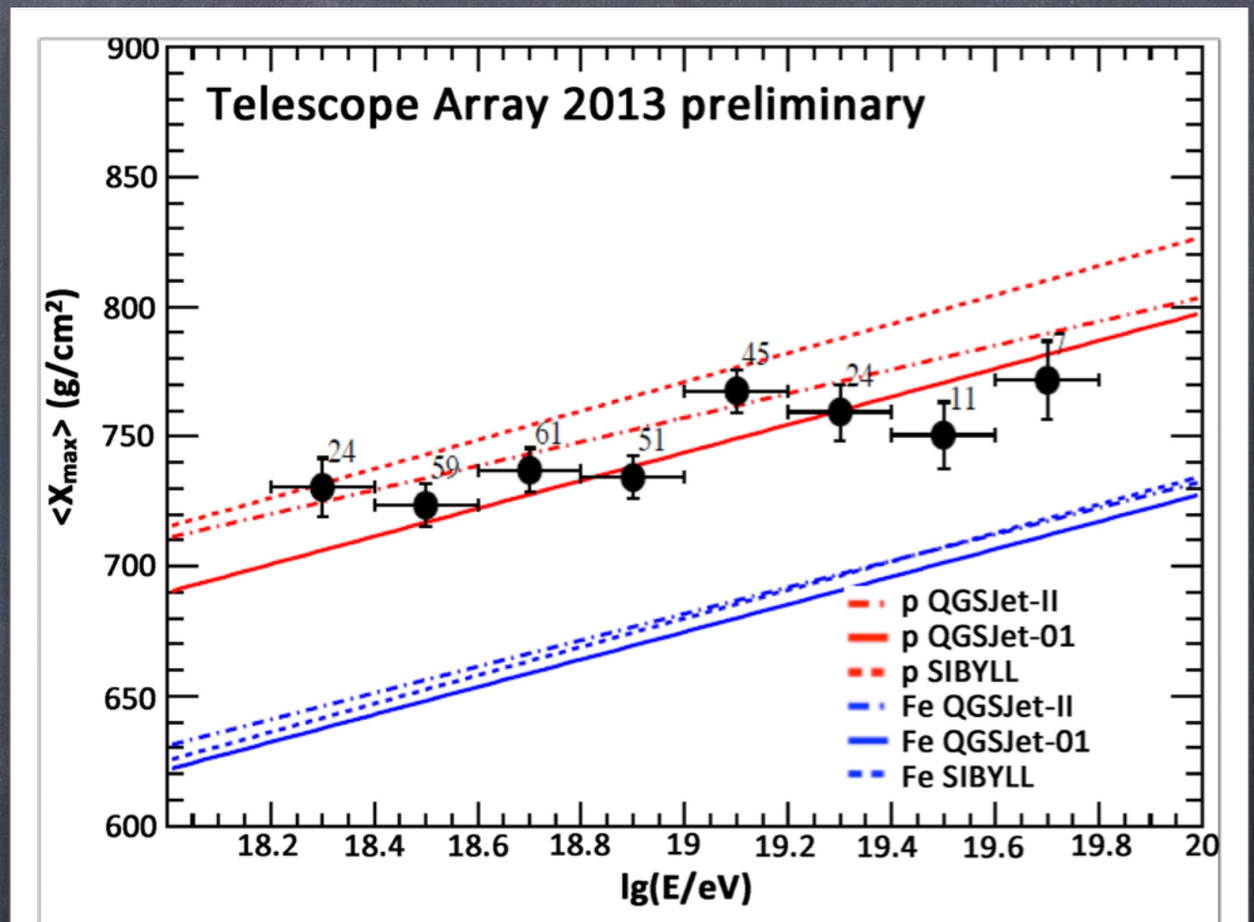


potential tension with air shower simulations and some hadronic interaction models because a mixed composition would predict larger RMS($X_{max}$)

# Muon number measured at 1000 m from shower core systematically higher than predicted

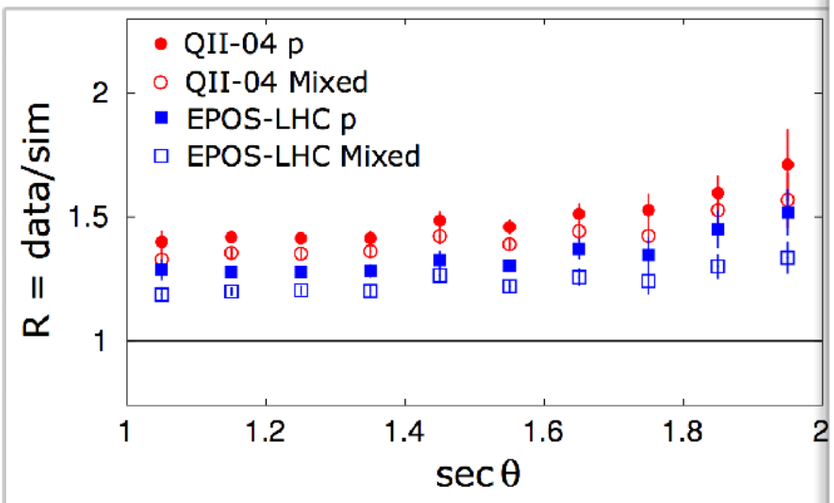


FIG. 2. The average ratio of S(1000) for observed and simulated events as a function of zenith angle, for mixed or pure proton compositions.

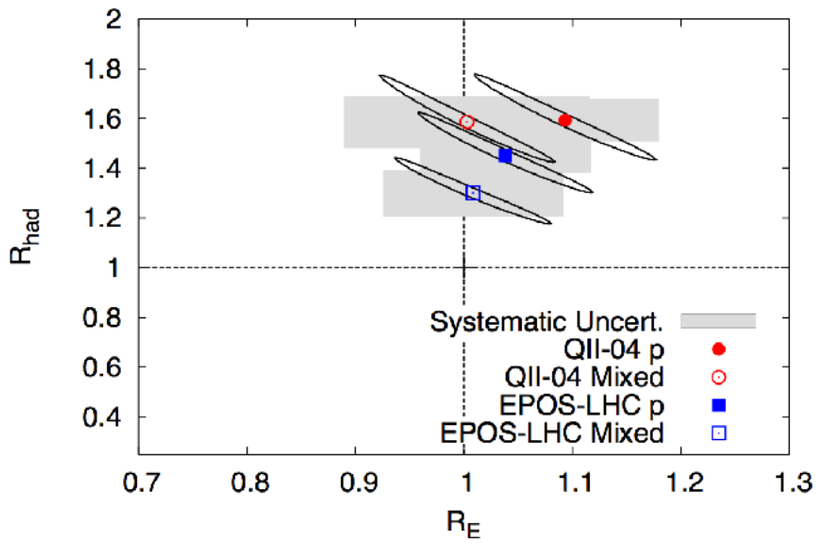


FIG. 4. Best-fit values of $R_E$ and $R_{\rm had}$ for QGSJet-II-04 and EPOS-LHC, for pure proton (solid circle/square) and mixed composition (open circle/square). The ellipses and gray boxes show the 1-$\sigma$ statistical and systematic uncertainties.

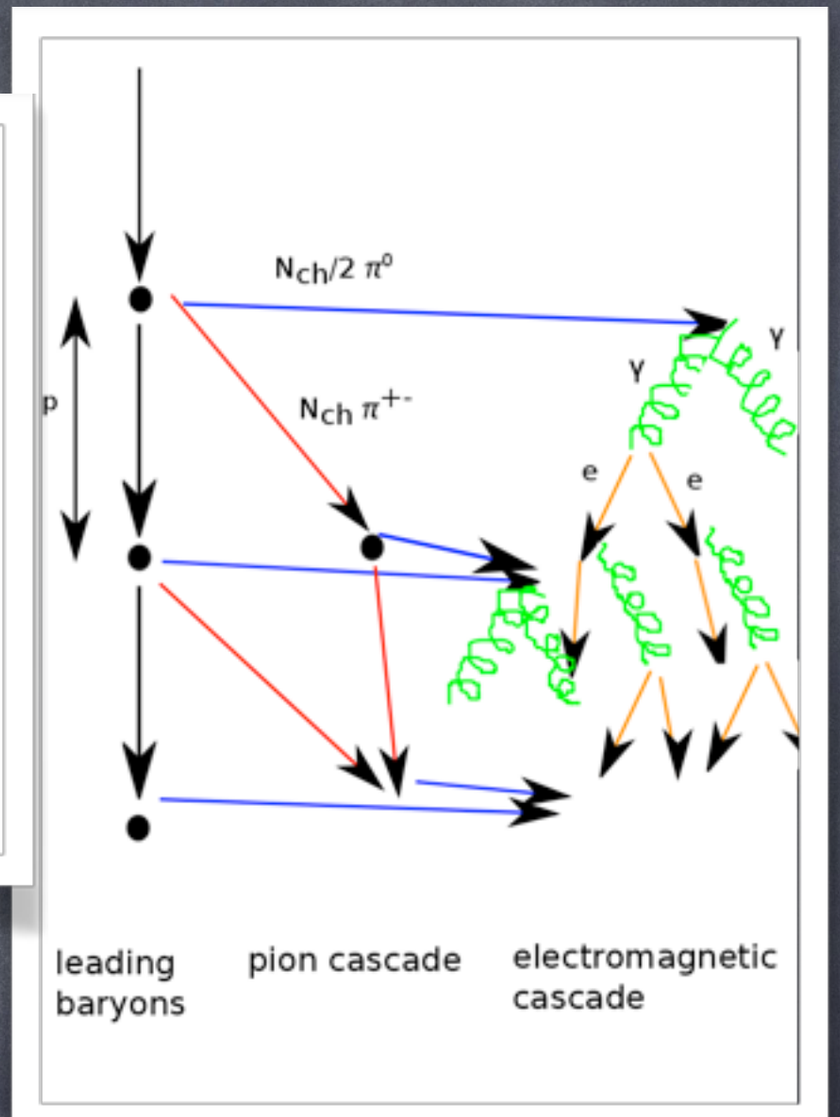


Pierre Auger Collaboration, PRL 117, 192001 (2016) [arXiv:1610.08509]

The muon number scales as

$$N_\mu \propto E_{\rm had} \propto (1 - f_{\pi^0})^N \ ,$$

with the fraction going into the electromagnetic channel $f_{\pi^0} \simeq \frac{1}{3}$ and the number of generations $N$ strongly constrained by $X_{\rm max}$. Larger $N_\mu$ thus requires smaller $f_{\pi^0}$ ! The production of $\rho^0$ could also play a role.

# Spectrum and Composition

fits to spectrum and composition for a homogeneous source distribution neglecting deflection (which generally is a good approximation for the solid angle integrated flux) tend to favor very hard injection spectra with low cut-off rigidities

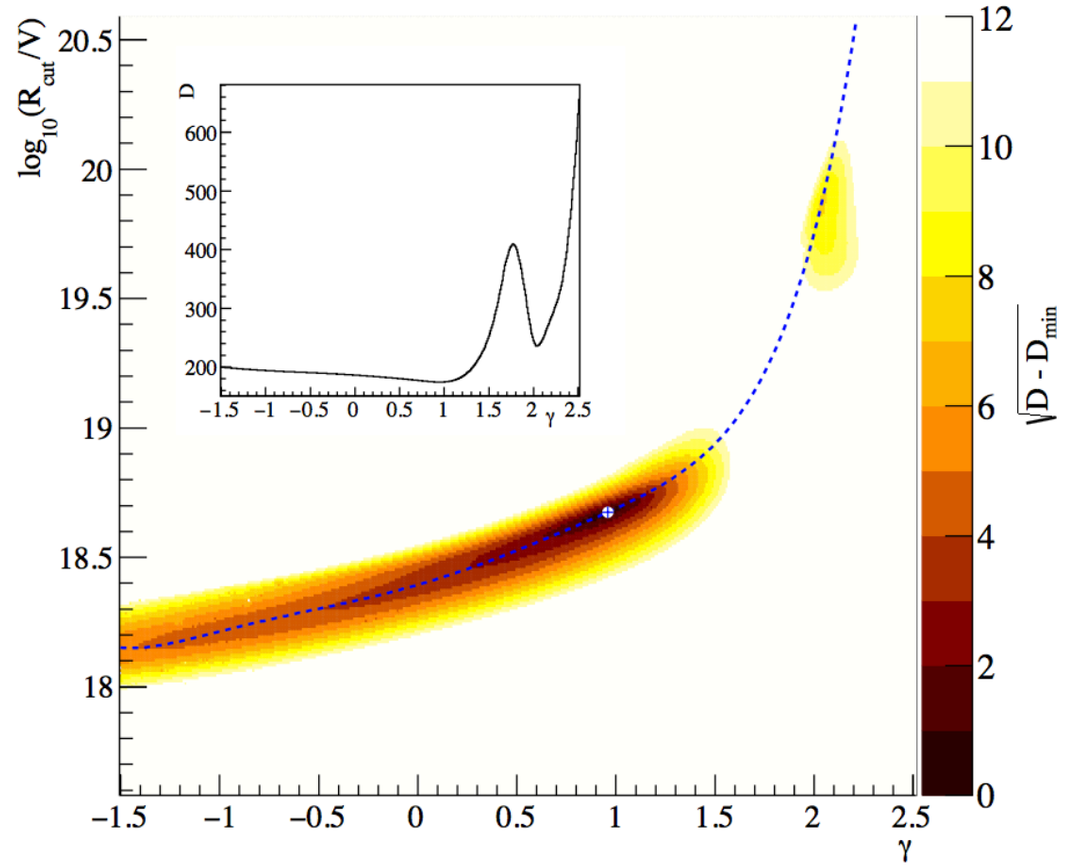


Pierre Auger collaboration, JCAP 1704 (2017) 028 [arXiv:1612.07155]

**Figure 1**. Deviance $\sqrt{D - D_{\rm min}}$, as function of $\gamma$ and $\log_{10}(R_{\rm cut}/{\rm V})$. The dot indicates the position of the best minimum, while the dashed line connects the relative minima of D (valley line). In the inset, the distribution of $D_{\rm min}$ in function of $\gamma$ along this line.

AugerPrime extension aims at event-by-event measurement of composition; other future experiments include space-based missions JEM-EUSO, POEMMA, ..

# Newest Results on Anisotropy

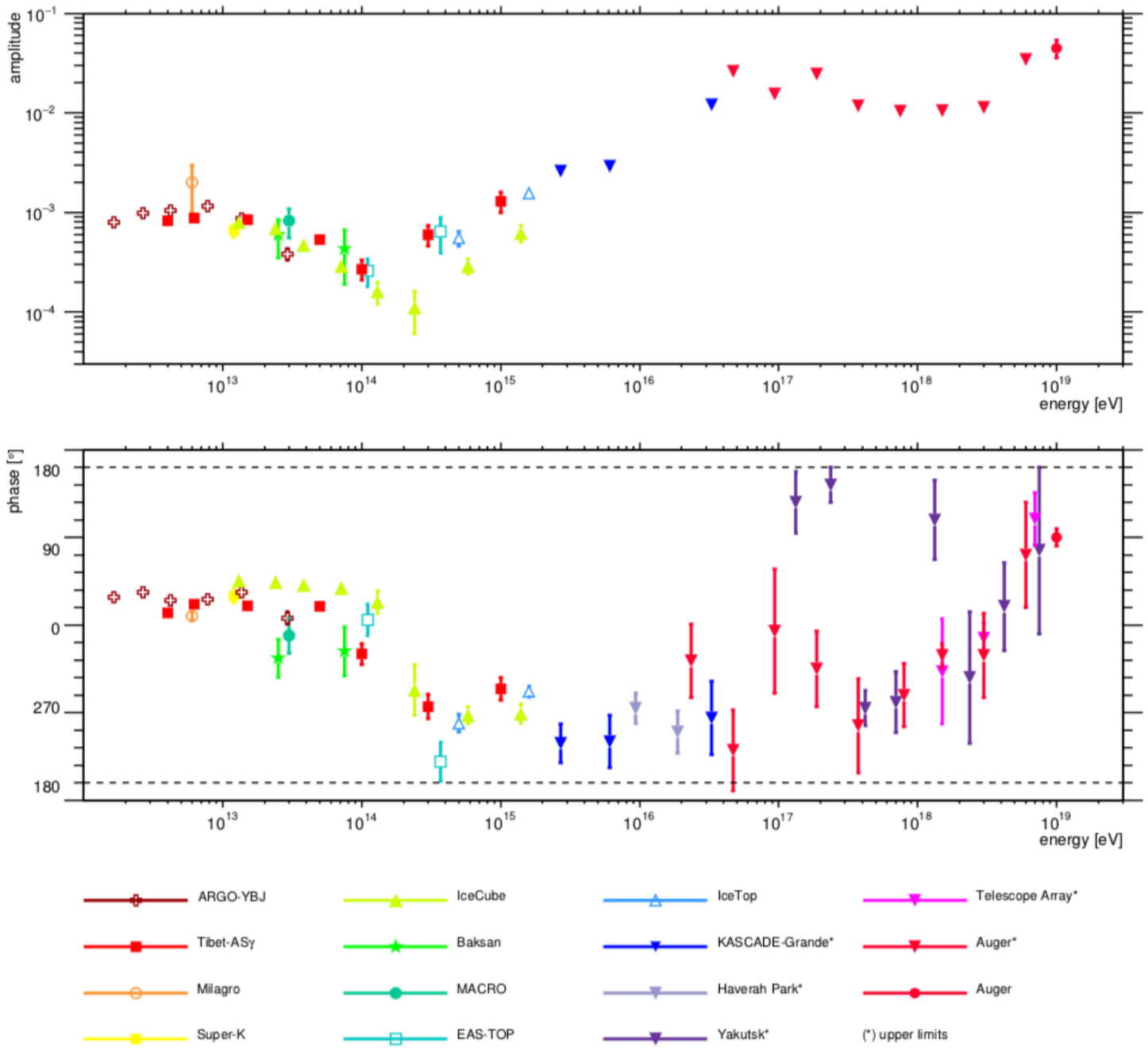


Figure 7: Amplitude (top) and phase (bottom) measurements of the first harmonic in right ascension as a function of energy, from various reports. Amplitudes drawn as triangles with apex pointing down are the most stringent upper limits up to date in the considered energy ranges.

Amplitude and phase of dipole as function of energy

O. Deligny, arXiv:1808.03940

# A Significant Anisotropy around $8\times10^{18}$ eV is now seen

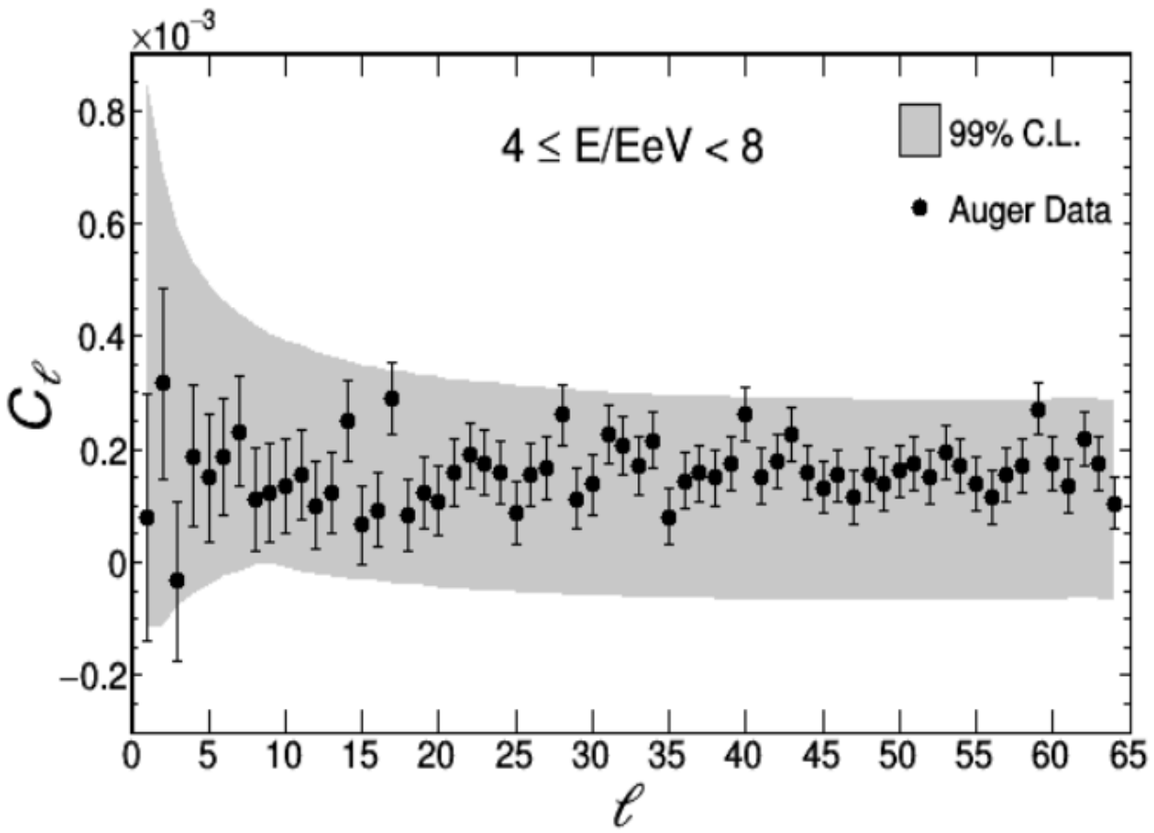


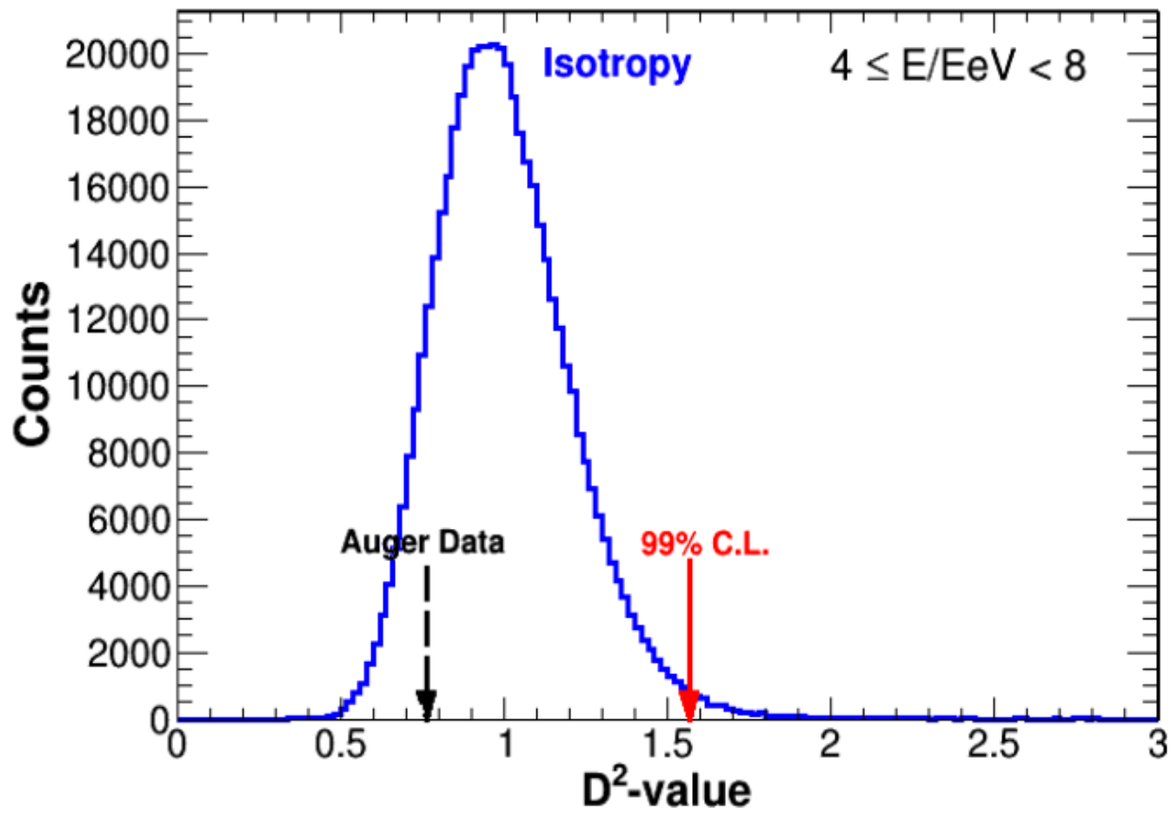


Figure 2: Angular power spectrum for $4 \leq E/\mathrm{EeV} < 8$. On the left there is no visible departure from the isotropic expectation. On the right the $D^2$-value distribution from 500,000 isotropic sky maps is shown. The red arrow represents the threshold to accept/reject the isotropy hypothesis with 99% C.L.. The $D^2$-value from data, represented by the black (dashed) arrow, is smaller than that threshold supporting the isotropy hypothesis.

Pierre Auger Collaboration, JCAP 1706 (2017) 026 [arXiv:1611.06812]

# A Significant Anisotropy around $8\times10^{18}$ eV is now seen

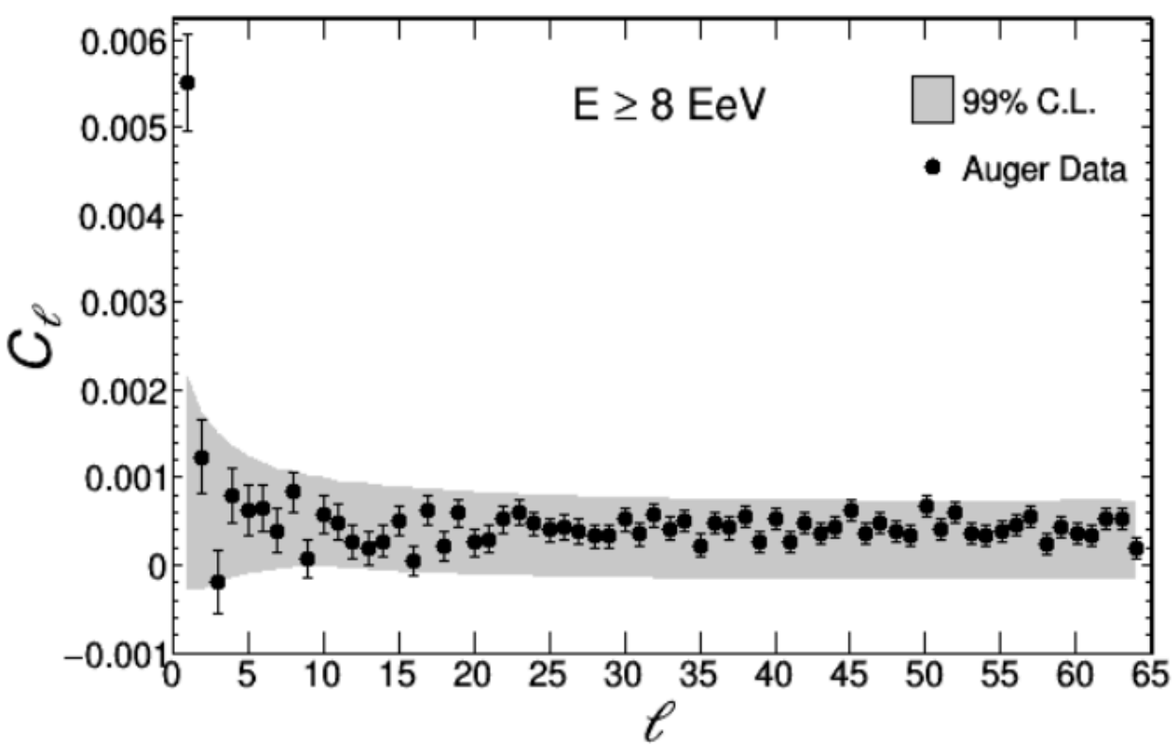


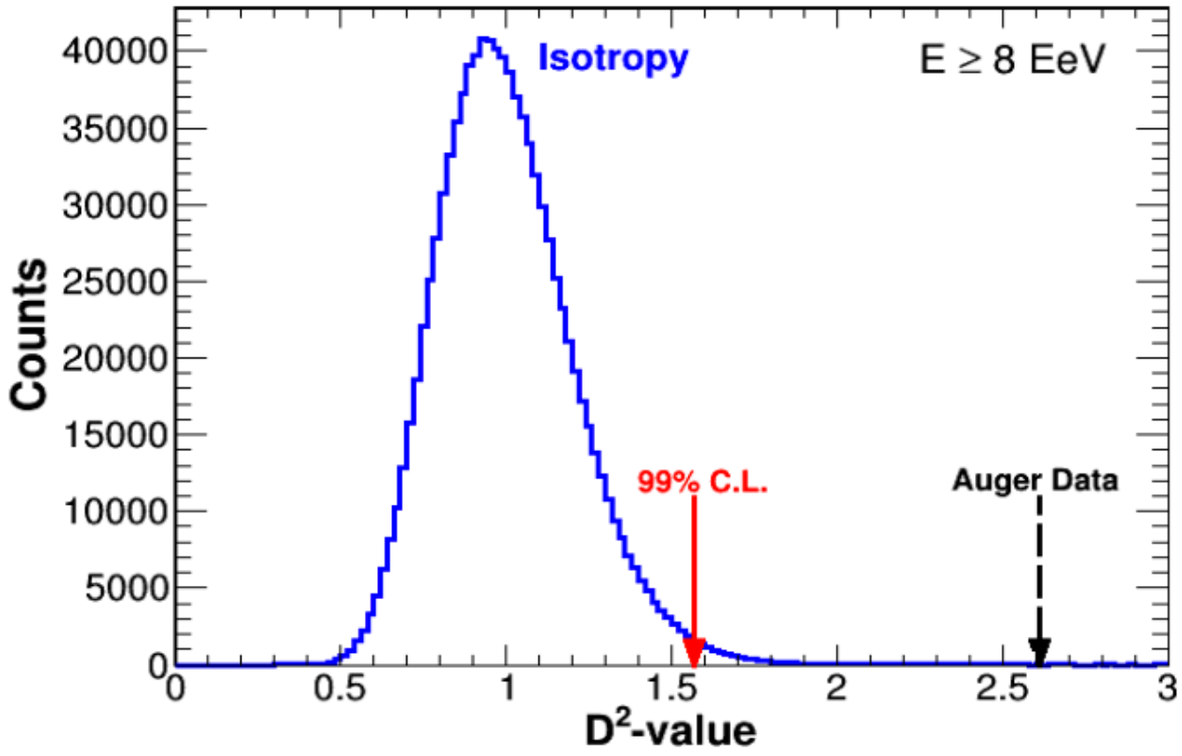


Figure 3: Angular power spectrum for $E \geq 8$ EeV. On the left a clear indication for a departure from isotropy is captured in the dipole scale. On the right the $D^2$-value distribution from 1,000,000 isotropic sky maps is shown. The $D^2$-value from data, represented by the black (dashed) arrow, is larger than the threshold of isotropy presenting an indication of anisotropy with $> 99\%$ C.L..

Pierre Auger Collaboration, JCAP 1706 (2017) 026 [arXiv:1611.06812]

# 3-Dimensional Effects in Propagation

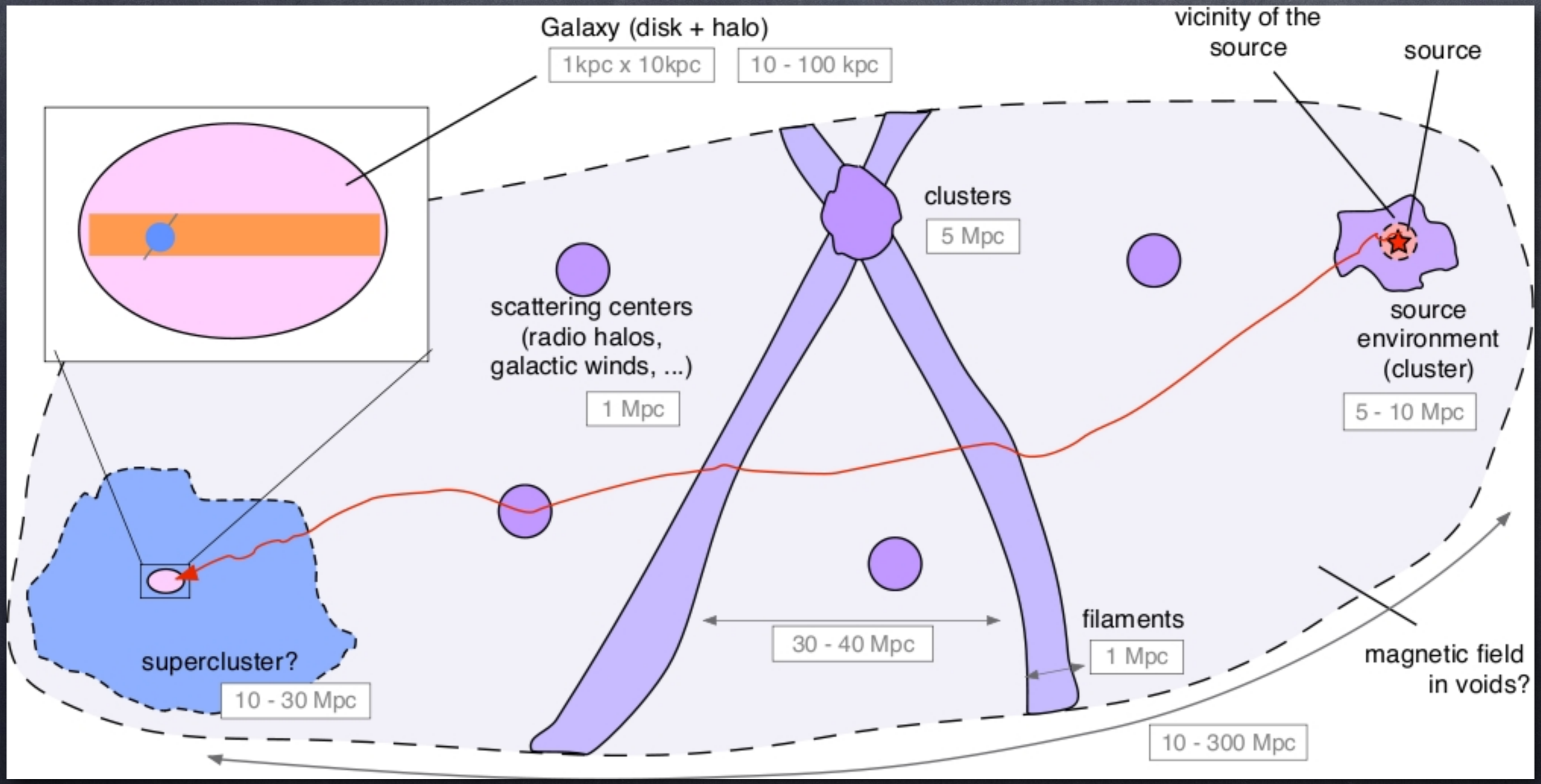


Kotera, Olinto, Ann.Rev.Astron.Astrophys. 49 (2011) 119

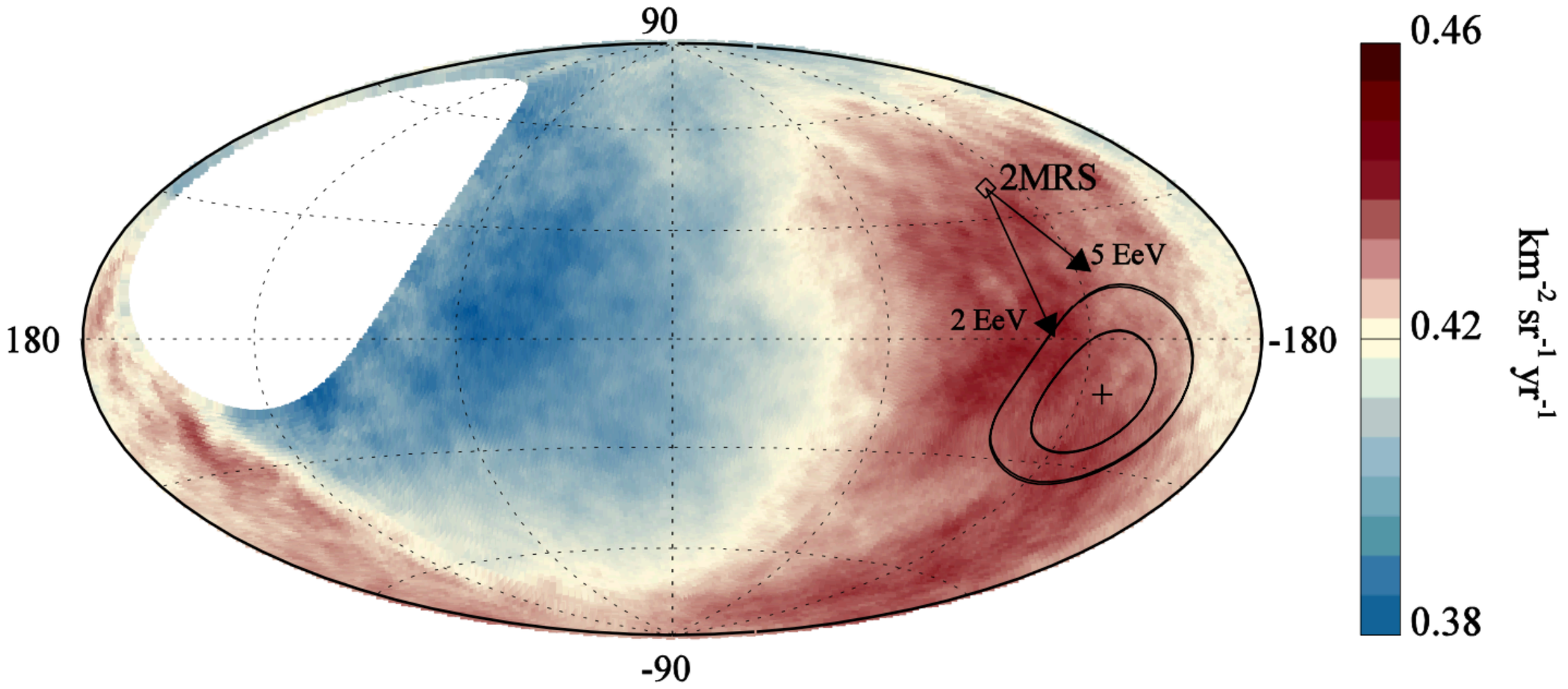


**Fig. 3. Map showing the fluxes of particles in Galactic coordinates.** Sky map in Galactic coordinates showing the cosmic-ray flux for $E \geq 8$ EeV smoothed with a 45° top-hat function. The Galactic center is at the origin. The cross indicates the measured dipole direction and the contours the 68% and 95% confidence-level regions. The dipole in the 2MRS galaxy distribution is indicated, while arrows show the deflections expected for a particular model of the Galactic magnetic field (*8*), for $E/Z$=5 EeV or 2 EeV.

Pierre Auger Collaboration, Science 357 (22 September 2017) 1266 [arXiv:1709:07321]

# Extragalactic Magnetic Field Filling Factors from recent Simulations

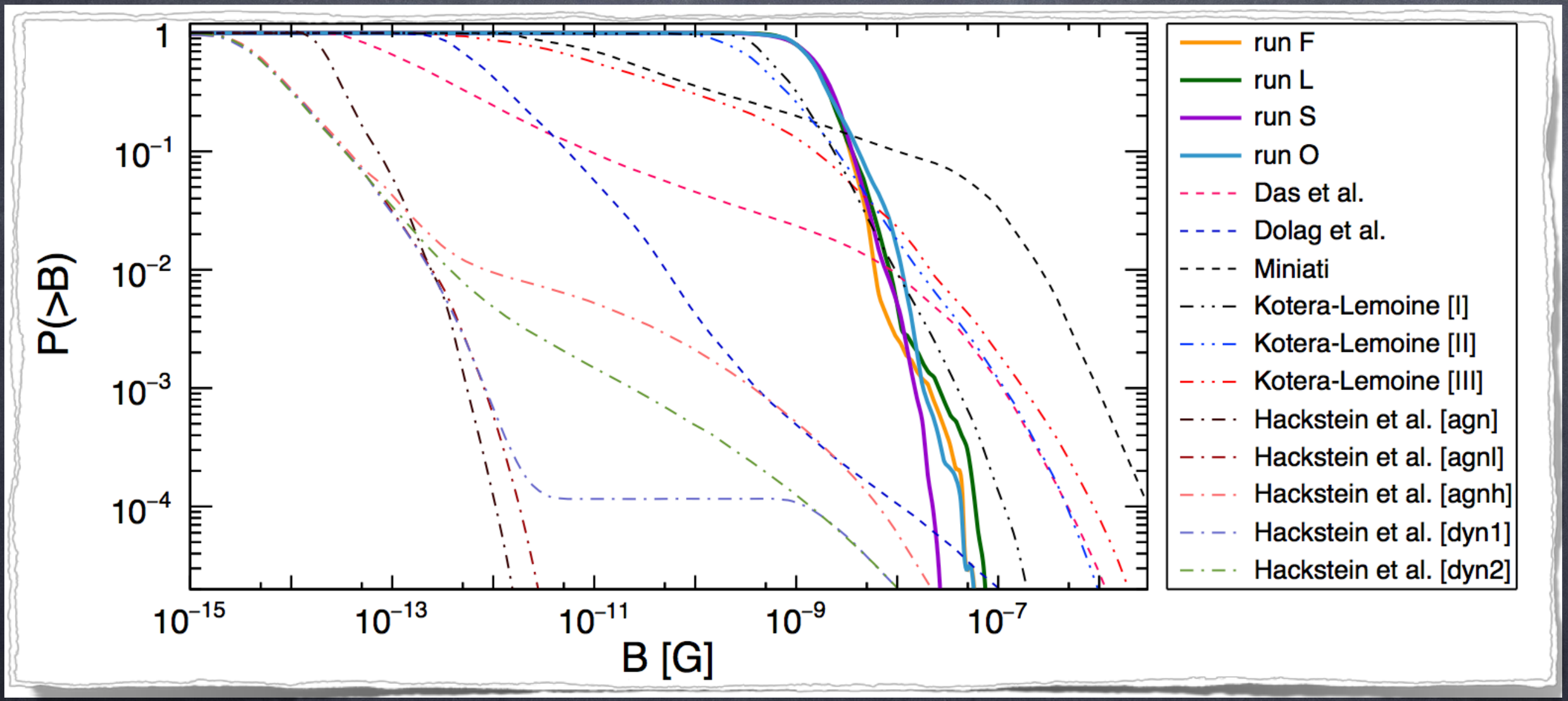


Alves Batista et al, PRD 96 (2017) 023010 [arXiv:1704.05869]

Extragalactic iron propagation produces nuclear cascades in structured magnetic fields:

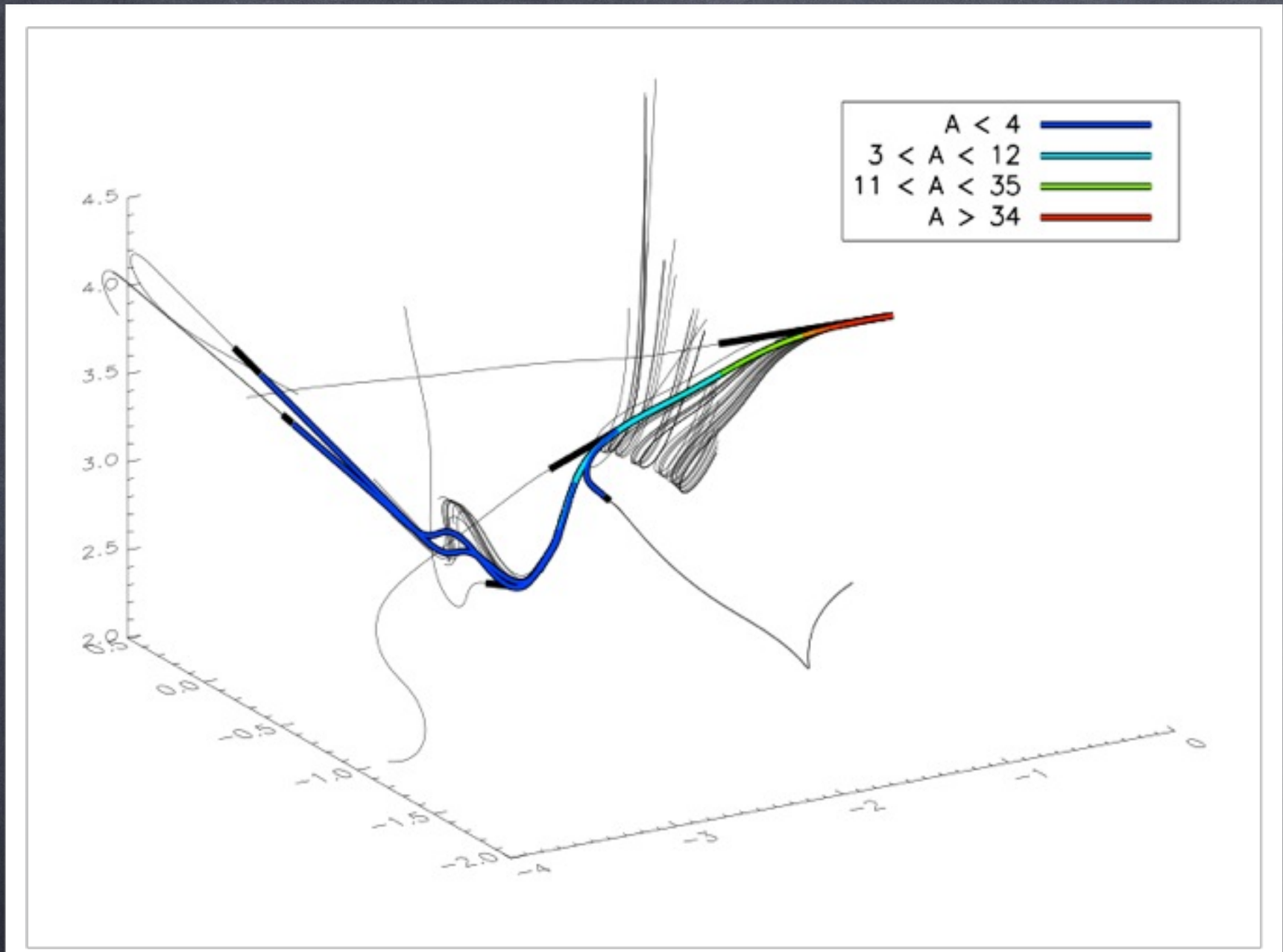


Initial energy 1.2 x $10^{21}$ eV, magnetic field range $10^{-15}$ to $10^{-6}$ G. Color-coded is the mass number of secondary nuclei

# CRPropa 2.0/3.0

**CRPropa is a public code for UHE cosmic rays, neutrinos and γ-rays being extended to heavy nuclei and hadronic interactions**

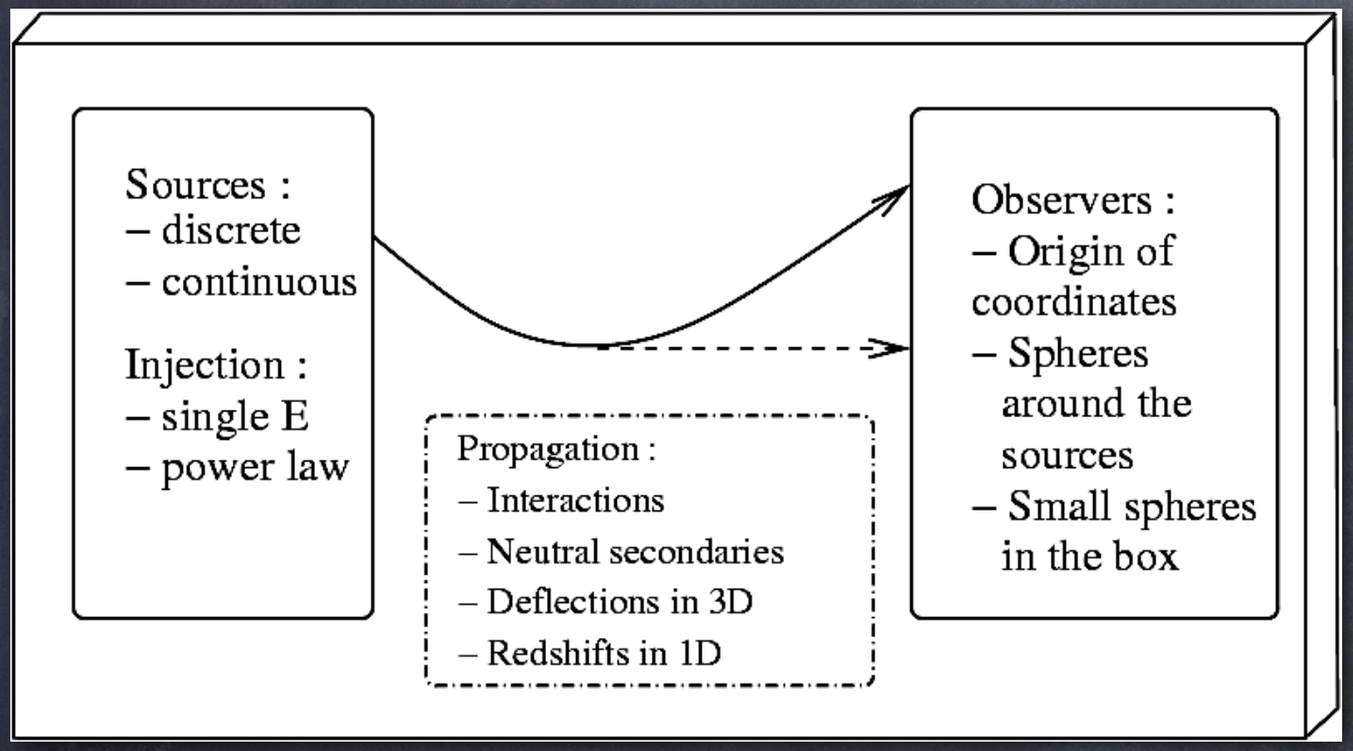


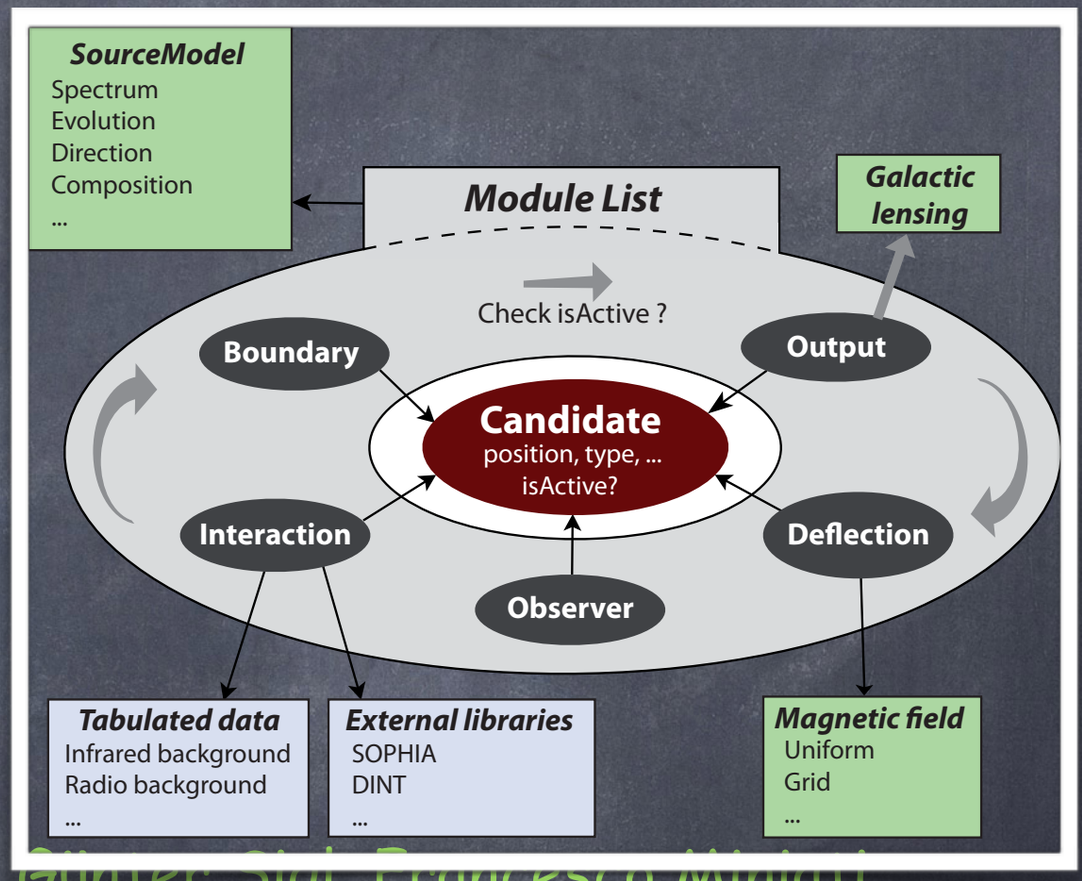


Version 1.4: Eric Armengaud, Tristan Beau, Günter Sigl, Francesco Miniati, Astropart.Phys.28 (2007) 463.

https://crpropa.desy.de/Main_Page

https://github.com/CRPropa/CRPropa3/

Version 2.0: Luca Maccione, Rafael Alves Batista, David Walz, Gero Müller, Nils Nierstenhoefer, Karl-Heinz Kampert, Peter Schiffer, Arjen van Vliet Astroparticle Physics 42 (2013) 41

# Discrete Sources in nearby large scale structure

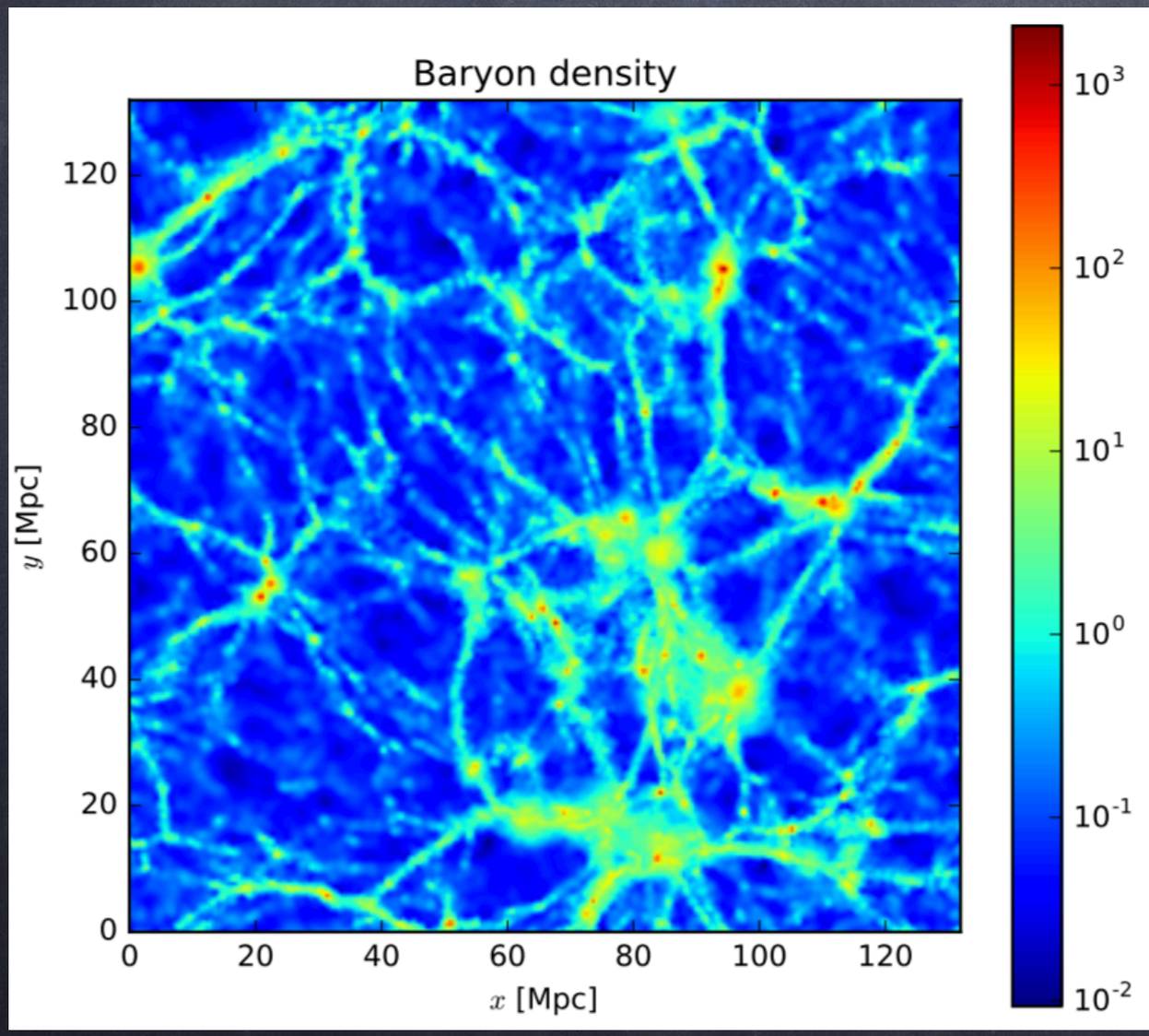


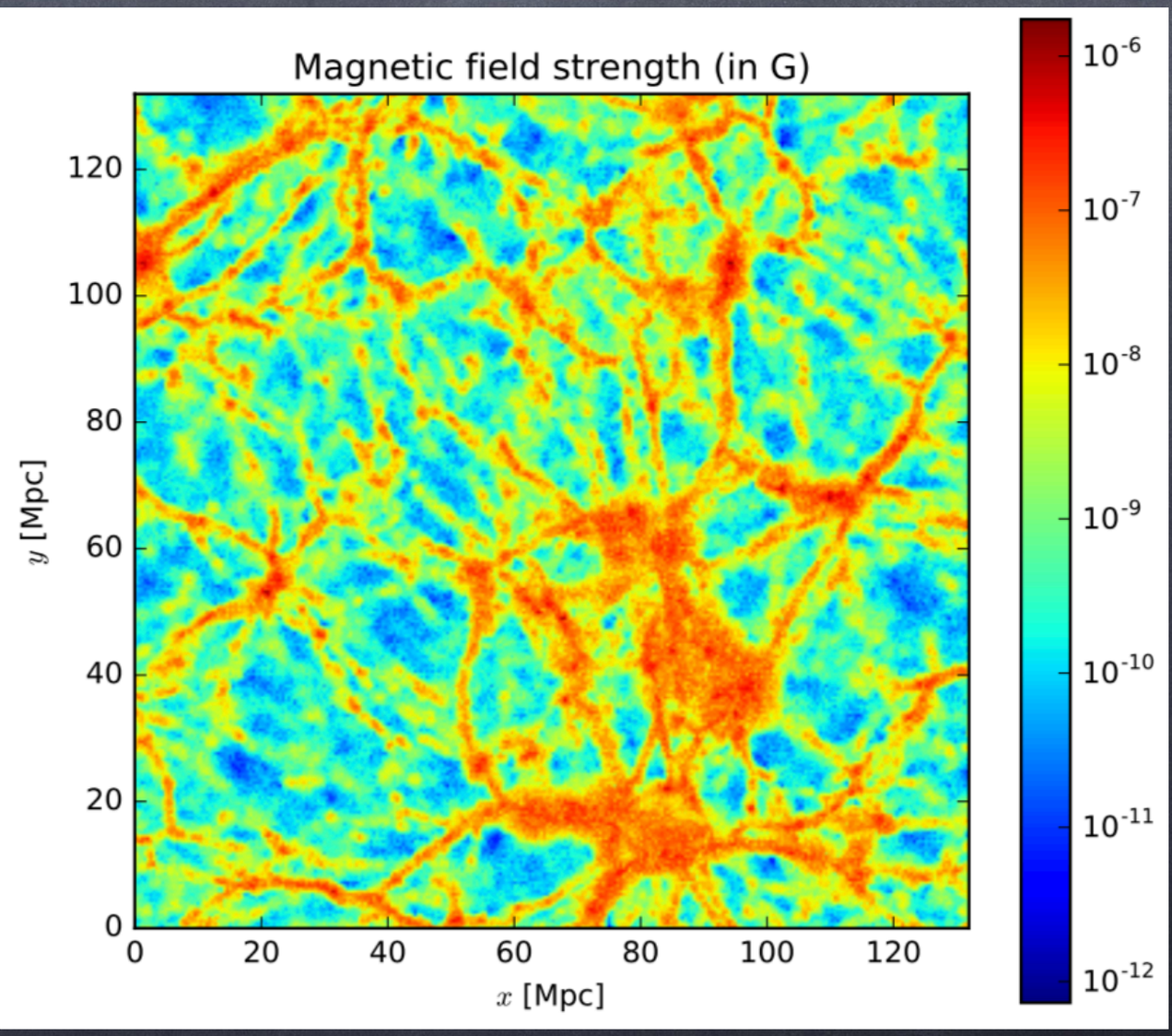

# Building Benchmark Scenarios

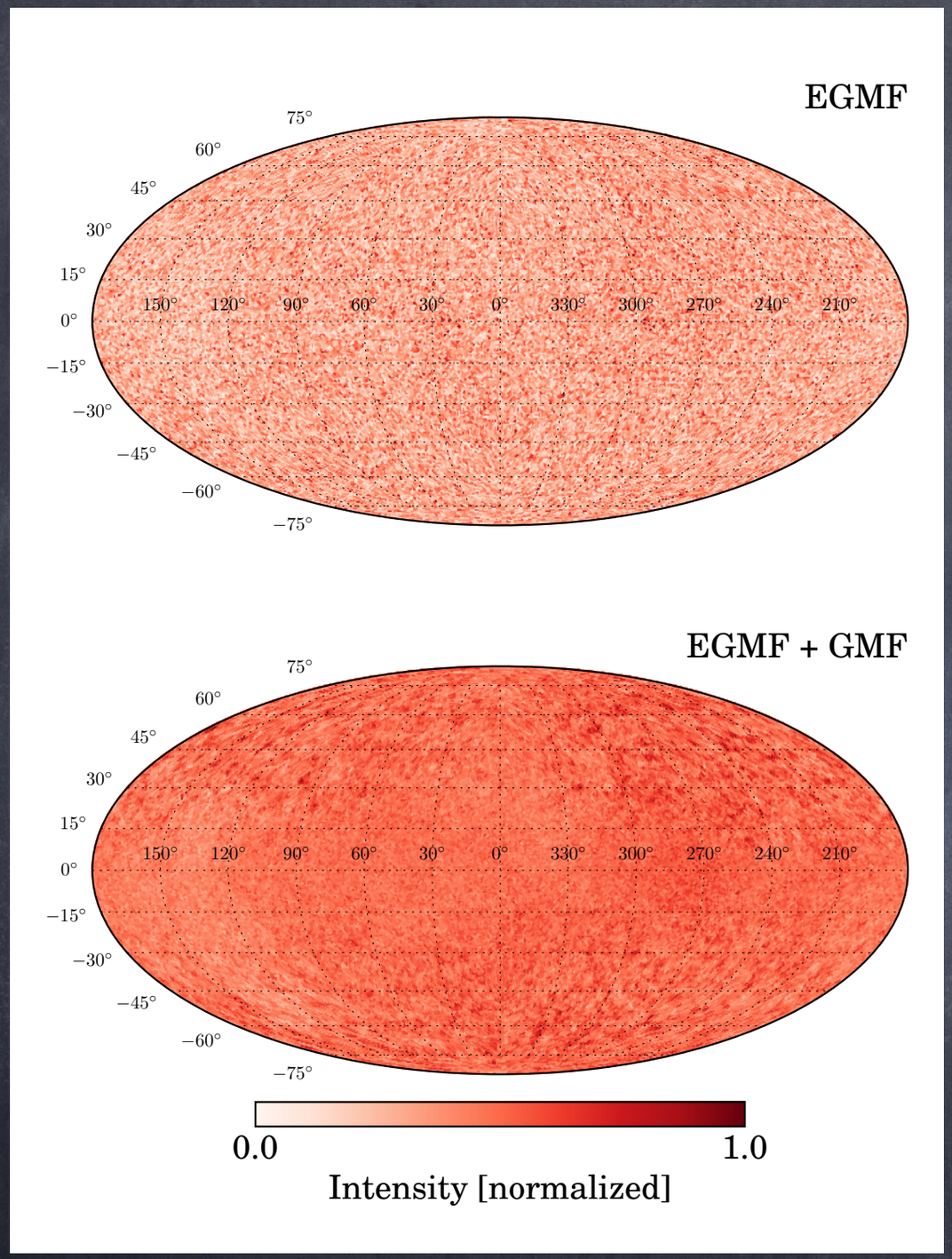


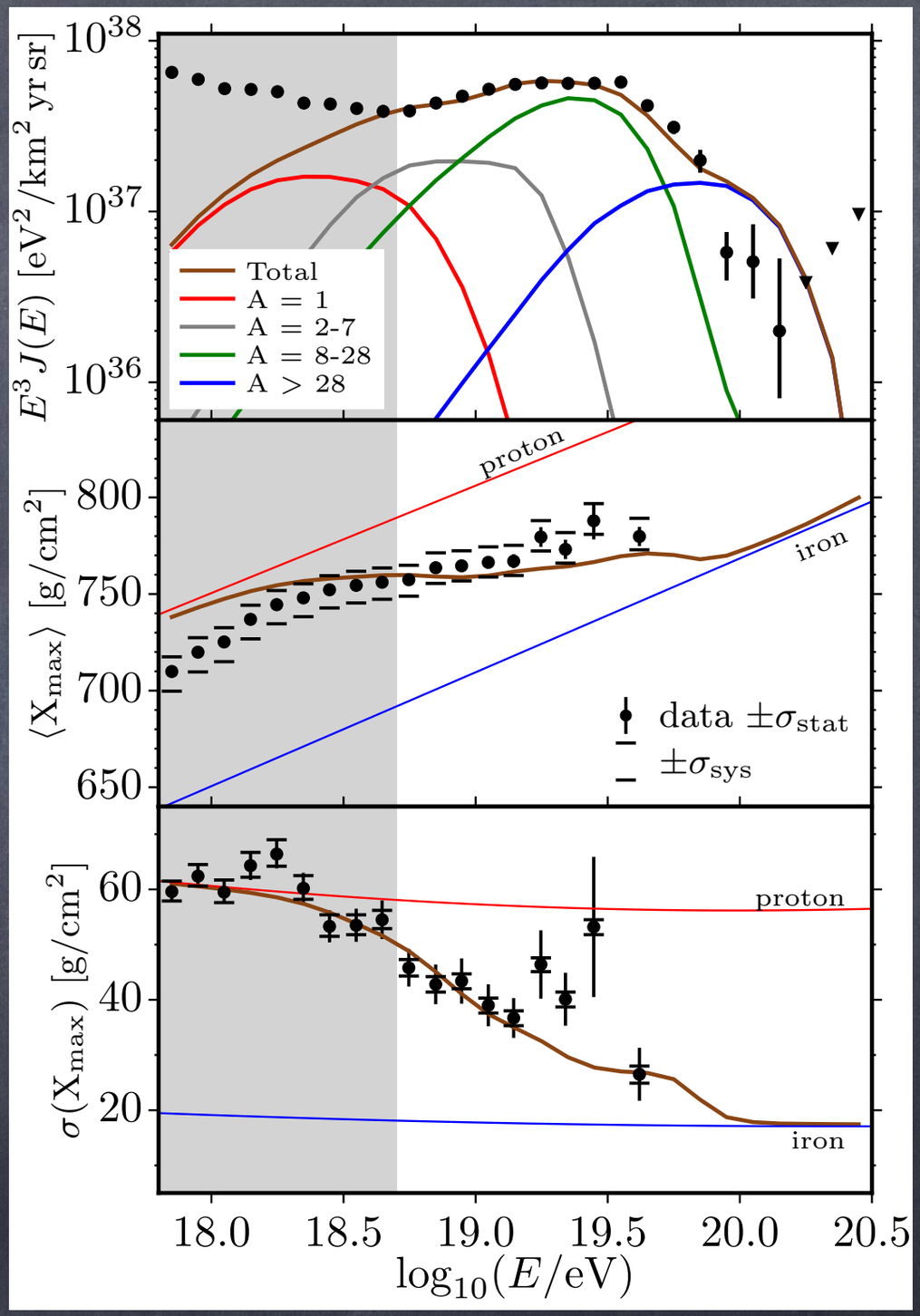


combining spectral and composition information with anisotropy can considerably strengthen constraints on source characteristics, distributions and magnetization

# Very High High Energy Neutrinos

The „grand unified" differential neutrino number spectrum

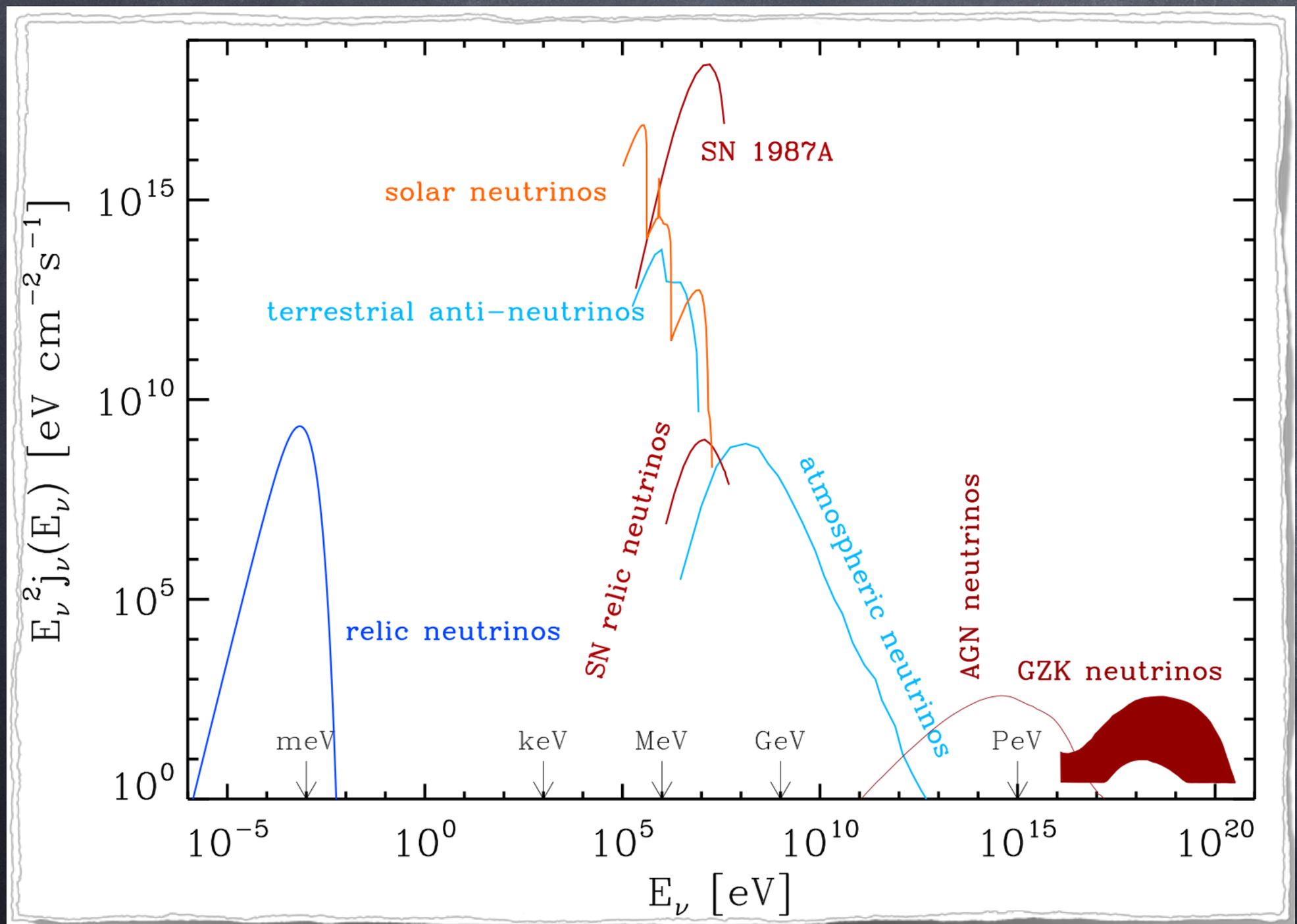


G. Sigl, book "Astroparticle Physics: Theory and Phenomenology", Atlantis Press/Springer 2016

# Summary of neutrino production modes

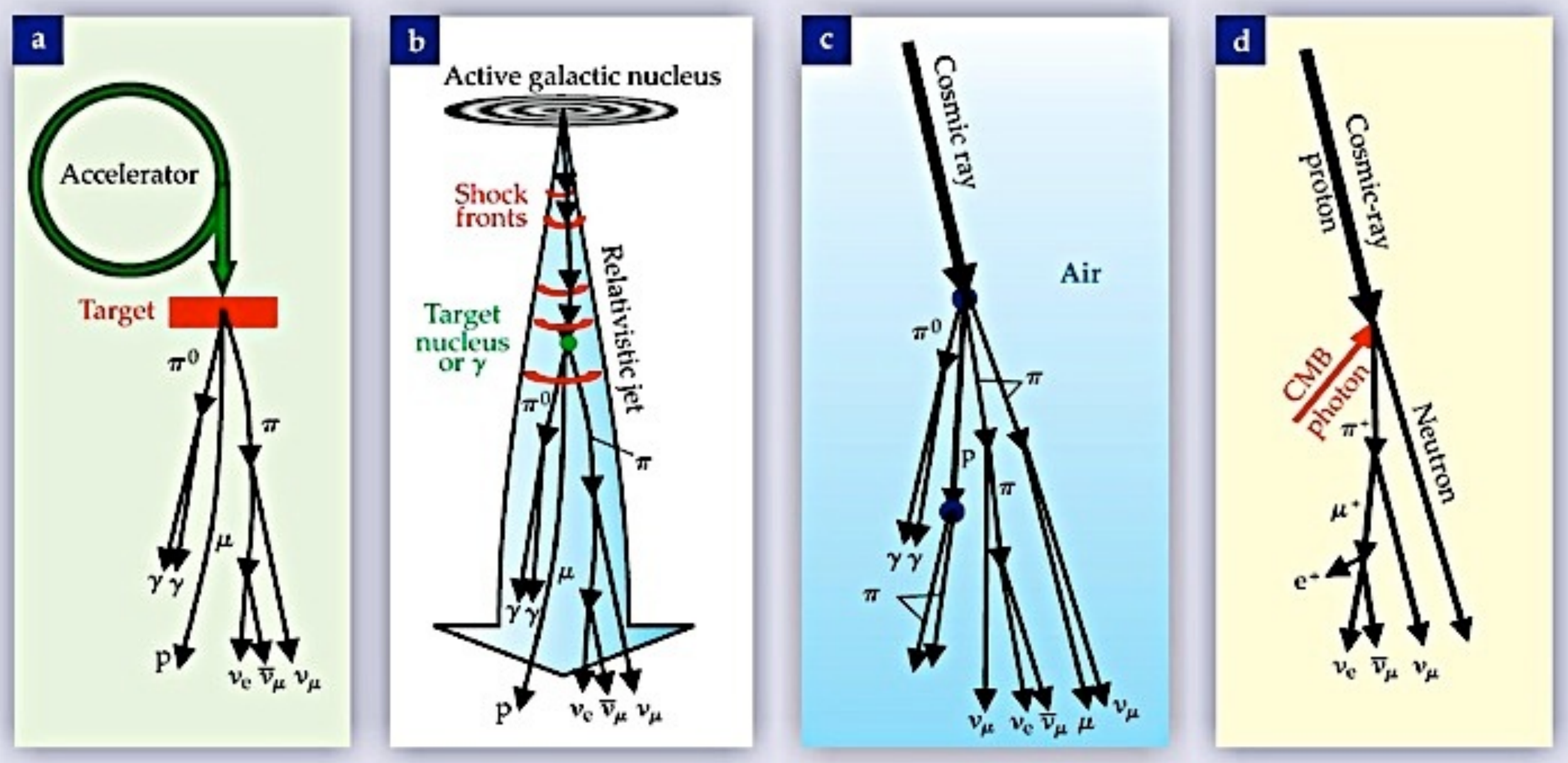


From Physics Today

# A combination of the measured diffuse flux with upper limits on individual sources constrains source type

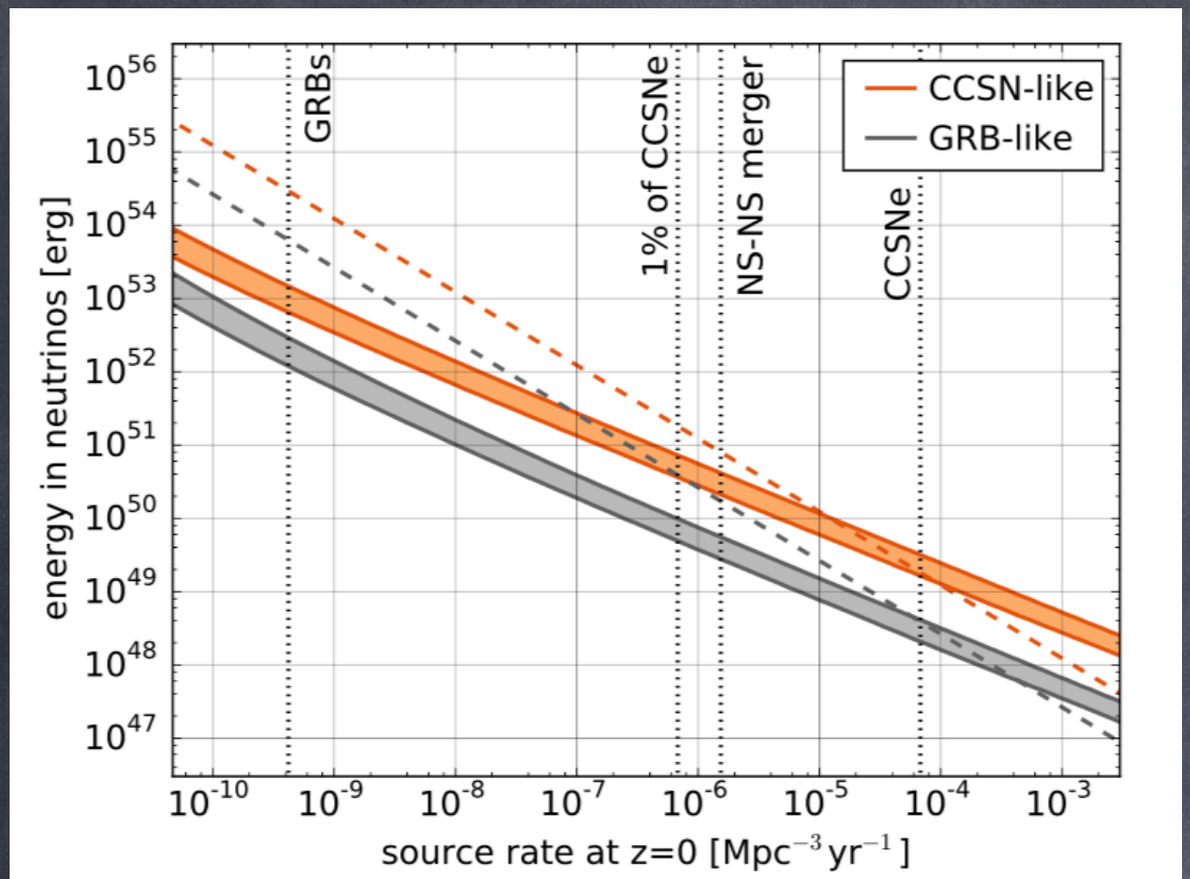


FIG. 2: Limits on the median source energy (90% c. l.) emitted in neutrinos between 100 GeV and 10 PeV within 100 s. The area above the bands is excluded for CCSN-like (orange) and GRB-like (gray) populations respectively. The upper edge of the limit corresponds to an $E^{-2.5}$ neutrino spectrum and the lower one to an $E^{-2.13}$ spectrum. The dashed lines show which source energy corresponds to 100% of the astrophysical flux for an $E^{-2.5}$ spectrum. The corresponding lines for an $E^{-2.13}$ spectrum would be lower by a factor of 13. The rate of long GRBs, NS-NS mergers and CCSNe is indicated. Beaming is included for long GRBs, but not for NS-NS mergers or CCSNe due to the unknown jet opening angles.

Aartsen et al [IceCube collaboration], arXiv:1807.11492

# Sensitivity of existing and future experiments to ultra-high energy neutrinos

A.N. Otte, arXiv:1811.09287

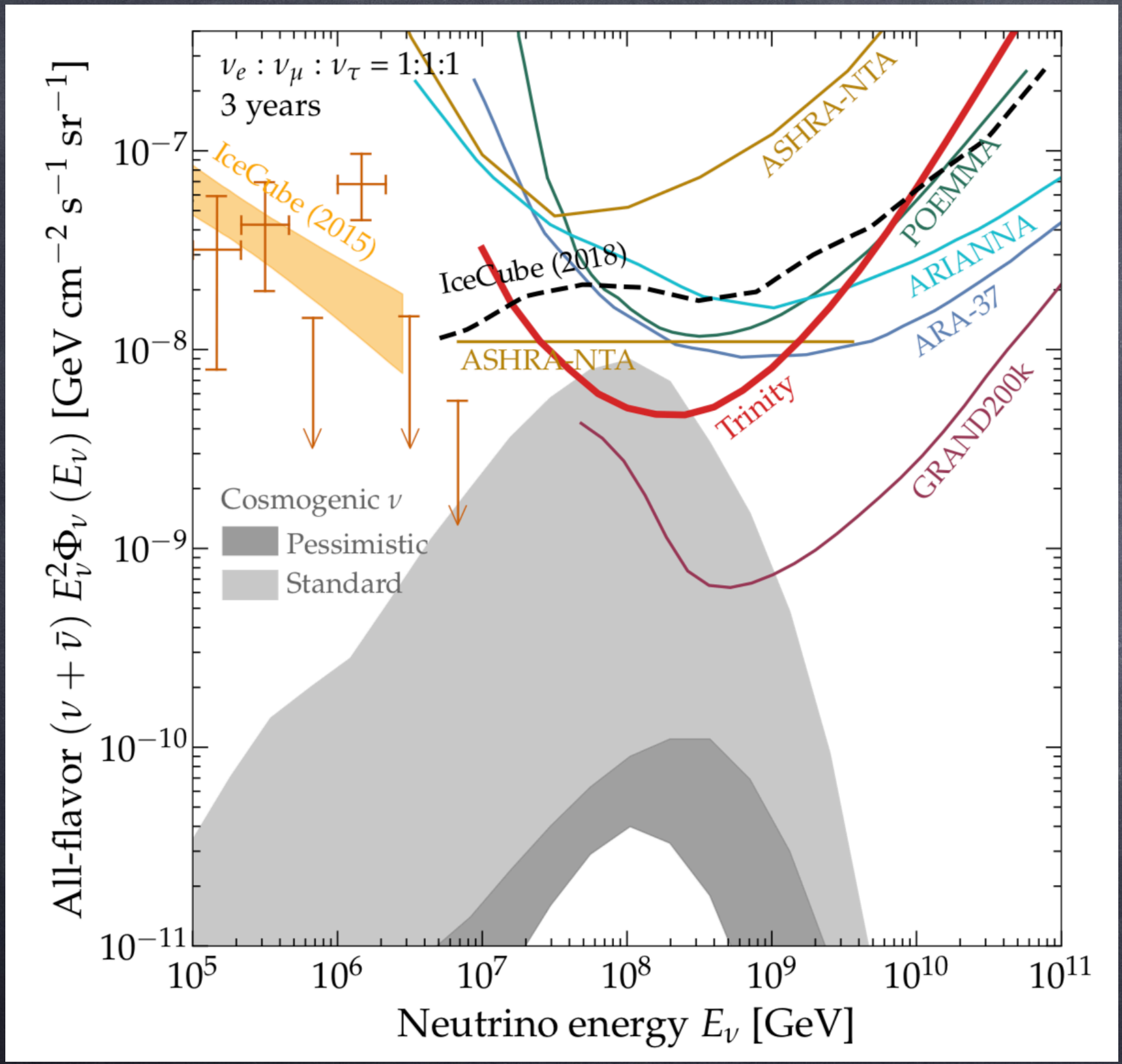

# Multi-Messengers: The Big Picture

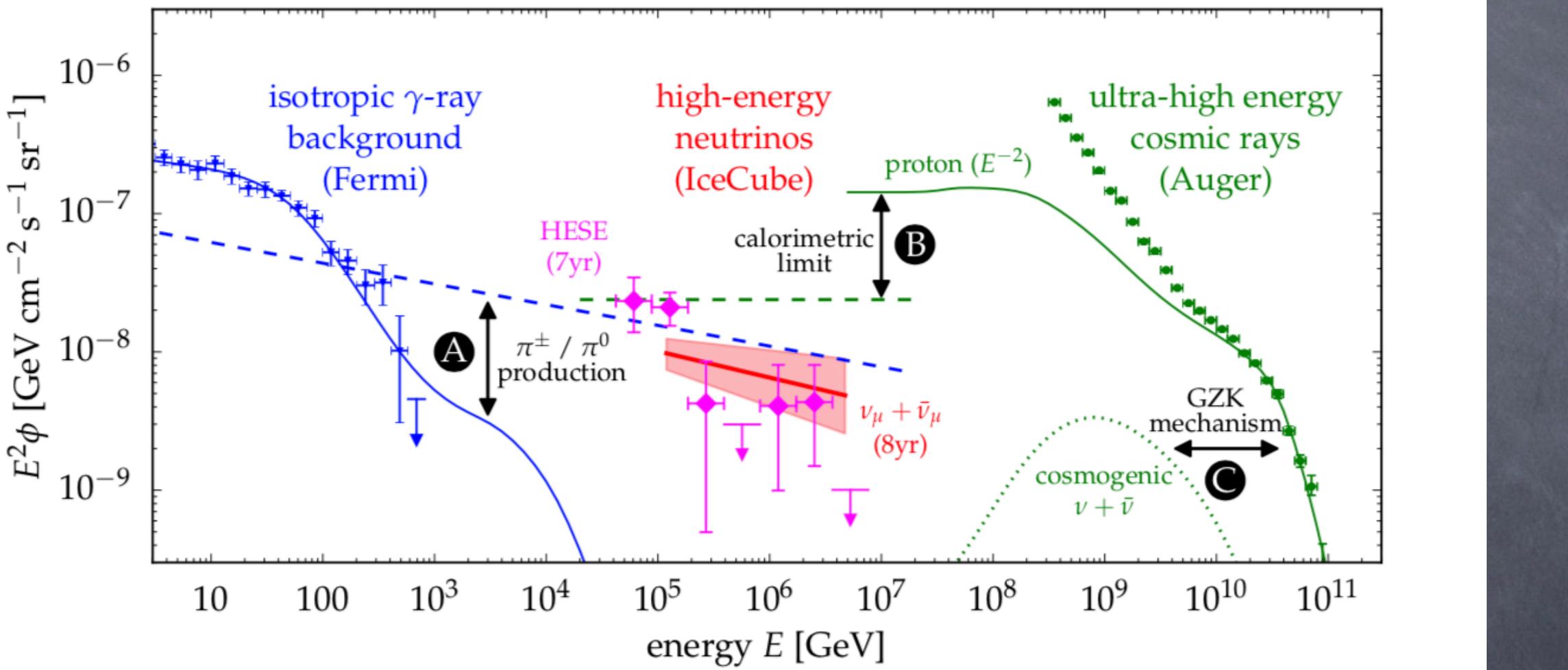


M. Ahlers, arXiv:1811.07633

**Figure 1.** The spectral flux ($\phi$) of neutrinos inferred from the eight-year upgoing track analysis (red fit) and preliminary results of the seven-year HESE analysis [8] (magenta data) compared to the flux of unresolved extragalactic $\gamma$-ray sources [10] (blue data) and ultra-high-energy cosmic rays [11] (green data). The $\nu_\mu + \bar{\nu}_\mu$ spectrum is indicated by the best-fit power-law (solid line) and $1\sigma$ uncertainty range (shaded range). We highlight the various multimessenger relations: **A:** The joined production of charged pions ($\pi^{\pm}$) and neutral pions ($\pi^0$) in cosmic-ray interactions leads to the emission of neutrinos (dashed blue) and $\gamma$-rays (solid blue), respectively. **B:** Cosmic ray emission models (solid green) of the most energetic cosmic rays imply a maximal flux (calorimetric limit) of neutrinos from the same sources (green dashed). **C:** The same cosmic ray model predicts the emission of cosmogenic neutrinos from the collision with cosmic background photons (GZK mechanism).

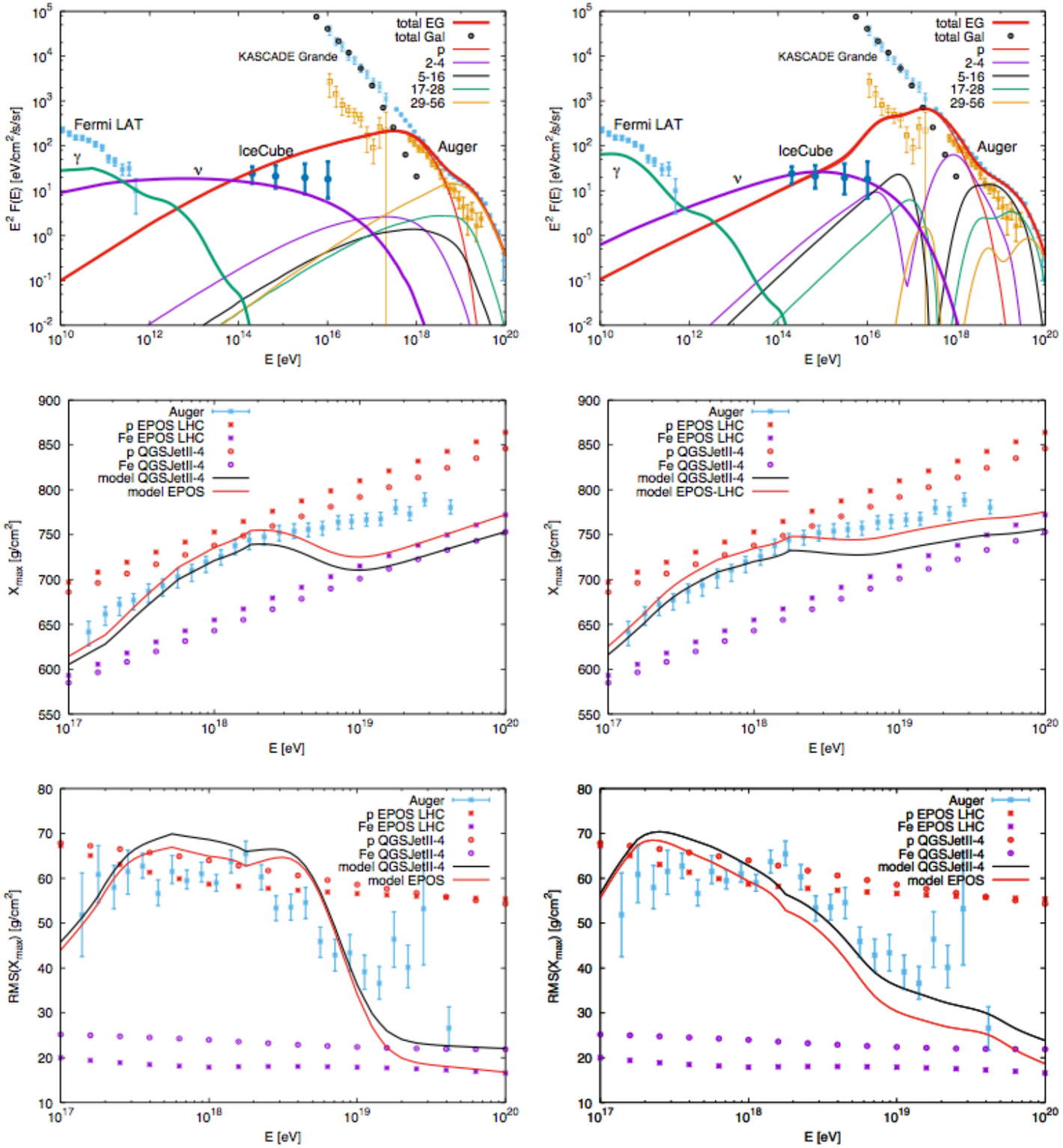


FIG. 1: Predictions for the diffuse flux (top) of five elemental groups together with the proton (orange errorbars) and total (blue errorbars) flux from KASCADE, KASCADE-Grande [9] and Auger (black errorbars) [8, 33], the EGRB from Fermi-LAT (red errorbars) [2], and the high-energy neutrino flux from IceCube (magenta errorbars) [3]; the middle and lower panels compare predictions for $X_{\rm max}$and RMS($X_{\rm max}$) using the EPOS-LHC [35] and QGSJET-II-04 [26] models to data from Auger [34]. Left panels for only hadronic interactions with $\alpha = 1.8$, $E_{\rm max} = 3 \times 10^{18}$ eV and BL Lac evolution. Right panels for both $A\gamma$ and Ap interactions with $\alpha = 1.5$, $E_{\rm max} = 6 \times 10^{18}$ eV, $\tau^{p\gamma} = 0.29$ and AGN evolution. The hadronic interaction depth is normalised as $\tau_0^{pp} = 0.035$.

a recent "minimal" model that explains diffuse spectra of primary cosmic rays, secondary gamma-rays and neutrinos in which primary cosmic rays interact hadronically and/or photo-hadronically around the sources

M. Kachelriess et al., arXiv: 1704.06893

# Dark Matter Candidates

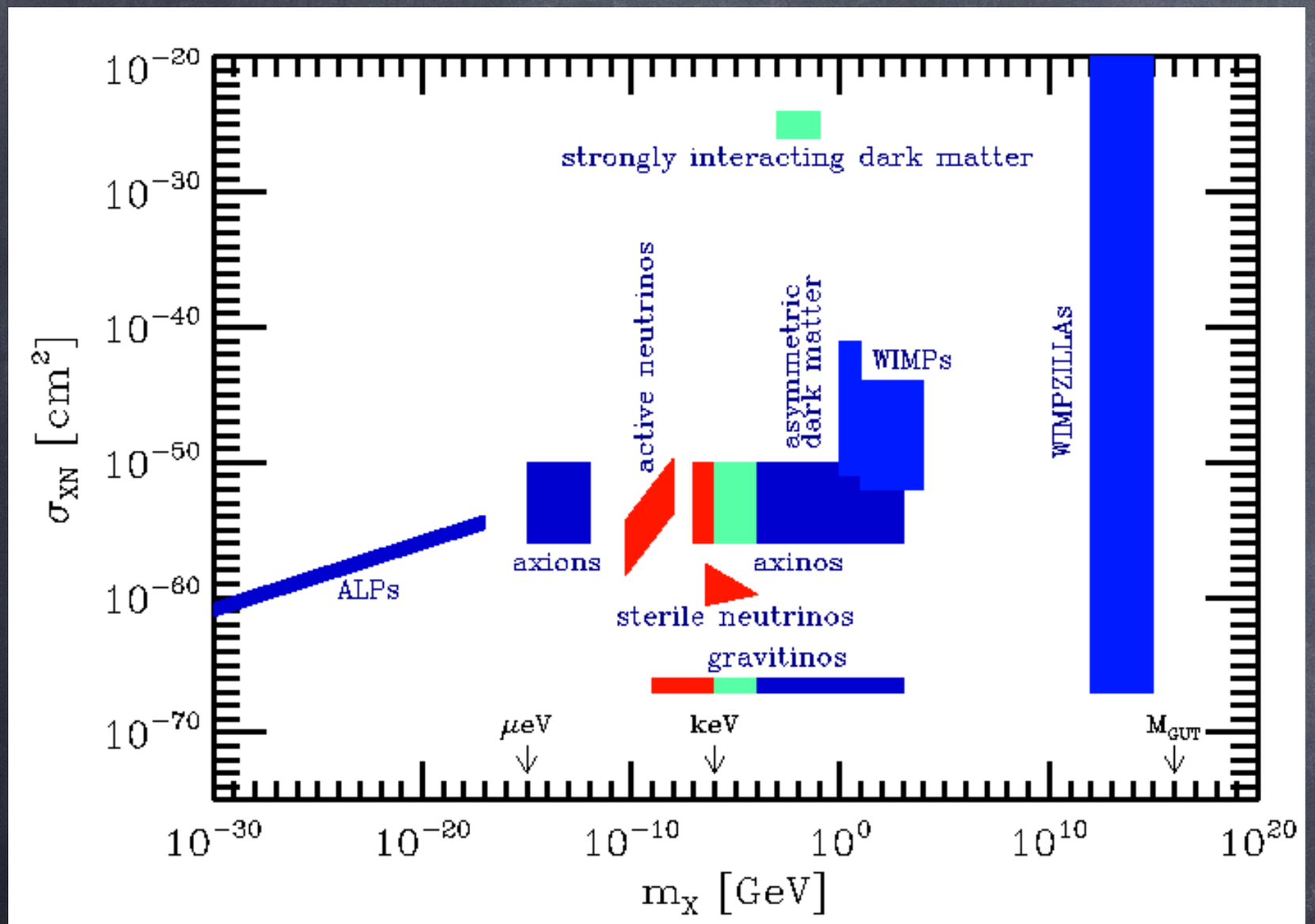


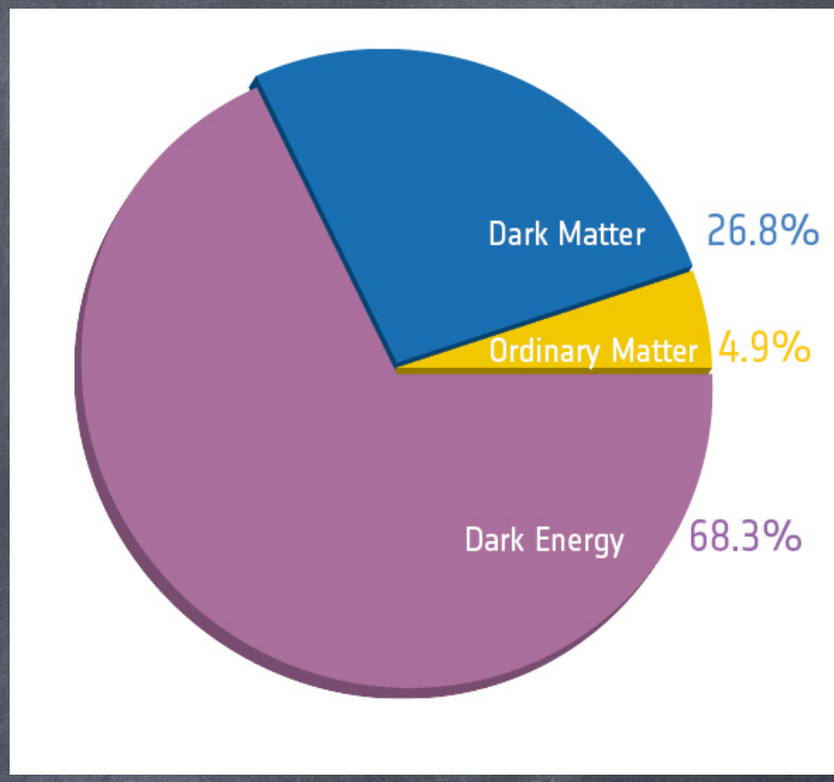


[PLANCK]

G. Sigl, book "Astroparticle Physics: Theory and Phenomenology", Atlantis Press/Springer 2016

# Axions, the strong CP problem and cosmology

breaking of global symmetry at temperature $T < f_a$: axion is would be pseudo Nambu-Goldstone boson

axion acquires mass at QCD scale due to mixing with pions -> tilted Mexican hat, solves strong CP-problem

$$m_a \simeq 6 \times 10^{-6} \left( \frac{10^{12}\,\mathrm{GeV}}{f_a} \right) \mathrm{eV}\,.$$

axion field frozen for $H > m_a$ with random values uncorrelated over causal distances

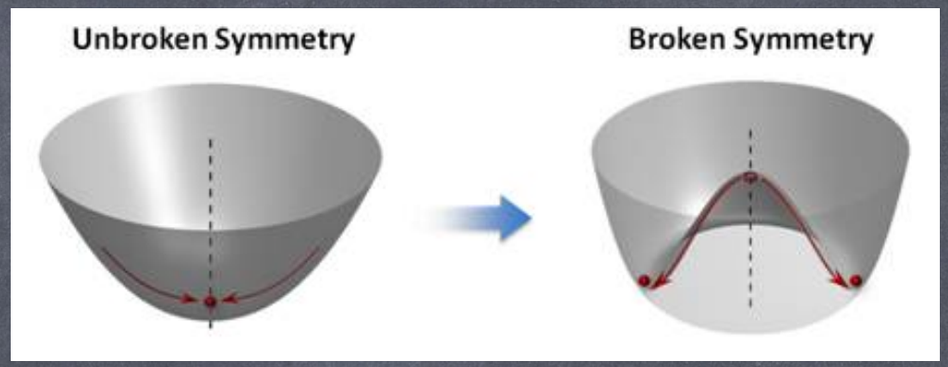


[Peking University]

$$\Phi(x) = \left[ f_a + \rho(x) \right] e^{ia(x)/f_a}$$

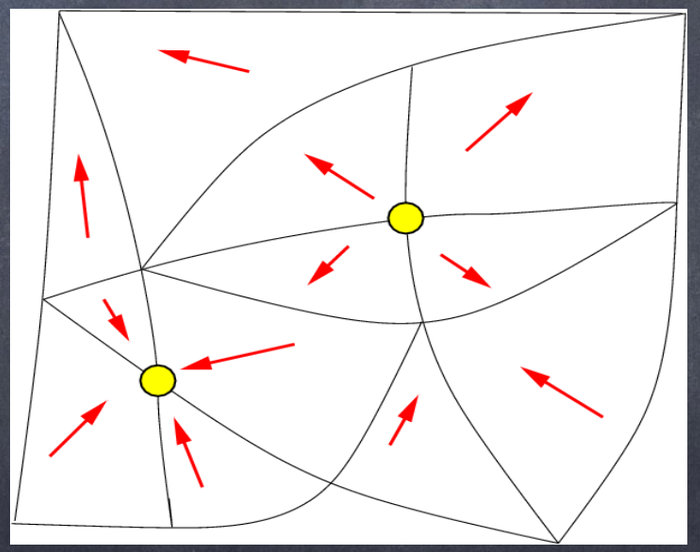

[Uhlmann et al. `10]

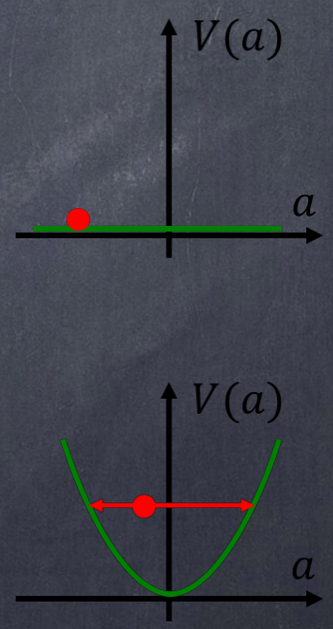


[Raffelt]

Once H < $m_a$ axion field starts to oscillate in its potential and behaves as pressure-less non-relativistic cold dark matter

resulting relic density has contributions from inflationary quantum fluctuations, possible cosmic string decays and the misalignment mechanism. The latter contributes

$$\Omega_a h^2 \simeq 7.4 \times 10^{-4} \left(\frac{m_a}{\mu\mathrm{eV}}\right)^{1/2} \left(\frac{f_a}{10^{12}\,\mathrm{GeV}}\right)^2 \theta_{a,0}^2 \,.$$

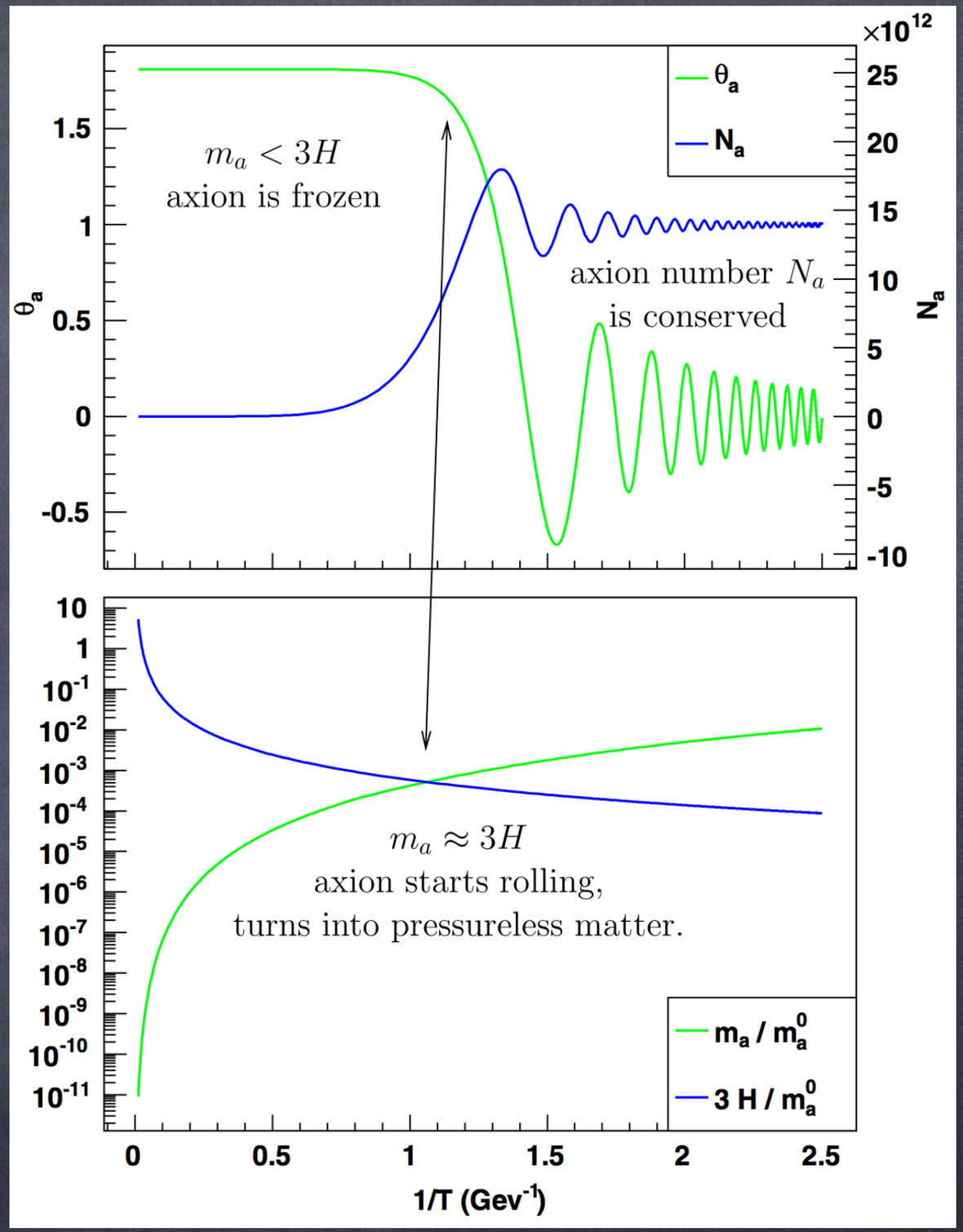


[Wantz,Shellard `09]

# ALP-photon Coupling

fundamental coupling:

$$\frac{\alpha_{\rm em}}{8\pi}\frac{C_{a\gamma}}{f_a}\,a\,F_{\mu\nu}\tilde{F}^{\mu\nu} = \frac{e^2}{32\pi^2}\frac{C_{a\gamma}}{f_a}\,a\,F_{\mu\nu}\tilde{F}^{\mu\nu} = \frac{\alpha_{\rm em}}{8\pi}\frac{C_{a\gamma}}{f_a}\,a\,F_{\mu\nu}\tilde{F}^{\mu\nu} = \frac{g_{a\gamma}}{4}\,a\,F_{\mu\nu}\tilde{F}^{\mu\nu}\,, \tag{4}$$

where $\alpha_{\rm em} = e^2/(4\pi\epsilon_0)$ and

$$g_{a\gamma} \equiv \frac{\alpha_{\rm em} C_{a\gamma}}{2\pi f_a}\,. \tag{5}$$

gives rise to two effects:

- Primakoff conversions between ALPs and photons in background electromagnetic fields -> shining light through a wall, helcioscopes, haloscopes
- modified photon refraction in ALP background -> Mathieu-type equations

For ALPs the mass $m_a$ and coupling energy scale $f_a$ are uncorrelated.
For axions they are related by

$$m_a \simeq 6 \times 10^{-6}\left(\frac{10^{12}\,\text{GeV}}{f_a}\right)\,\text{eV}\,.$$

# Overview Current Constraints

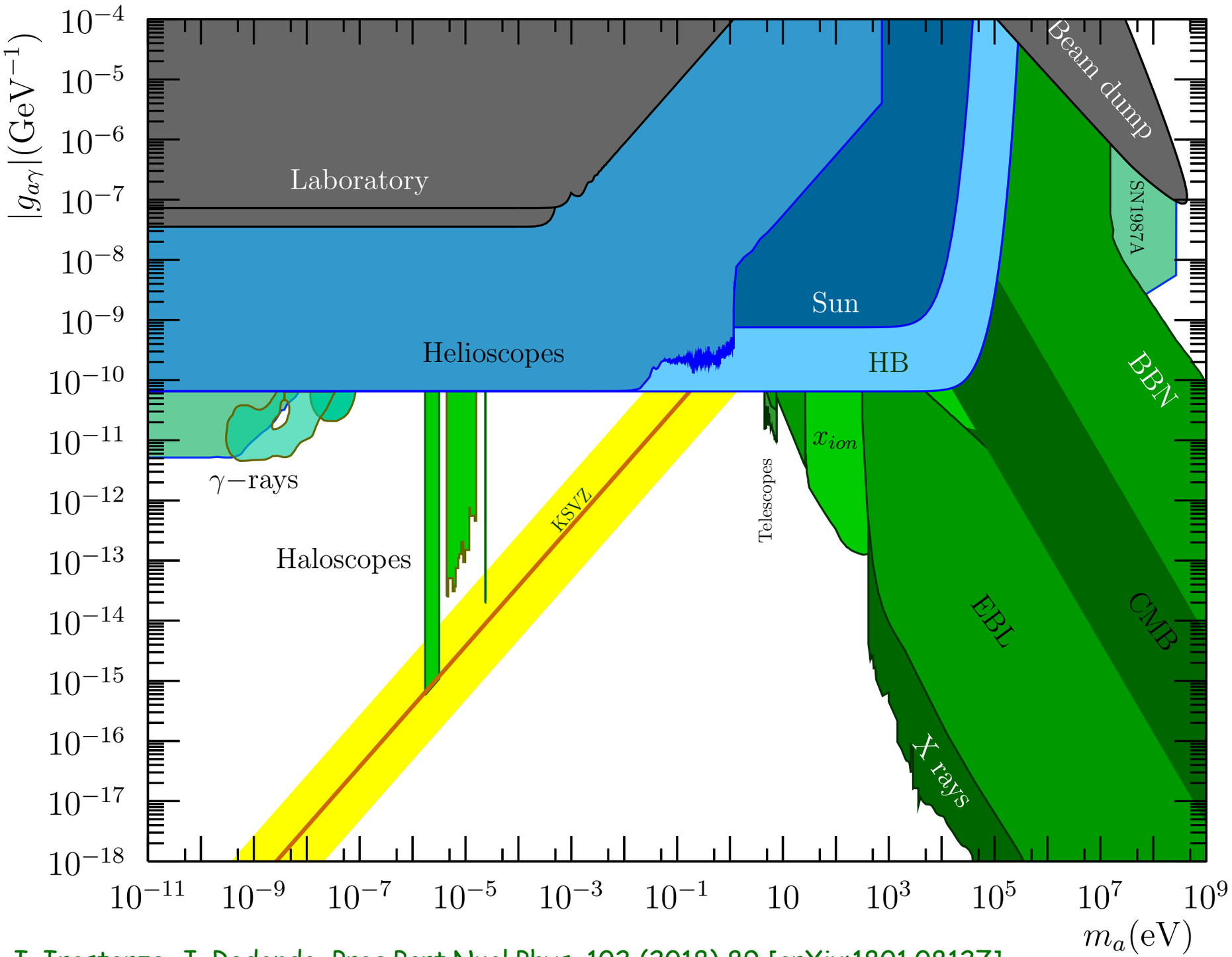


I. Irastorza, J. Redondo, Prog.Part.Nucl.Phys. 102 (2018) 89 [arXiv:1801.08127]

recently K. Kelley and P. J. Quinn, Astrophys. J. 845, 1 (2017) [arXiv:1708.01399] pointed out the possibility to search for ALP dark matter with radio telescopes; they used standard magnetic field estimates but assumed most of the power is on meter scales which is unlikely.

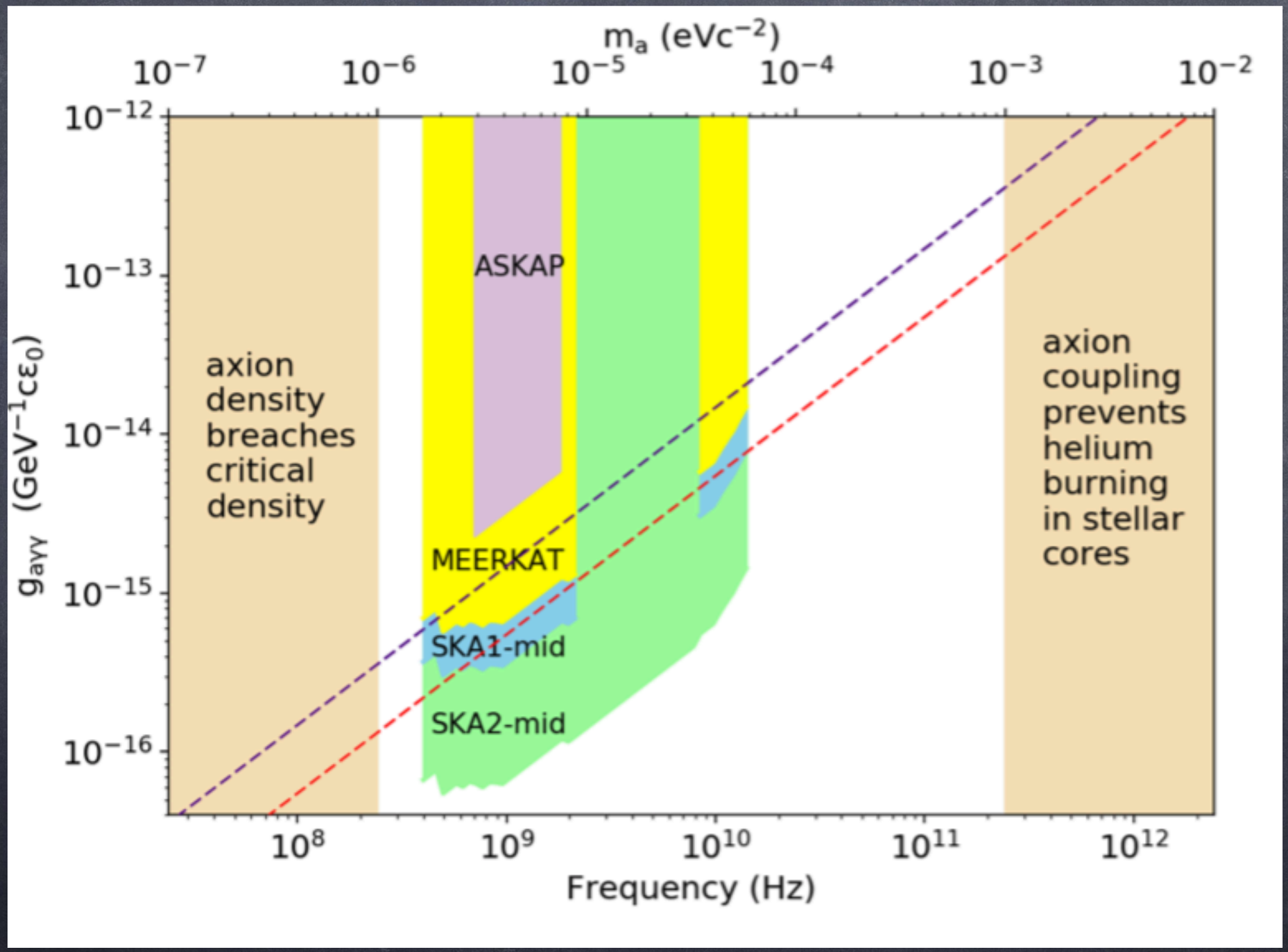

More compactly this can be written in terms of the magnetic field (static) power spectrum defined as

$$\rho_m = \frac{1}{2\mu_0 V}\int d^3\mathbf{r}|\mathbf{B}(\mathbf{r})|^2 = \frac{1}{2\mu_0 V}\int d^3\mathbf{k}|\mathbf{B}(\mathbf{k})|^2 = \int d\ln k \rho_m(k)\,,$$

Using $|\mathbf{k}_\gamma - \mathbf{k}_a| \sim k_\gamma \sim m_a$ and assuming a **homogeneous ALP distribution** with total mass $M_a = n_a m_a V$ this gives

$$R_{a\to\gamma} \simeq \pi g_{a\gamma}^2 \frac{M_a}{m_a^2}\rho_m(m_a)\,,$$

Integration over the line of sight dl this results in a **specific intensity per solid angle** [Jansky per steradian where 1 Jy = $10^{-26}$ W/(cm$^2$ Hz) = $10^{-23}$ erg/(cm$^2$ s Hz)]

$$I \simeq \pi \frac{g_{a\gamma}^2}{m_a^2}\frac{1}{\Delta}\int_{\text{l.o.s.}} dl \rho_a(l)\rho_m(m_a, l)\,,$$

For example, for a supernova remnant at distance d for which $\rho_m(m_a) = f(m_a)\rho_m$ SKA would be sensitive to couplings

$$g_{a\gamma} \gtrsim 2\times 10^{-13}\,[m_a/\mu\text{eV}][\Delta/10^{-3}]^{1/2}[d/(2\,\text{kpc})]^{1/2}\,\text{GeV}^{-1}/f(m_a)$$

Unfortunately f(k) is poorly known and might be <<1 [GS, PRD Phys.Rev. D96 (2017) 103014 [arXiv:1708.08908]]

# Resonant Primakoff Conversion around Compact Objects

Full conversion (e.g. resonance between ALP mass and plasma frequency at distance $r_s$ from neutron star center) gives

$$S_{\rm max} \simeq \frac{\rho_a}{m_a}\frac{v_a}{\Delta}\left(\frac{r_s}{d}\right)^2 \simeq 10^{-10}\left(\frac{m_a}{\mu{\rm eV}}\right)^{-1}\left(\frac{r_s}{10^6\,{\rm cm}}\right)^2\left(\frac{d}{\rm kpc}\right)^{-2}{\rm Jy}\,,$$

see also M.S.Pshirkov, J.Exp.Theor.Phys. 108 (2009) 384 [arXiv:0711.1264] who obtained higher fluxes, see also A. Hook et al., arXiv:1804.03145, F.P. Huang et al., arXiv:1803.08230

This would be detectable out to ~ pc distances, see also D. Marsh (Cambridge)

Hook et al., arXiv:1804.03145 made a more detailed calculation of resonant conversion (when plasma frequency matches ALP mass) around neutron stars which results in

$$\frac{d\mathcal{P}(\theta=\frac{\pi}{2},\theta_m=0)}{d\Omega} \approx 4.5\times10^8\ \mathrm{W}\left(\frac{g_{a\gamma\gamma}}{10^{-12}\ \mathrm{GeV}^{-1}}\right)^2 \left(\frac{r_0}{10\ \mathrm{km}}\right)^2\left(\frac{m_a}{1\ \mathrm{GHz}}\right)^{5/3}\left(\frac{B_0}{10^{14}\ \mathrm{G}}\right)^{2/3}\left(\frac{P}{1\ \mathrm{sec}}\right)^{4/3} \left(\frac{\rho_\infty}{0.3\ \mathrm{GeV/cm}^3}\right)\left(\frac{M_{\mathrm{NS}}}{1\ M_\odot}\right)\left(\frac{200\ \mathrm{km/s}}{v_0}\right),$$

$$S = 6.7\times10^{-5}\ \mathrm{Jy}\left(\frac{100\ \mathrm{pc}}{d}\right)^2\left(\frac{1\ \mathrm{GHz}}{m_a}\right)\times \left(\frac{200\ \mathrm{km/s}}{v_0}\right)^2\left[\frac{d\mathcal{P}/d\Omega}{4.5\times10^8\ \mathrm{W}}\right].$$

Advantage: Depends on plasma and magnetic field structure only through adiabaticity of conversion

A. Hook et al., arXiv:1804.03145

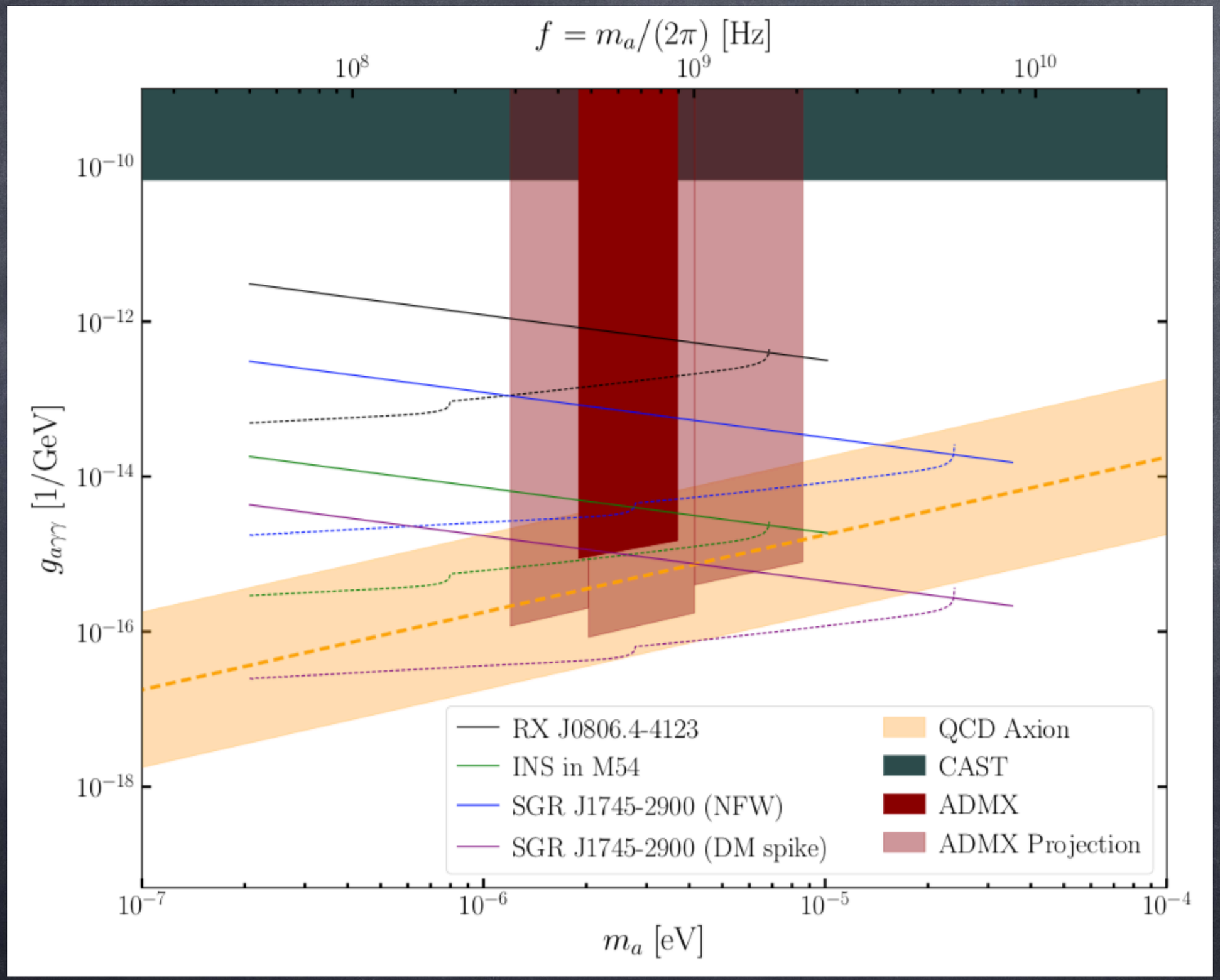

# Spontaneous and Stimulated Decays

compare Primakoff conversion rate

$$\frac{1}{\tau_a} \simeq \frac{\pi g_{a\gamma}^2}{m_a} \rho_m(m_a) \simeq 9.7{\times}10^{-38} \left(g_{a\gamma} 10^{14}\,\mathrm{GeV}\right)^2 \left(\frac{m_a}{\mathrm{meV}}\right)^{-1} \left(\frac{B}{\mathrm{mG}}\right)^2 f(m_a)\,\mathrm{s}^{-1}\,,$$

with spontaneous decay rate

$$\frac{1}{\tau_a} = \frac{g_{a\gamma}^2 m_a^3}{64\pi} \simeq 1.5 \times 10^{-38} \left(g_{a\gamma}\, 10^{14}\,\mathrm{GeV}\right)^2 \left(\frac{m_a}{\mathrm{meV}}\right)^3 \mathrm{s}^{-1}\,.$$

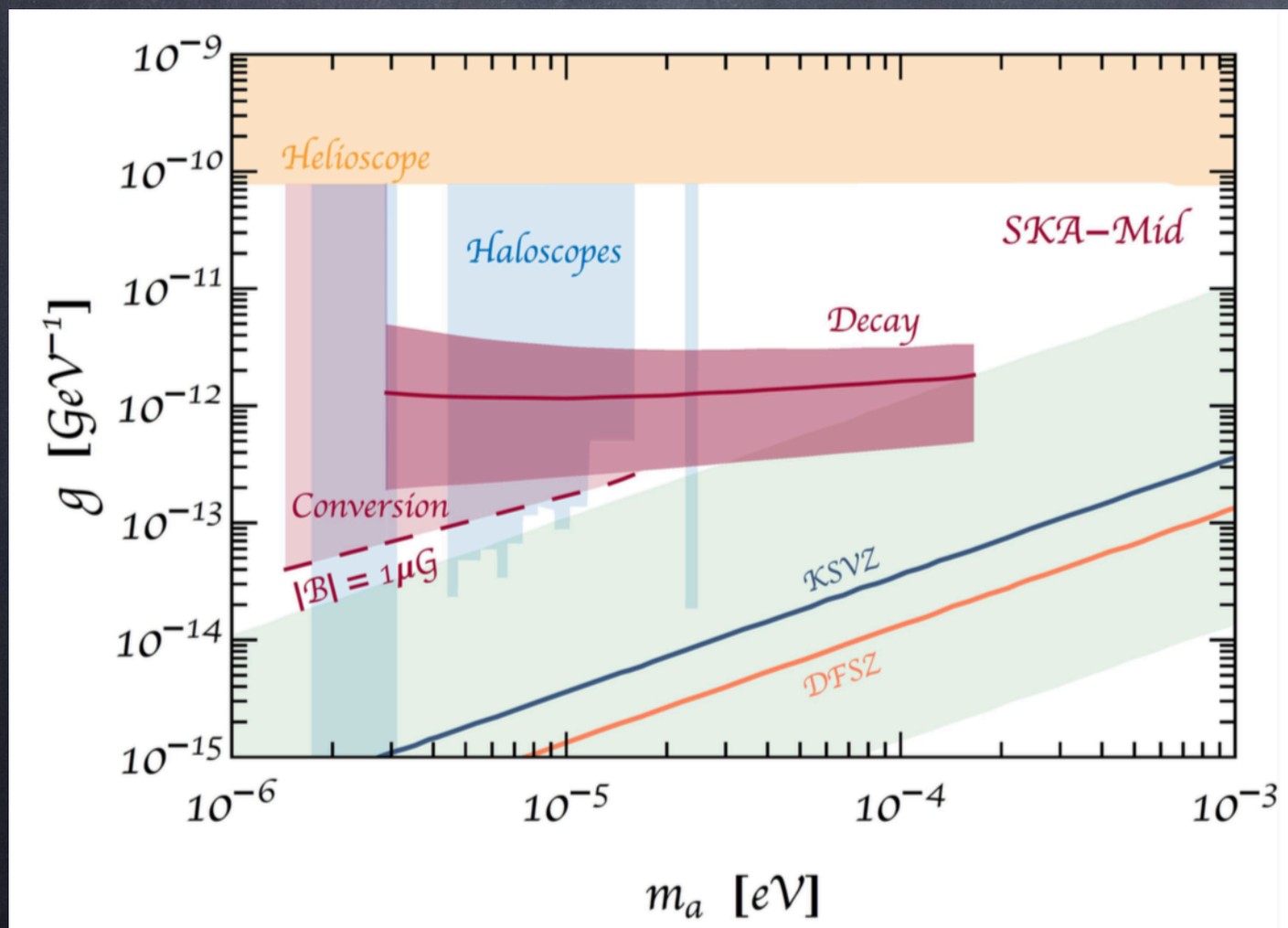


A. Caputo et al., PRD 98, 083024(2018) [arXiv:1805.08780], see also I.Tkachev, PLB 191 (1987) 41;
T.W. Kephart and T.J. Weiler, PRD 52, 3226 (1995)

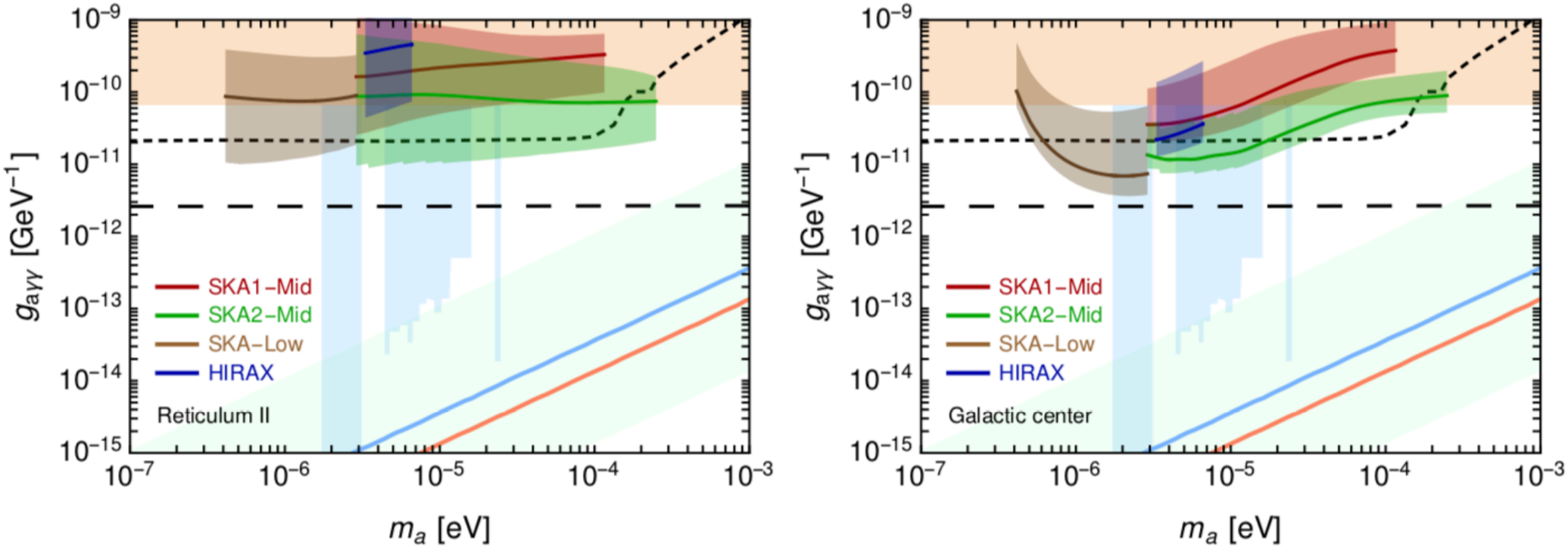


**Figure 2.** Projected sensitivities for the Reticulum II dwarf galaxy (left) and the Galactic center (right). Results are displayed alongside current bounds from haloscopes (light blue) [14–17] and helioscopes (orange) [18], projected bounds from ALPS-II [62] (black, short dashed) and IAXO [19, 20] (black, long dashed), and benchmark QCD axion models (light green band, blue line, orange line) [45]. The width of the expected exclusion contours reflect the astrophysical uncertainty in each environment.

A. Caputo et al., arXiv:1811.08436

# ALP-Photon Conversion through Parametric Resonance

Tkachev Sov.Astron.Lett. 12 (1986) 305, Pisma Astron.Zh. 12 (1986) 726,
see also M.P. Hertzberg and E.D. Schiappacasse, arXiv:1805.00430,

From the modified Maxwell equations

$$\boldsymbol{\nabla}\cdot\mathbf{E} = \frac{\rho_{\rm em}}{\epsilon_0} + \frac{\mathbf{B}\cdot\boldsymbol{\nabla}a}{\epsilon_0 M_a}\,, \quad \boldsymbol{\nabla}\times\mathbf{B} = \frac{\partial\mathbf{E}}{\partial t} + \mu_0\,\mathbf{j}_{\rm em} + \frac{\mathbf{E}\times\boldsymbol{\nabla}a - \mathbf{B}\partial_t a}{\epsilon_0 M_a}$$

with $g_{a\gamma} = 1/M_a$ for an ALP field $a(t)=a_0 \sin m_a t$ one obtains a Mathieu-type equation of the form

$$\left[\frac{d^2}{dx^2} + A - 2q\cos(2x)\right] A_\pm = 0$$

for the two circularly polarised photon fields $A_\pm$ with $x=m_a t/2$ and

$$A = \frac{4k^2}{m_a^2}\,, \quad q = \pm\frac{2k}{\epsilon_0 M_a}\frac{a_0}{m_a}$$

For $q<1$ (narrow resonance) there are resonances at $A = 1 \pm q$ growing with a rate in x of ~ q/2. The resulting band width is $k = m_a(1 \pm q)/2$

This corresponds to the crossed spontaneous decay into $k=m_a/2$ photons.

For $q>1$ other resonances are at $A\sim 2q$ growing with a rate in x of ~1 (probably not relevant here)

## Case 1: Diffuse galactic dark matter

$$\rho_a \simeq \frac{1}{2} m_a^2 a_0^2 \longrightarrow a_0 \simeq 2.2 \left( \frac{\mu\text{eV}}{m_a} \right) \text{keV}$$

which implies a narrow resonance with

$$q \sim 2.3 \times 10^{-19} \left( g_a \cdot 10^{14}\,\text{GeV} \right) \left( \frac{\mu\text{eV}}{m_a} \right)$$

could give a few e-folds in Galaxy, but extremely narrow line

## Case 2: ALP stars

estimates based on Visinelli et al., Phys Lett. B 777 64 (2018) [arXiv:1710.08910]

$a_0 \sim f_a^2/M_{pl}$ -> narrow resonance parameter

$$q \simeq C_{a\gamma} \frac{\alpha_{\text{em}}}{2\pi} \frac{f_a}{M_{\text{Pl}}} \sim 10^{-9} \left( \frac{f_a}{10^{12}\,\text{GeV}} \right)$$

The radius of an axion star is $R \sim 1/(q m_a)$ and the kinetic energy of axions in an axion star is $\sim q m_a$. Therefore, impinging radio photon beams could be enhanced by $m_a\, q/(m_a q)$ thus potentially by several e-folds.

But axion stars probably cover too small a fraction of the sky to give observable effects. On the other hand, if a large fraction of the axion star could be converted to radio photons [Hertzberg and Schiappacasse, arXiv:1805.00430, Tkachev, PLB 191, 41]. Note that spontaneous ALP decay probably not crucial to seed this because radio photons are always around.

Interesting conceptual questions when back reaction becomes important

$$\Box a + \frac{\partial V_a}{\partial a}(a) = \frac{\mathbf{E}\cdot\mathbf{B}}{M_a}\,.$$

For example, does momentum conservation lead to recoil when photon beam is enhanced ? Energy conservation ?

Potentially strong constraints from the diffuse radio background.

However, details depend on detailed structure of axion stars and their formation history: much interesting recent work on this
e.g. Buschmann, Levkov, Niemeyer, Pargner, Redondo, Schwetz, …

on small length scales the Mathieu equation leads to the dispersion relation

$$\omega = k \mp \frac{m_a g_{a\gamma}}{2\epsilon_0} a_0 \cos(m_a t + \delta) \,,$$

which leads to birefringence with a phase shift

$$\Delta\phi_1 \simeq \frac{g_{a\gamma}}{\epsilon_0} a_0 \simeq 10^{-20} \left( g_{a\gamma} 10^{14}\,\mathrm{GeV} \right) \left( \frac{\mu\mathrm{eV}}{m_a} \right) .$$

Note that this does not depend on photon wavenumber and thus any waveband can be applied. Adding in quadrature phase shifts from domains $l_c > 1/m_a$ in which the axion field is coherent (i.e. phase $\delta$ ~ constant) yields

$$g_{a\gamma} \lesssim 3 \times 10^{-13}\, \Delta\phi\, v_a^{-1/2} \left( \frac{m_a}{10^{-22}\,\mathrm{eV}} \right)^{1/2} \left( \frac{10\,\mathrm{kpc}}{d} \right)^{1/2} \mathrm{GeV}^{-1} \,,$$

where $\Delta\phi$ is an upper limit on the observed phase shift.

Same effect also used in experimental approaches, e.g. birefringent cavities, arXiv:1809.01656

# Application to CMB Polarization angle rotation limits

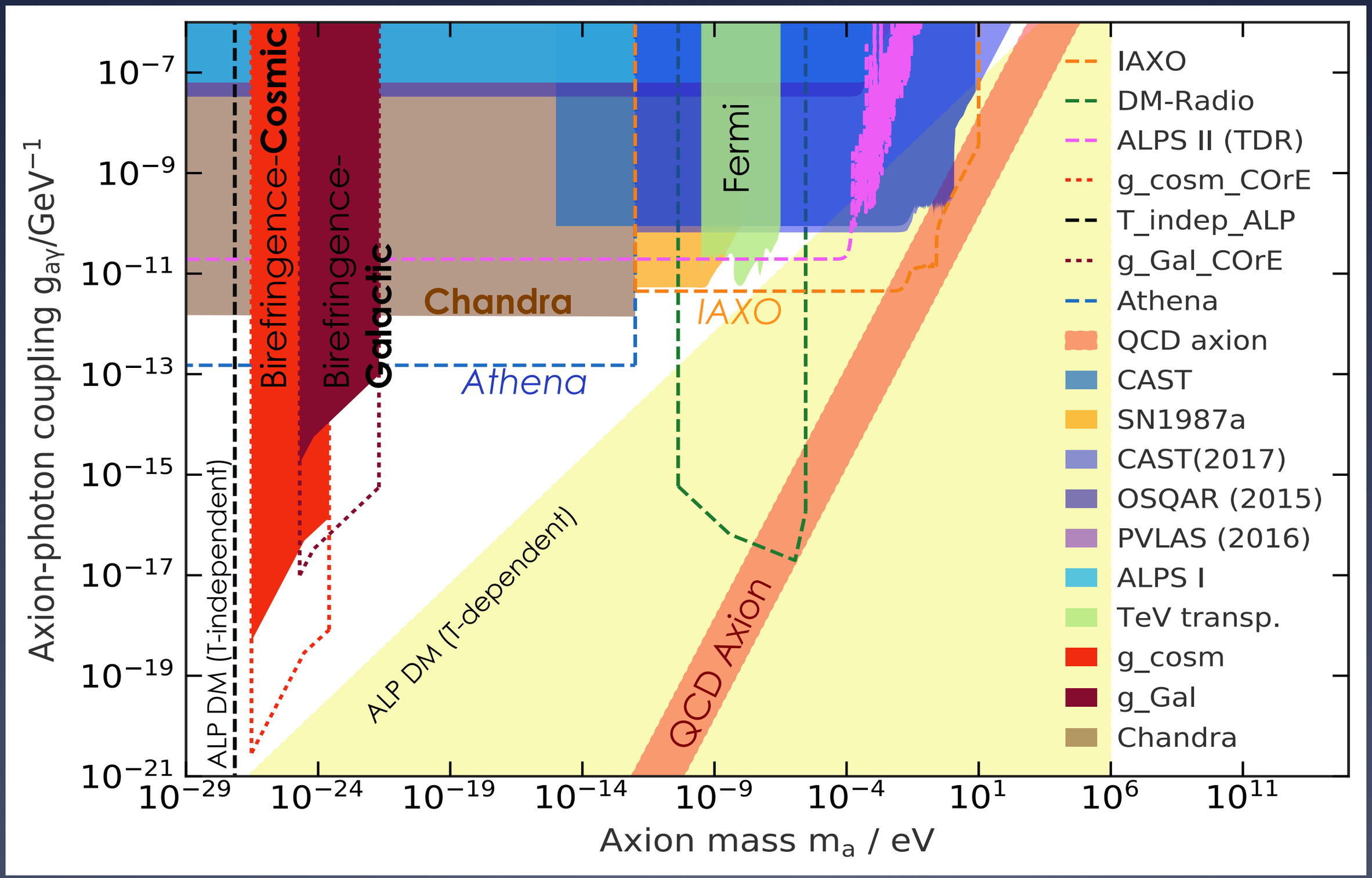


G. Sigl, P. Trivedi, arXiv:1811.07873

# Conclusions 1

1.) The sources of ultra-high energy cosmic rays are still not identified due to rather small anisotropies; composition seems to become heavier at the highest energies which appears economic in terms of shock acceleration power

2.) The observed $X_{max}$ distribution of air showers provides potential constraints on hadronic interaction models: Some models are in tension even when "optimizing" unknown mass composition; however, systematic uncertainties are still significant.

3.) IceCube neutrinos already constrain their sources which should be sufficiently numerous: Gamma-ray bursts are unlikely as main sources

4.) Multi-messenger modeling sources including gamma-rays and neutrinos start to constrain the source and acceleration mechanisms

# Conclusions 2

1.) Linelike radio emissions from dark matter-ALP conversion into photons in magnetic fields may be detectable with current and future radio telescopes such as LOFAR and SKA

2.) However, the most crucial (and least known) parameter is the magnetic field power on the ALP mass scale which is in the meter regime for μeV ALP masses. MHD modes in the presence of coherent magnetic fields would play an important role but their intensity is currently unclear.

3.) Spontaneous decay (interesting above ~$10^{-5}$ eV) and parametric amplification in ALP stars are independent of magnetic fields, but the latter depends a lot on ALP star structure and their formation (not well understood yet but many opportunities for collaboration !)

4.) Resonant conversion around compact stellar objects may give interesting signals less dependent on magnetic field structure

5.) Birefringence induced in photons propagating in an oscillating axion background should be wavelength independent (thus also relevant e.g. for X-rays) and could lead to further constraints.